Dissertation
submitted to the
Combined Faculties for the Natural Sciences and for Mathematics
of the Ruperto-Carola University of Heidelberg, Germany
for the degree of
Doctor of Natural Sciences

presented by

NIRUPAMA RAMANATHAN; M.Sc., B.Tech.
Born in Chennai, India

Oral-examination: 17th July 2015

MONITORING THE RESPONSE OF CELLS AND ORGANISMS TO DIFFERENT CHEMICAL CUES USING MICROFLUIDICS

Referees:
DR. RAINER PEPPERKOK
PROF. DR. WALTER NICKEL

Abstract

Microfluidic devices allow precise control to manipulate fluids within micrometer sized channel networks. In single phase microfluidic systems where miscible fluids are infused, laminar flow can be generated. This means liquid streams can flow parallel to each other without convective mixing. In two phase microfluidic systems where two immiscible fluids are infused, droplets are generated. Using this system, uniformly sized aqueous micro compartments can be generated in oil. This dissertation describes the development of novel microfluidic devices based on single phase and two phase systems to monitor responsiveness of cells and organisms to different chemical cues. Firstly, the possibility to apply a specifically designed single-phase microfluidic chip to study zooplankton ecology has been demonstrated. Zooplankton perceive their surrounding using chemical cues and rely on these cues for development and survival. However, with the current rapid global climatic changes affecting the ocean chemistry, it is unclear on how plankton, which form the base of the marine food chain, are coping. So far, measurements on zooplankton ecology have been hampered by technical impracticalities of exposing actively swimming plankton species to different chemical conditions simultaneously while monitoring their behavior on an individual level. Using the microfluidic device, first measurements on behavioral preferendum of zooplankton species to changes in pH and salinity could be made with a precision that additionally allowed estimating the "responsiveness", which is the minimum change in concentration required for the plankton to elicit a response, to an environmental stimulus. *Platynereis dumerilii,* cosmopolitan model plankton were more sensitive to changes in pH than salinity. In addition, comparing different species lead to the observation that *Euterpina acutifrons,* a copepod species showed a narrower pH preferendum than *P.dumerilii*. These measurements allow making predications on sensitive and resilient species. Furthermore, the ability to study the interaction of zooplankton with their prey and predators and perform functional studies on identifying cell types responsible for a sensory response has been demonstrated.

For cell-based screening assays however, the high-throughput offered by droplet-based systems outcompetes single-phase systems. But, generating chemical diversity in droplets that can allow screening entire chemical libraries while being able to track the sample identity remains to be demonstrated. Here a novel approach has been devised that allows generating sample barcoded combinatorial mixtures. In addition the approach has been optimized to suit for screening rare

and sensitive cells like mouse embryonic stem (mES) cells. The ability to maintain viable mES cells in droplets for a period of 48 h has been demonstrated and in addition the possibility to differentiate them by encapsulating them together with 10^{-8} M retinoic acid (RA) has been shown.

Lastly, a new microfluidic approach combining the advantages of single phase and two phase microfluidics has been described. This approach allows high-content cell-based screening with freely accessible cells allowing regular tissue culture handling and potentially, immunostaining experiments which are not possible when cells are encapsulated. To maximize the throughput per chip, chemicals were encapsulated in droplets and were allowed to locally diffuse through the chip material to the cells. The usability of this approach has been demonstrated by localized induction of GFP in tetracycline inducible HeLa-TRex™ cells.

In conclusion, different microfluidic approaches have been described in this thesis and used for applications ranging from analyzing cells to organisms. The good spatial resolution, precise control over liquids, possibility of assays on the individual level and low cell number/reagent quantity requirement, enabled by microfluidics makes the devices an advantageous tool for biological applications.

Zusammenfassung

Mikrofluidik-Chips erlauben eine präzise Manipulation von Flüssigkeiten in Mikrometer großen Kanalnetzwerken. In einphasigen Mikrofluidik-Systemen werden zwei mischbare Flüssigkeiten in einem Mikrochip injiziert und dadurch eine laminare Strömung erzeugt. Dies bedeutet, die Flüssigkeiten fließen in parallelen Strömen ohne sich konvektiv zu vermischen. In zweiphasigen Mikrofluidik-Systemen werden durch Injektion zweier nicht mischbaren Flüssigkeiten Tröpfchen gebildet, in denen biologische Assays ausgeführt werden können. In dieser Dissertation wird die Entwicklung von neuen Mikrofluidik-Chips basierend auf ein- und zweiphasigen Mikrofluidik-Systemen beschrieben, die eine Analyse der Sensitivität von Zellen und Organismen in Bezug auf chemische Stoffe ermöglichen.

Der erste hier beschriebene Mikrofluidik-Chip verwendet ein einphasiges Mikrofluidik- System und wurde speziell dafür entwickelt, umdie Ökologie von Zooplankton zu analysieren. Wichtig für die Entwicklung und den Fortbestand von Zooplankton ist die chemische Komposition der Umgebung. Wie Plankton, welches die Basis der marinen Nahrungsnetzwerke bildet, mit dem momentanen schnellen Klimawandel zurechtkommt, ist noch unerforscht. Studien der Ökologie von Plankton wurden bisher oft durch die Problematik behindert, dasses technisch nicht möglich war, frei schwimmende Plankton gleichzeitig verschiedenen chemischen Umgebungen auszusetzen und das individuelleVerhalten einzelner Organismen zu beobachten. Mit dem hier beschriebenen Mikrofluidik-Chip konnte zum ersten Mal die Verhaltensvorlieben von Zooplankton in Bezug auf Veränderungen von pH und Salzgehalt gemessen werden, wobei die Genauigkeit der Messwerte erlaubt,die Sensitivität der Arten auf Umwelteinflüsse abzuschätzen. *Platynereis dumerilli*, eine weltweit vorkommende Modell Plankton Art, reagierte empfindlicher auf Veränderungen des pH-Werts als auf Variation der Salzkonzentration. Der Vergleich verschiedener Arten zeigte zusätzlich, dass der Ruderfusskrebs *Euterpina acutifrons* einen kleineren pH-Toleranzbereich als *P. dumerilli* hat. Die erhaltenen Messergebnisse erlauben daher Abschätzungen über empfindliche und belastbare Spezies. Zusätzlich erlaubt dieser Mikrofluidik-Chip, Jäger-Beute Interaktionen von Zooplankton zu beobachten, und funktionale Studien durchzuführen, um Zelltypen zu identifizieren, die an der Sinneswahrnehmung beteiligt sind.

Für Studien an einzelnen Zellen hingegen eigenen sich die auf Tröpfche- basierenden Mikrofluidik-Systeme mit hohem Durchsatz besser als einphasige Methoden. Allerdings fehlte bisher die Möglichkeit, diverse chemische Bibliotheken in Tröpfchen einzukapseln, und die chemische Komposition einzelner Tröpfchen nachzuverfolgen. Hier wird nun ein neuer Ansatz dargestellt, mit dem einzigartige kombinatorische Barcodes der Proben hergestellt werden., Zudem wurde ein neuer Mikrofluidik-Chip für die Analyse von empfindlichen Zellen, wie z.B. ES Zellenentwickelt. Dieser ermöglicht es, die. mES Zellen für 48 h in Tröpfchen am Leben zu erhalten und die Differenzierung mit 10^{-8} M Retinsäure einzuleiten. .

Zuletzt wird eine neueMikrofluidik-Methode beschrieben, welche die Vorteile von einzel- und zweiphasigen Mikrofluidik-Chips vereint. Diese Methode erlaubt frei-zugängliche Zellen unter Verwendung von Standard Zellkulturtechniken zu analysieren, und potentiell Antikörperfärbungen durchzuführen, was mit eingekapselten Zellen nicht machbar ist. Um den Durchsatz dieser Chips zu maximieren, werden hier Chemikalien in Tröpfchen eingekapselt, welche lokal durch das Material des Chips zu den Zellen diffundieren. Eine Machbarkeitsstudie hierzu wurde mit lokaler Tetrazyclin-induzierter GFP HeLaTRex™ Zellen erläutert.

Zusammenfassend beschreibt diese Dissertation verschiedene Methoden der Mikrofluidik und zeigt wie diese für Anwendungen an Zellen und Organismen genutzt werden können. Die hohe räumliche Auflösung, die Präzision der Flüssigkeitsmanipulation, die Möglichkeit der Hochdurchsatz-Analyse von Individuen und einzelnen Zellen, sowie die geringe Menge an notwendigen Reagenzien machen diese Mikrofluidik-Cchips zu einem hervorragenden Werkzeug für biologische Anwendungen.

Acknowledgements

It is an interesting journey that is near its conclusion. There were many whose counsel and contributions made this journey enriching and I would like to thank them. First and foremost, I would like to thank Dr. Christoph Merten, for giving me the opportunity to pursue my PhD in an exciting field: Microfluidics. His continuous guidance and critical suggestions were crucial for this work and also, I greatly appreciate the interest he took in improving my general scientific abilities including writing of this thesis. The collaboration with Ocean-on-a-chip project had an important bearing on my work. This was made possible by the help and guidance offered by Prof. Detlev Arendt. My thanks are also due to Dr. Oleg Simakov with whom I worked together on this project. I would also like to thank Dr. Dominic Eicher, Dr. Federica Eduati and Ramesh Utharala for their contributions to this thesis, and Mahmoud-Reza Rafiee and Dr. Aleksandra Pekowska for the informative discussions.

I would also like to extend my deepest gratitude to all my TAC members: Prof. Dr. Walter Nickel, Dr. Rainer Pepperkok, Dr. Jeroen Krijgsveld and Dr. Pierre Neveu, for all the active discussions during the yearly meetings that contributed significantly to improving this work. My heart-felt thanks to Prof. Dr. Walter Nickel for his support as my University advisor and Chairman of my defense and to Dr. Rainer Pepperkok who will be my first examiner. Furthermore, my sincere thanks go to Dr. Guido Grossmann and Dr. Kyung-Min Noh for promptly agreeing to be on my defense committee.

In addition, I am grateful to the people in the EMBL core facilities for their support, especially to Dr. Alexis Perez Gonzalez (Flow cytometer facility), Dr. Hüseyin Besir (PEPcore facility), Thomas Heinzmann (SIM), Leo Burger and Sascha Blättel (Mechanical Workshop), for their valuable assistances. Indeed this PhD would not have been possible without the administrative and personal support from the Graduate office: Dr. Helke Hillebrand, Meriam Bezohra and Matija Grgurinovic. My heartfelt gratitude goes to each of them.

I am thankful to all the members of the Merten group who made the work environment enjoyable. Thanks to Dr. Timm Schlegelmilch and Dr. Chawaree Chaipan for translating my abstract to German. The stay at Heidelberg, my home away from home was made comfortable by all my friends here. A big “Danke” goes to Timm for being with me during difficult situations in the last two years, constantly supporting me and for all the scientific advice. Last but not the least; I sincerely appreciate the encouragement and unconditional support from my family at home -my parents and my sister - who have brought me to the position I am today. Thank you!

Contribution

The work presented in Chapter 2 “Ocean on a chip: Quantifying preferences and responsiveness of marine zooplankton to changing environmental conditions” and Chapter 4 “Semi-compartmentalization” were parts of collaborative efforts.

The contributions of Nirupama Ramanathan were as follows:

Chapter 2: Nirupama Ramanathan designed the microfluidic devices, performed the microfluidic experiments and analyzed the data. Further, she was involved in writing the manuscript which has been submitted and is under review now.

Chapter 4: Nirupama Ramanathan conceived the idea of the membrane method where the cells are grown on membrane instead of inside channels, optimized cell culturing in PDMS, and contributed with troubleshooting of drug diffusion through PDMS. This chapter was previously published: Eicher, D., Ramanathan, N., and Merten, C.A. (2015). Soft compartmentalization: Combining droplet-based microfluidics with freely accessible cells. Engineering in Life Sciences. DOI: 10.1002/elsc.201400184.

Dr. Christoph A. Merten

Table of Contents

Chapter 1

General Introduction

1.1 Microfluidics

Microfluidic systems are devices with sub-millimeter sized structures through which fluids of pico- to micro-liter volume are infused and processed (Whitesides, 2006). Integrated microfluidic devices together with pumps, valves and detectors are also called micro total analysis systems (μTAS) or lab-on-a-chip systems (Auroux et al., 2002; Reyes et al., 2002). These systems allow precise control of fluids, require low amounts of reagents and allow good spatial (μm scale) and temporal (ms scale) resolution. Further they enable automation, parallelization and high-throughput while being economical to produce. All these benefits have propelled research in this field over the last two decades. In the field of biology, these systems are an attractive tool because of several reasons including the possibility to use fewer cells for high-throughput which means that it is possible to work with rare samples and patient materials (Sia and Whitesides, 2003). Moreover polydimethylsiloxane (PDMS)-based microfluidic devices are also biocompatible and transparent for imaging (McDonald and Whitesides, 2002). These advantages have allowed several miniaturized bioassays to be performed in microfluidics which are further discussed in section 1.3.

1.2 Physics of microfluidics

Fluids behave differently in microfluidic devices because of the small dimensions. These properties are discussed below. Depending on the miscibility of the fluid, microfluidics is classified as single- and multi-phase microfluidics.

1.2.1 Single-phase systems

Miscible fluids, i.e. fluids of a single phase infused through a microfluidic channel do not undergo convective mixing because of the dominant viscous forces (Squires and Quake, 2005). Reynold's number (Re) gives the ratio between inertial and viscous forces. (Equation 1). For Re < 10 the flow is laminar and for Re = 2000 the flow is fully turbulent. In microfluidic device the Re is close to 1.

$$Re = \rho v L/\eta \qquad \rightarrow \text{Equation 1}$$

Where ρ is the density, v is the velocity, L is the length and η the shear viscosity.

Although the flow in a microfluidic device is laminar, diffusion by Brownian motion causes mixing of fluids over time. The longer the streams travel parallel to each other the greater the diffusion (Figure 1.1A). The diffusion is also dependent on the diffusion coefficient of the molecules in the streams (Equation 2).

$$d^2 = 2Dt \qquad \rightarrow \text{Equation 2}$$

Where d is the diffusion, t is the time and D is the diffusion coefficient. In a microfluidic device the time linearly correlates with the length of the channel.

It is known that in a static system a solute ion diffuses faster than a large protein during the same time (Beebe et al., 2002; Squires and Quake, 2005). In microfluidics, this has been favorably used for filtering without membranes by simply increasing the length of the channel depending on the diffusion coefficient of the molecule to be extracted (Brody et al., 1996) (Figure 1.1B).

In a microfluidic device where there is a flow, the length of the channel required to achieve complete mixing can be determined by also taking into account the velocity of the fluid in the channel. Using the Péclet number (Pe), which is the ratio between convective and diffusive flow, it is possible to determine when the flow is diffusive (Equation 3). For $Pe < 1$ the flow is diffusive, and for $Pe > 1$ the flow is convective.

$$Pe = vL/D \qquad \rightarrow \text{Equation 3}$$

Using the above principles, it is possible to generate on-chip gradients. This has been demonstrated previously to generate both linear and non-linear gradients (Irimia et al., 2006; Jeon et al., 2000; Toh et al., 2014).

Another parameter facilitating mixing in micro channels is dispersion. In pressure-driven microfluidic devices, where the liquids are infused using positive displacement pumps, the flow profile in the channel is parabolic (Figure 1.1C). This is because the flow velocity experienced by

the molecule in the center is higher than the flow velocity close to the walls. At a certain time point, this parabolic flow profile disperses the molecules resulting in a Gaussian distribution of their concentration (Figure 1.1C). This phenomenon is called Taylor dispersion (Taylor, 1953, 1954).

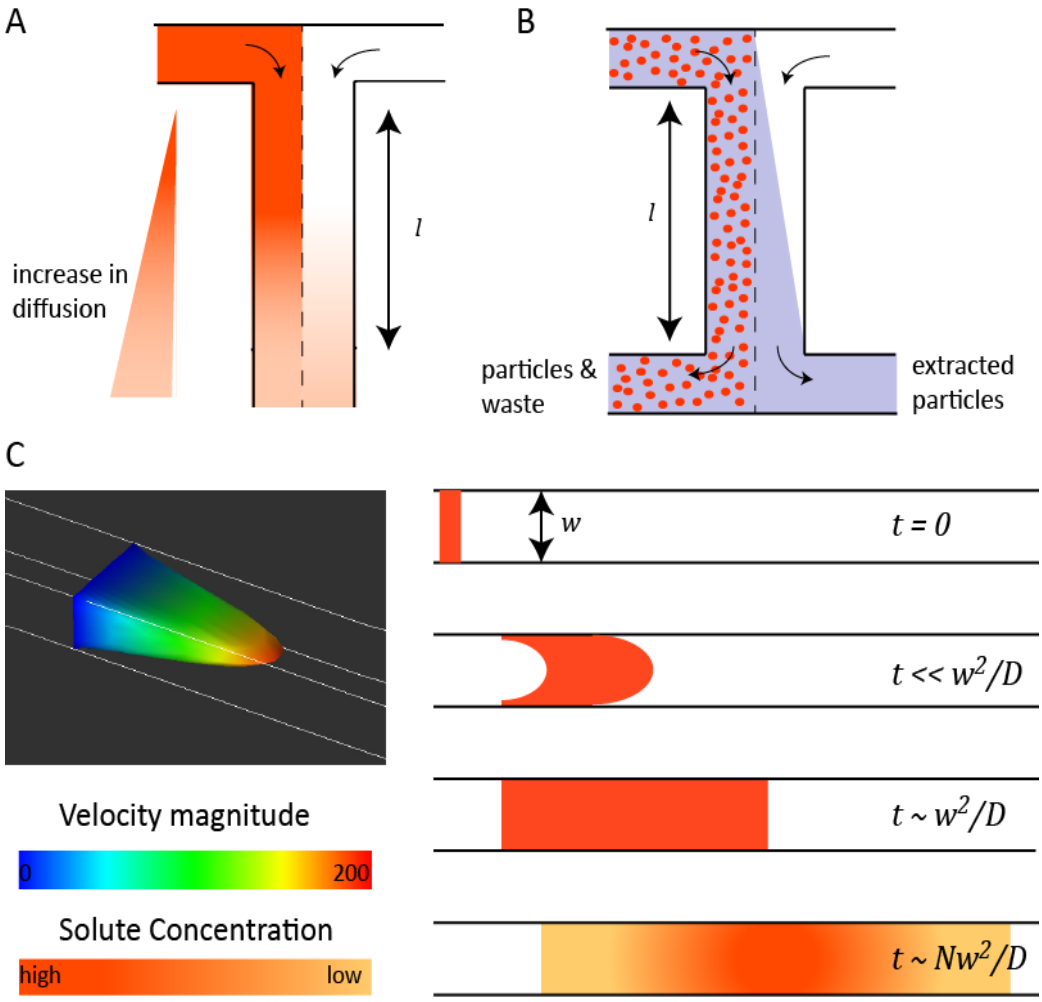

Figure 1.1 Flow profile in microfluidic channel. (A) Laminar flow of two streams. The dotted line indicates the interface between the two streams. Diffusion increases along the length *(l)* of the channel until a homogenous distribution of solutes is achieved. (B) A membraneless H-filter that separates molecules based on their diffusion coefficients. Larger molecules (red dots) diffuse slower than smaller molecules (blue) and to separate them a defined length *(l)* of the channel is required. Modified from (Brody et al., 1996). (C) Velocity profile of a pressure-driven flow inside a microfluidic channel (left). Adapted from (Schilling, 2001). The flow profile is parabolic which results in taylor dispersion of solutes with time (Tatistcheff et al.). The time required for dispersion depends in the diffusivity (D) of the solute and the width (w) of the channel.

1.2.2 Multi-phase systems

Interaction between two or more immiscible fluids/phases causes the formation of droplets and emulsions. This is because when immiscible fluids interact, surface tension γ affects the dynamics. Lowering the surface tension using microfluidics can allow producing smaller droplets. Uniformity in droplet size is necessary, especially if droplets are used as individual reaction vessels or assay compartments, where volume has to be the same. There are different ways reported to generate monodispersed droplets (Anna et al., 2003; Lee et al., 2009; Thorsen et al., 2001; Umbanhowar et al., 2000), however, the most commonly used methods are using either a T-junction (Thorsen et al., 2001) or a flow-focusing geometry (Anna et al., 2003) as illustrated in Figure 1.2B.

The T-junction geometry, described by Thorsten *et al.*, allows the generation of droplets by injecting water into a stream of oil (Thorsen et al., 2001). In this case, there is no interfacial tension between the two phases; however competing stresses drive the interface: surface tension reduces the interfacial area and viscous stresses extend and drag the interface downstream. These stresses destabilize the interface causing droplet formation (Figure 1.2A).

Flow focusing geometry allows producing significantly smaller droplets with the same channel dimensions. Here, an aqueous stream is focused between two opposing oil streams causing breakage of the aqueous stream into droplets due to Rayleigh-Plateau instability (Rayleigh, 1879)(Figure 1.2B). The size of the droplets can be adjusted by changing the nozzle dimension and the flow rates. Four different droplet breakup regimes have been reported using flow focusing geometry: squeezing, dripping, jetting and thread formation (Figure 1.2C) (Lee et al., 2009). To increase the flexibility of flow focusing devices, additional active elements like electrodes have been coupled. By changing voltage of the electrodes, the interfacial tension between the oil and aqueous phase could be altered, switching droplet breakup regimes (Gu et al., 2008).

Capillary number (*Ca*) comes into play whenever interfacial stresses compete with viscous stresses as in the formation of droplets. It is the ratio between the viscous forces and surface tension acting between immiscible fluids (Equation 4).

$$Ca = \frac{\eta v}{\gamma} \qquad \rightarrow \text{Equation 4}$$

Where η is the dynamic viscosity, v is the characteristic velocity of the fluid and v is the surface or interfacial tension between two fluids.

This dimensionless number influences the droplet formation. De Menech et al. reported theoretical evidence on the influence of Ca in droplet breakup regime (De Menech et al., 2008).

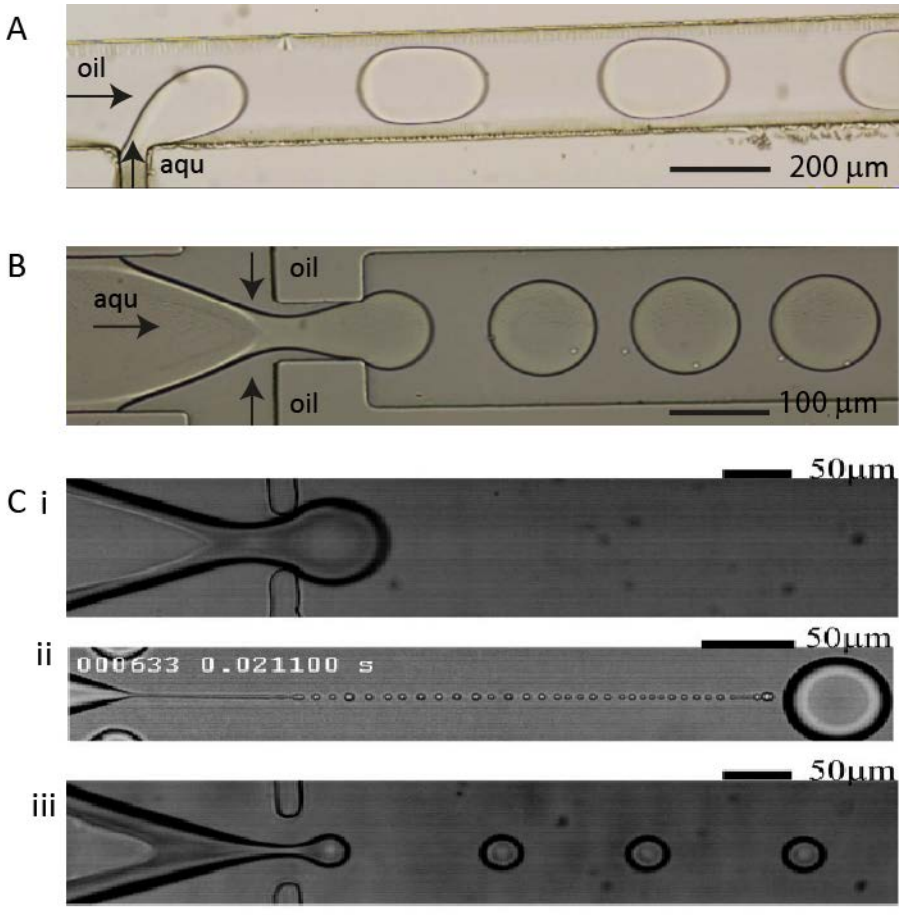

Figure 1.2 Different drop-makers. (A) A T-junction geometry where the aqueous phase (aqu) is injected into an oil career phase. (B) Flow focussing geometry requires two opposing oil streams in between which the aqueous phase (aqu) is injected to form droplets. (C) Different droplet breakup regimes (i) squeezing (ii) thread forming (iii) dripping. Reprinted from (Lee et al., 2009) with permission from *American Institute of Physics*. Scale bars are as indicated.

1.3 Applications of microfluidics in biology

Most cell-based assays are performed in conventional tissue culture plastic dishes and microtiter plates. There are established protocols refined since 1912 (Carrel, 1912), for assaying cells including primary and stem cells in these conventional methods. There is also abundant literature for 3D culturing of mammalian cells (like stem cells) which is physiological and mimics the *in vivo* complexity (Lee et al., 2008). With advances in tissue engineering, the possibilities of generating tissue scaffolds *in vitro* have also been demonstrated (Chung and Burdick, 2008; Lee and Mooney, 2001). However, there are limitations to these well-established methods. One of which is that it is not possible to mimic dynamic mechanical forces such as shear force in blood vessels, peristalsis in the gut, tension in skin, breathing in lungs etc., that naturally exist *in vivo* (Ingber, 2006). These factors are important for both developmental studies and to recreate organs that can serve for therapy or as disease models. In this context, microfluidic technology can circumvent the limitations of conventional methods. Some recent advances in the technology have extended the use far beyond cell culturing ((Chiu et al., 2000) and ibidi® flow chambers) to recreate organs (Organ-on-a-chip) (Huh et al., 2010). Together with the aforementioned physical properties of microfluidics, mechanical functionalities like valves, pumps and actuators can be used to imitate the dynamic environment that exists in vascular and musculoskeletal systems. For instance, Huh et al. used programmed pumps and vacuum to produce cyclic stretching of the tissue-tissue interface thereby mimicking breathing (Figure 1.3A). By this they were able to reconstitute key structural, functional and mechanical properties of the human alveolar-capillary interface which is the functional unit of a living lung (Huh et al., 2010). They even demonstrated the usability of the Lung-on-a-chip as a pulmonary disease model (Huh et al., 2012).

Microfluidic systems further allow mimicking complex biochemistry and geometries of the extra-cellular matrix (ECM) that exists in the *in vivo* niche micro-environment which is not possible in conventional plastic plates (Gobaa et al., 2011; Marx, 2013). Sustaining the niche environment is a critical parameter for sensitive cells like stem cells. This is because they rely on the cues received from the ECM for their cell fate decisions (Hattori et al., 2011). The biocompatible materials used for fabricating microfluidic devices are modifiable with regard to stiffness, elasticity and topography to suit different ECMs. Engler and co-workers found that varying the stiffness and elasticity of the substrate can define cell fate of mesenchymal stem cells (MSC):

soft matrices mimic the brain and lead to neuronal differentiation, stiffer matrices mimic muscles and form myogenic cells and more rigid matrices mimic collagenous bones and give rise to osteogenic fate (Engler et al., 2006). In another study microvalves were used to regulate oxygen concentrations in MSC cultures to mimic hypoxic conditions (Csete, 2005).

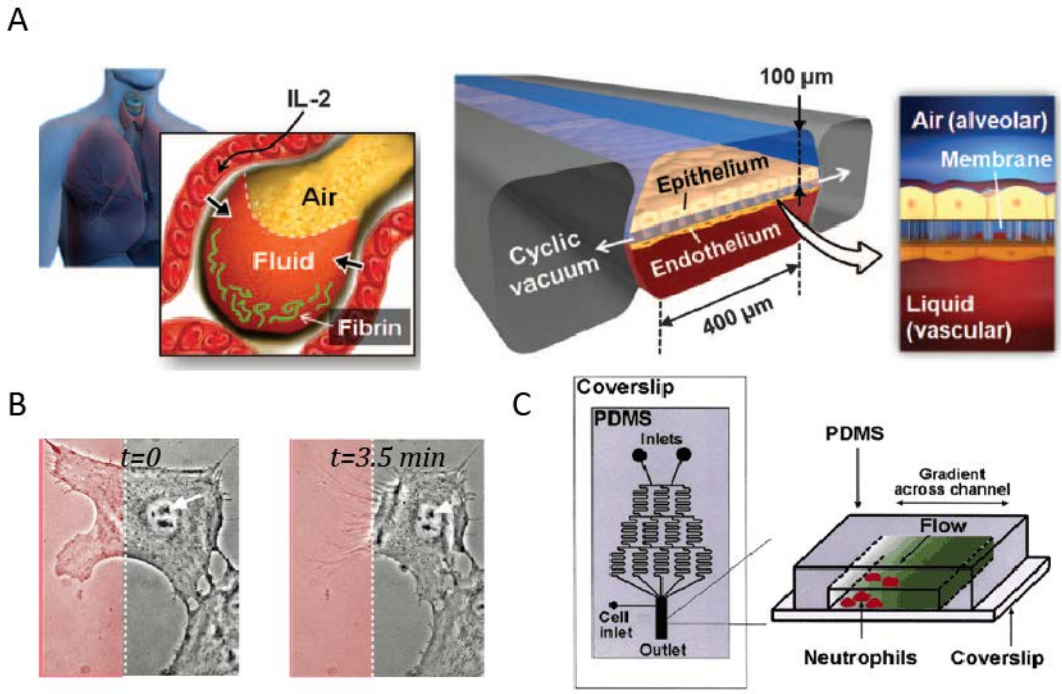

Figure 1.3 Applications of single-phase microfluidics. (A) Lung-on-a-chip as described by Huh and co-workers (Huh et al., 2012). The central channel is divided by a porous PDMS membrane over which epithelial cells are spread on one side and endothelial cells are on the other. A vacuum is created in the two side channels periodically that stretch the membrane, mimicking the breathing motion of the lung. Reprinted from (Huh et al., 2012) with permission from *American Association for the Advancement of Science* (B) Sub-cellular partitioning using laminar flow as shown by Takayama et al. Reprinted from (Takayama et al., 2003) with permission from Elsevier. The red stream contains trypsin to which the cell responds within 3.5 minutes. (C) A chemotaxis experiment using a gradient generator PDMS device. Jeon et al. exposed neutrophils to a linear gradient of IL-8 to study the chemotactic response. Reprinted from (Jeon et al., 2002) with permission from *Nature Publishing Group*.

Other important biological assays that greatly benefit from the physics of microfluidics are localized perturbation and chemotaxis assays. With the spatial resolution that is possible to achieve using microfluidics, a single cell can be partitioned by laminar flow and locally exposed to a different chemical (Figure 1.3B) (Takayama et al., 2001; Takayama et al., 2003). Developing embryos of *Drosophila melanogaster* (Lucchetta et al., 2005), *Arabidopsis thaliana* (Meier et al., 2010) etc. could also be spatially and temporally divided and exposed to different factors. These

methods were used to study developmental changes and cell-cell communication by local perturbations in intact embryos. The ability to generate laminar flows and using them to generate gradients are attractive assets for chemotaxis studies on cells (Jeon et al., 2002) and organisms (Albrecht and Bargmann, 2011). For example, Jeon et al. cultured neutrophils in a microfluidic chamber and exposed them to different chemokine interleukin-8 (IL-8) gradients to show the attraction of neutrophils to the chemokine (Figure 1.3C) (Jeon et al., 2002).

So far applications of single-phase microfluidic systems were discussed. Droplet-based systems offer different advantages for biology. These systems are generally used when compartmentalization is necessary, for example in library or secretome screens which are generally done in microtiter plates. Although single-phase microfluidic systems have been proposed for screening, they are limited by the number of chambers or unique spots that can be fitted in a 2D array (Hung et al., 2005; Upadhyaya and Selvaganapathy, 2010). Droplets have the benefit of high-throughput: monodispersed droplets can be produced at kilohertz frequencies (Park et al., 2011). Every droplet is comparable to a well in a microtiterplate in terms of the uniqueness of the samples it can contain. Furthermore, droplet-based microfluidics enable up to 10^8 droplets to be screened in one day (Guo et al., 2012) and require fewer cells (down to 1 cell per droplet) than microtiter plates (~10,000 cells per well). Owing to these advantages, not only has droplet microfluidics provided convenient automated solutions of producing uniform hydrogel 3D cultures such as embryoid bodies (EBs) with pluripotent stem cells (Serra et al., 2011; Wilson and McDevitt, 2013), but also a promising replacement to conventional microtiter plate assays using robots.

To imitate pipetting steps, there are several approaches developed with microfluidics such as: droplet adding (Abate et al., 2010) and splitting (Christopher et al., 2009). These droplet manipulations (Figure 1.4) are achieved by using unique geometries, physical properties and external elements like valves and electrodes (Ahn et al., 2006; Song et al., 2003). Additionally downstream processing such as sorting of desired assay droplets can also be automated within the microfluidic device (Baret et al., 2009). This is possible because of the dielectric properties (DEP) of the aqueous phase. Sorting of desired droplets can be achieved by coupling an electrode to the detector unit which allows the detector to send a trigger feedback to the electrode upon detection of a desired droplet. Subsequently the electric field is switched on thus

pulling the selected droplet into the collection channel, while all other droplets end up in the waste channel.

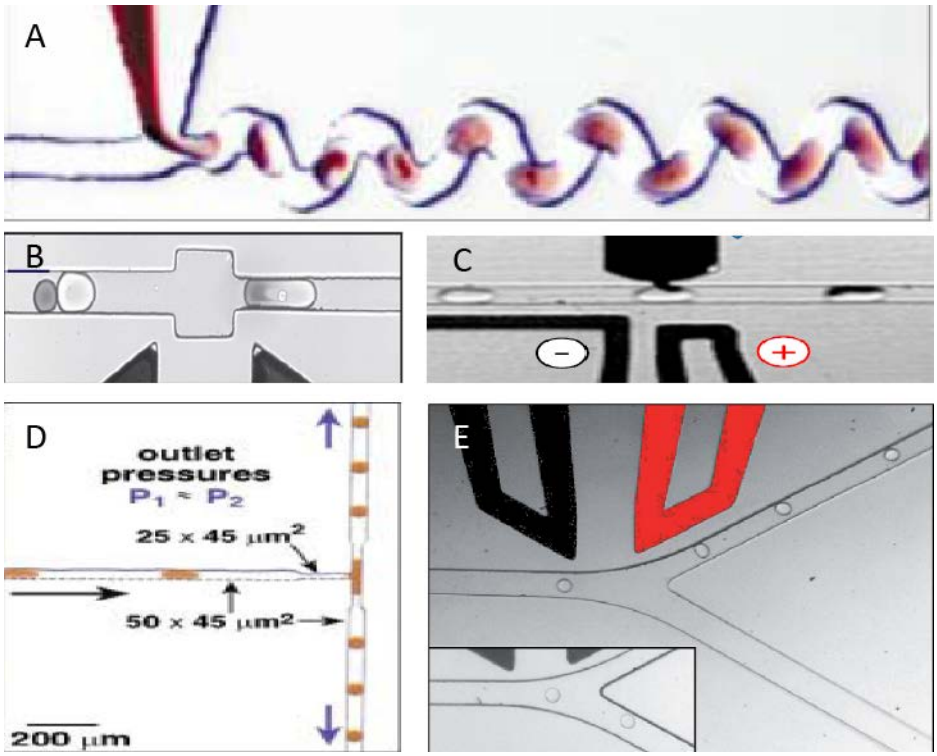

Figure 1.4 Different droplet manipulations. (A) Rapid mixing inside droplet. This mixing happens by chaotic advection that is enhanced by the serpentine channel geometry. Reprinted from (Song et al., 2003) with permission from John Wiley and Sons. (B) Fusing two droplets using an electric field generated by programmable electrodes. (C) Adding reagents to droplets using a picoinjector. Reprinted from (Abate et al., 2010) with permission from *Proceedings of the National Academy of Sciences*. (D) Splitting of a droplet into two, using withdrawal pressures as indicated. Reprinted from (Song et al., 2003) with permission from John Wiley and Sons. (E) Sorting droplets at a Y shaped junction using DEP. Reprinted from (Baret et al., 2009) with permission from *Royal Society of Chemistry*.

All these capabilities with droplets have allowed assaying biological samples (Agresti et al., 2010). However, for screening chemical compounds, there is an additional requirement for droplet barcoding in order to know which chemical is encapsulated in which droplet. Unlike microtiter wells that are spatially positioned, droplets (of picoliter volume) are prone to shuffling. The use of fluorescent barcodes (Han et al., 2001) can circumvent the issue but is restricted to the detectable differences in spectral windows. Nonetheless, the possibility to form “plugs”, which are larger droplets that fill the entire cross section of the channel, can overcome

the above problems by serving as a spatial barcoding method (Figure 1.5). Reports of screens using this strategy have already been proposed (Cao et al., 2012; Clausell-Tormos et al., 2010; Zeng et al., 2009; Zheng and Ismagilov, 2005).

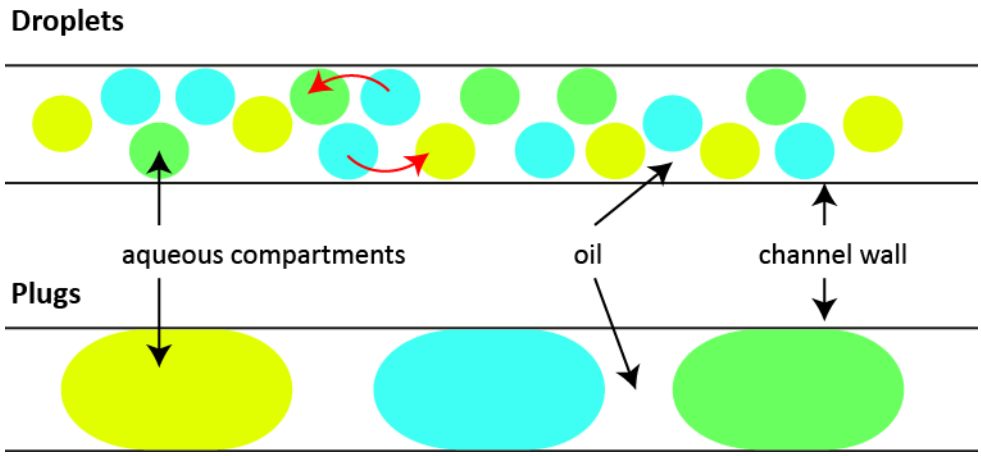

Figure 1.5 Droplets and plugs. Droplets are surfactant stabilized aqueous microcompartments that are smaller than the channel and hence can shuffle (as indicated by the red arrows), whereas plugs are unstabilized microcompartments that fill the entire cross-section of the channel and cannot be shuffled inside a channel.

1.4 Large scale integration in Lab-on-a-chip platforms

Large scale integration and parallelization of several procedures using multiple reagents can be made possible using micromechanical valves in microfluidic devices (Thorsen et al., 2002). A valve in microfluidic channels is used to control and direct flow through channel networks. Different micromechanical valves have been proposed as reviewed by Au and co-workers (Au et al., 2011). One of the most commonly used microvalve method was described by Stephen Quake's lab (Unger et al., 2000). This pneumatic valve requires a bilayer chip where the upper layer is comprised of a channel network filled with air and the lower layer has the liquid channels that need to be controlled. The liquid channel can be selectively closed off by increasing air pressure in the channels above. Thereby flow can be regulated in the microfluidic channels.

The use of valves make it possible to have highly complex, integrated designs, with several functionalities stitched together, just like how digital electronics made it possible to have more complex microprocessor designs. These valves can be computer controlled and have been used in applications like protein crystallography (Hansen et al., 2006), genetic analysis (Liu et al.,

2003), amino acid analysis (Skelley et al., 2005), chemical synthesis (Lee et al., 2005; Wang et al., 2006) and single cell analysis (Marcus et al., 2006). Figure 1.6 shows one such integrated microfluidic device for cDNA synthesis, where 50 reactions can be performed simultaneously. These large scale integrated devices are promising tools to automate complete protocols from adding reagents to analyzing, while supporting the advantages of small volume reactions.

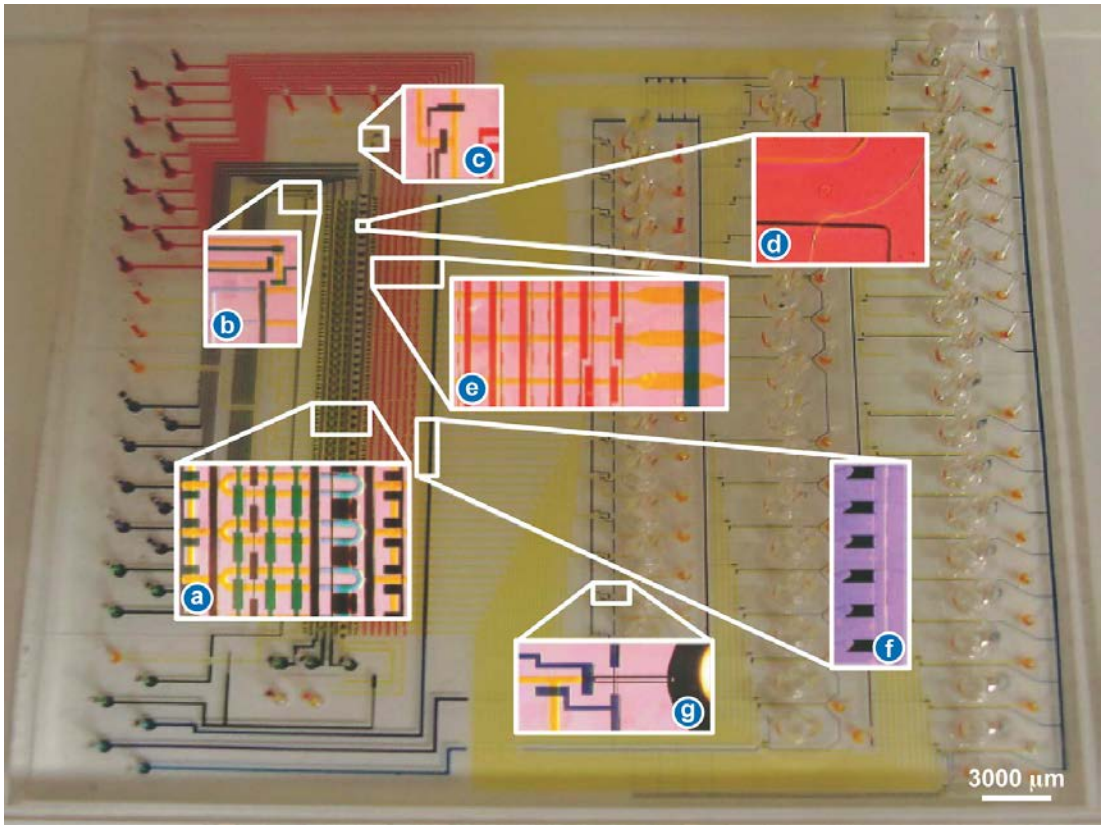

Figure 1.6 A 50-plex cDNA synthesis device. All flow channels are filled with a yellow dye, multiplexer control channels are filled with a red dye, and waste and control collection channels are filled with a blue dye. The device has seven functionalities integrated in a single device. (a) Cell lysis module. Cells are portioned in the flow channels filled with blue dye. The pump valves are in green. (b) Buffer inlets. (c) Bead and lysis inlets. Beads enter through one inlet and lysis buffer pushes residual beads into the sieve valves through the other inlet. (d) Capturing module. (e) Multiplexer control channels and sieve valve channel. (f) Six stacked bead columns. (g) Outlet and collection module with outlet and waste valves, as well as a portion of the collection port (Marcus, 2006).

Aim & Outline

This main aim of this thesis is to develop novel microfluidic approaches based on single- and multi-phase systems for monitoring responsiveness of cells (including rare cells like stem cells) and organisms to different chemical cues. The chapters are divided based on the type of microfluidics used (single or multi-phase). Every chapter contains an individual introduction to the corresponding subject, motivation to the work and a discussion of the results with some possible future experiments. Briefly, in **Chapter 2: "Ocean on a chip: Quantifying preferences and responsiveness of marine zooplankton to changing environmental conditions"** a specially designed single-phase microfluidic device is used to monitor the ecological preferences of marine zooplankton. For the first time, the possibility to quantitatively determine the ecological preferendum of these marine organisms is reported. This is especially relevant in the current situation of rapid global environmental changes because the system allows identifying species sensitive and resilient to environmental changes. In **Chapter 3: "Generating combinatorial mixtures in droplets to assay stem cell niche"** a novel multi-phase microfluidic approach for screening entire libraries of molecules both individually and in combination is discussed. Furthermore, this novel approach is optimized to screen for optimal directed differentiation conditions for stem cells. Thus, this chapter is not only about the development of a novel combinatorial screening platform but also shows, for the first time, the usability of microfluidics for high-throughput screening (HTS) with mouse embryonic stem cells. Finally, **Chapter 4: "Soft-compartmentalization: Combining droplet-based microfluidics with freely accessible cells"** is a brief report on a new method combining single-phase with multi-phase systems for high content screening of adherent mammalian cells. A **General Conclusion** then connects the individual chapter discussions and gives an outlook on future perspectives.

Chapter 2

Ocean on a chip: Quantifying preferences and responsiveness of marine zooplankton to changing environmental conditions

2 Introduction

Laminar flows in microfluidics have been favorably used for several chemotaxis experiments of both single cells (Takayama et al., 2003) and the organism *Caenorhabditis elegans* (Albrecht and Bargmann, 2011). In light of fast worldwide climate changes, this ground work is extended by presenting the first study that uses microfluidics to analyze the response of zooplankton, both from established lab cultures and fresh marine field isolates, to environmental conditions. First, quantitative measurements on the ecological preferences of zooplankton in terms of pH, salinity and food are reported here. In addition, the possibility to use microfluidics for functional studies is demonstrated.

2.1 Plankton and their significance

Plankton are microscopic, freely drifting, aquatic organisms that constitute 75 % of the ocean biomass. They are composed of phyto- and zooplankton aside bacteria and viruses. Phytoplankton are the “plants of the sea” and hence are the photosynthesizing primary producers. Zooplankton (animal plankton) can be either secondary or tertiary producers and can be holozooplankton (remain as plankton throughout their life cycle), or meroplankton (transform into benthos or nekton) (Rawlinson et al., 2004). Zooplankton graze on phototrophic phytoplankton and in turn provide them with the nitrogen required for their growth, thus maintaining a symbiotic relationship. On the whole, being the energy producers of the ocean, plankton form the base of the food web and all higher organisms (from small fishes to whales), in essence, rely on plankton for their survival.

Interestingly, unlike the terrestrial ecosystem, where the largest animals such as ungulates are herbivores (feeding solely on plants), the largest animals in the marine ecosystem are carnivores and especially baleen whales are known to feed mainly on zooplankton (Kann and Wishner, 1995). In fact there is no similarly large herbivore in the ocean, presumably because of the size of the primary producers (phytoplankton) being too small for efficient grazing. Furthermore, zooplankton also support the microbial community of the ocean (Ruhl and Smith, 2004): marine microbes colonize faecal pellets and carcasses of zooplankton which are rich sources of organic carbon. These zooplankton products also rain down on the seabed sustaining diverse benthic communities of sponges, echinoderms, anemones, crabs and fishes.

In addition to zooplankton playing a crucial role in the food web, they are also known to sink atmospheric carbon dioxide which is necessary to maintain a balance in the planet's atmosphere (Siegenthaler and Sarmiento, 1993). Phytoplankton sequesters the CO_2, uses it for photosynthesizing; and releases oxygen just as land plants. When phytoplankton are consumed by zooplankton the carbon is transferred and deposited on the seabed through their excreta. In addition dying plankton sink the carbon in the oceans. Figure 2.1 is an illustration of the carbon cycle in the ocean. Globally, plankton transfers more than a hundred million tonnes of carbon in the form of CO_2 from the atmosphere to the deep ocean each day (Behrenfeld et al., 2006). Even small changes in the growth of phytoplankton may reflect on atmospheric carbon dioxide concentrations, which in turn would affect global surface temperatures. Thus, plankton contribute to maintaining the ocean ecosystem and balancing the earth's climate which ultimately profits the human society by providing food through fishery, and by providing a habitable planet.

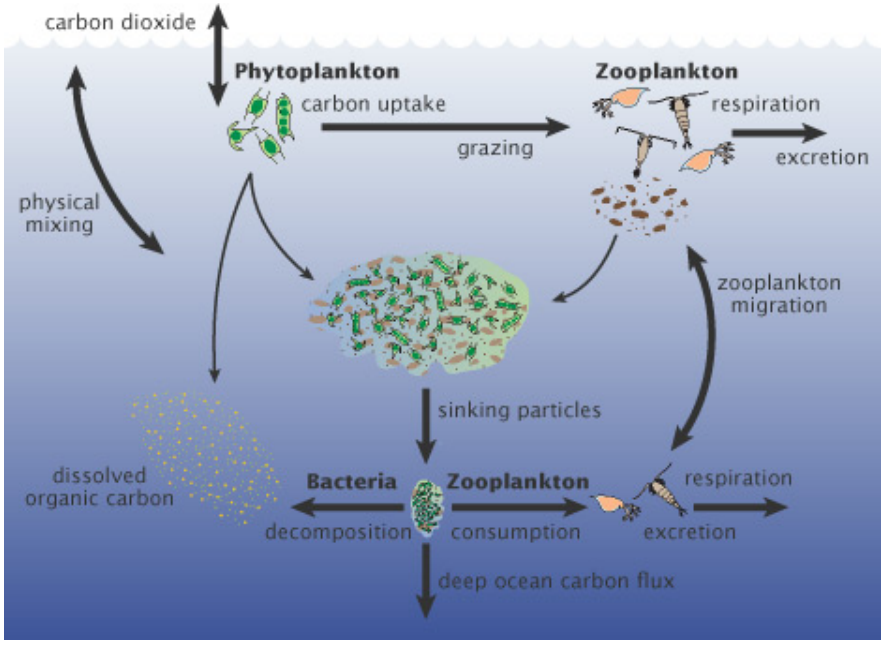

Figure 2.1 Ocean carbon cycle. Atmospheric carbon dioxide is fixed by phytoplankton during photosynthesis. When zooplankton graze on phytoplankton, this carbon is transferred and finally accumulates in the deep oceans through the excreta of zooplankton or the decomposition of their carcasses. Reprinted from (Lindsey and Scott, 2010), NASA Earth Observatory.

2.2 Impact of global climate changes on the oceans and plankton

Since the industrial revolution in the 18th century, 3.67 trillion tonnes of anthropogenic CO_2 have been released into the atmosphere (Allen et al., 2009) mainly from the burning of fossil fuels (Marland et al., 1999) and due to deforestation, urbanization and other land-use practices (Houghton et al., 2001). This has caused many changes in the environment including an overall 2 ^{o}C raise in surface temperatures because of the CO_2 mediated greenhouse effect, and acid precipitation because of the excessive CO_2 in the atmosphere. It is evident from the bleaching of coral reefs that all these environmental changes are affecting the marine ecosystem (Figure 2.2) (Anthony et al., 2008; Hoegh-Guldberg et al., 2007). Furthermore, oceans have absorbed a third of the CO_2 released from human activity since 1800 and it is predicted that, by the year 2100, the oceans' capacity to sink atmospheric CO_2 will reduce by 14 % compared to if there was no climate change (Matebr and Hirst, 1999). It is also predicted that with the current amounts of CO_2 emission, the pH of the ocean will drop (acidification) from pH 8.2 (pre-industrialization period) to ~pH 7.9 which is an almost 30 % increase in H^+ ion concentrations (Caldeira and Wickett, 2003, 2005; Fabry et al., 2008). This ocean acidification, coupled with the reducing ability of oceans to sink CO_2 resulting in increasing surface temperatures, does have both direct and indirect implication on the marine ecosystem (Doney et al., 2012; Hoegh-Guldberg and Bruno, 2010).

This chapter focusses on the effect of environmental changes on plankton because of their pivotal role in the food web (Figure 2.2, section 2.1). In addition, plankton are considered sensitive beacons of climate changes because the non-linear response of plankton communities can amplify even subtle environmental changes (Taylor et al., 2002). On the one hand this highlights the benefit of using plankton to assess the impact of global environmental changes to the ecosystem, on the other hand it also underscores the urgent need to understand and, in the best case, predict the drastic response that might occur with the present rapid pace of climate changes. Despite the critical necessity, our current knowledge on how these changes are affecting the microscopic plankton community is still rudimentary. It is known that the acidification is already affecting zooplankton with calcareous skeletons (Beare et al., 2013) but knowing how the plankton community is coping with these adversities is necessary to take precautions.

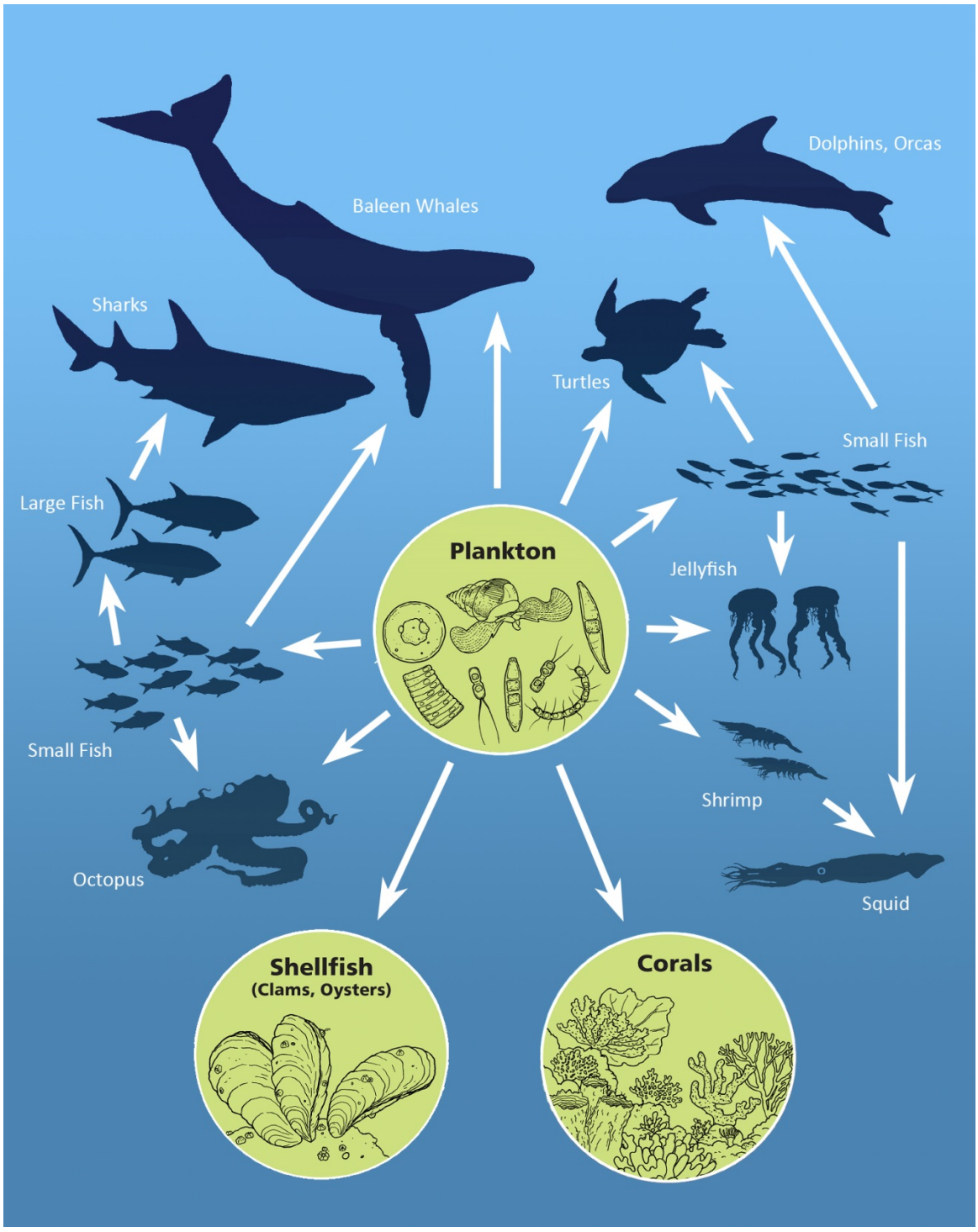

Figure 2.2 Impact of ocean acidification on the marine ecosystem. Plankton form the base of the food web and are the energy producers of the ocean. They, along with other organisms in green circles are already being affected by acidification.

2.3 Existing methods

Most investigations of the effect of global environmental changes on planktonic organisms are based on case studies. These studies provide information on the current status and the trend over a certain past period. Much of our understandings arise from such documents and the majority of these studies use the Continuous Plankton Recorder (CPR) data sets (Warner and Hays, 1994). These CPR data sets are generated by periodic sampling at different locations using plankton tows and are valuable resources for researchers to evaluate the long-term impact of climate changes (Beare et al., 2013). For example, Edwards and Richardson used the CPR data set to infer that there was substantial phenological (timing of repeated seasonal activities like migration and reproduction) changes observed over a 45 year period (1958 - 2002) in the central North Sea (Edwards and Richardson, 2004). These case studies give insights on the abundance of plankton and the variations that has occurred in the past, however they do not allow making reliable predictions on future implications, especially considering the fact that the response of plankton to environmental changes is non-linear (Taylor et al., 2002).

In other experimental studies, layered water in “mesocosm” was used to study the effect of drop in pH on plankton (Riebesell et al., 2013). Mesocosms are experimental water enclosures in the ocean. Similar methods to stratify water in 40 m^3 boxes (Poulet and Ouellet, 1982) or 50 m^3 bags (Zhang et al., 2012) with layers containing different concentration of H^+ ions have been described. These methods allow estimating the abundance of plankton in a certain pH while retaining the ecosystem dynamics (species-species interaction); however, the method does not allow making species-specific predictions on the pH preference. Also, these layered water approaches do not maintain stable gradients with a good spatial resolution, so it is impossible to accurately quantify preferendum. Yet some other small-scale lab approaches in multi-well plates allow assessing individual plankton species at different pH conditions, but these experiments only give information on the lethal doses and tolerance of plankton in a certain condition (Yamada and Ikeda, 1999). The Y-maze approach has been previously described allowing exposing plankton trapped within a porous membrane chamber to two different conditions in a ‘Y’ shaped tube with two inlets. This approach facilitates binary preference measurements, however, in the ocean there exists a certain degree of pH variations and what is required to know is the “preferendum” or a preferred window of concentrations of a certain parameter. And

this cannot be achieved using a Y-maze because of the inability to expose plankton to more than two conditions in this approach.

Furthermore, for plankton species that are able to actively choose their environment, a more precise measure of their preference would be a quantification based on their behavior and not simply based on the count. None of the existing methods allow this possibility. Hence, an assay system that allows exposing plankton species to several different conditions simultaneously, while allowing the possibility to monitor their behavioral preferences is urgently needed. Also, this system should have a spatial resolution that can dissect a small area into different conditions to allow these microscopic organisms to detect the existence of neighboring conditions.

2.4 Need for microfluidics

The possibility to generate laminar flows in microfluidics allows liquid streams to flow parallel to each other without convective mixing. This ability has been used to not only expose adherent cells to different conditions, but also has allowed chemotaxis and behavior studies on actively moving *C. elegans* (Albrecht and Bargmann, 2011; Larsch et al., 2013). Figure 2.3 shows an experiment where *C. elegans* actively choose their preference when exposed to different chemokines.

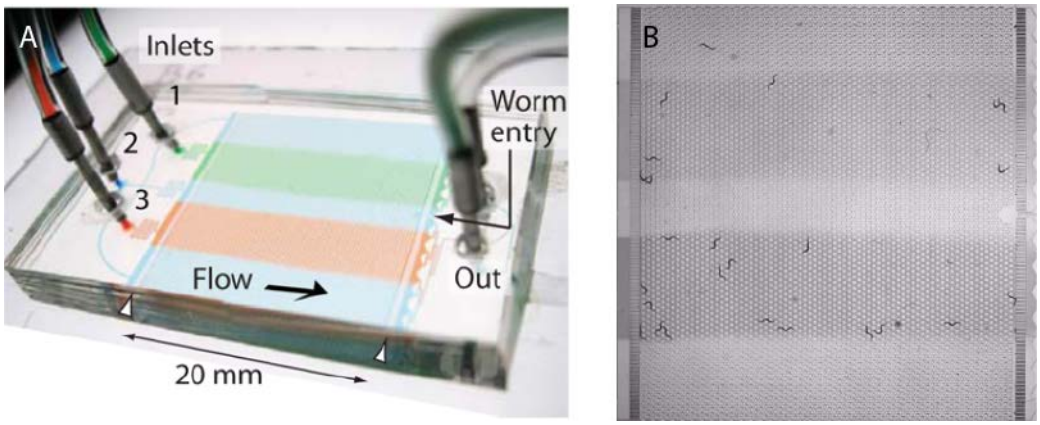

Figure 2.3 *C. elegans* exposed to different chemokine using laminar flow principle in microfluidics. (A) Microfluidic device with three inlets for three different chemokines (blue, green and red). (B) End of an experiment where *C. elegans* accumulated in its preferred streams. Reprinted from (Albrecht and Bargmann, 2011) with permission from *Nature Publishing Group*.

The spatial resolution and small dimensions of microfluidic could be a suitable platform to assess the behavioral preference of actively swimming plankton species. Roman Stocker´s lab at the Massachusetts Institute of Technology has used microfluidics to perform extensive ecological studies on marine bacteria and phytoplankton (Mayola et al., 2014; Seymour et al., 2010; Tout et al., 2015). However, the methods have not been applied for zooplankton.

2.5 Why focus on zooplankton?

Plankton play a central role in the marine food web. However zooplankton are more adversely affected than phytoplankton to changes in environmental conditions because of a couple of reasons. Firstly, most zooplankton are poikilothermic (organisms whose internal temperature varies considerably) and hence their physiological processes such as ingestion, respiration, reproduction are highly sensitive to ambient temperatures (Blaxter et al., 1998). Secondly, most zooplankton species are not only short-lived (< 1 year) but also their life-cycle is tightly coupled with the seasonal changes (Hays et al., 2005). Hence, any small climatic changes can greatly influence zooplankton population dynamics. Moreover, meroplankton, that only live a part of their life as plankton, were found to be more affected by subtle climate changes than their holozooplanktonic neighbors (Edwards and Richardson, 2004). In this work, a meroplankton, *Platynereis dumerilii* was used as a model species to test the preference to changing environmental conditions. The life cycle of *P. dumerilii* as illustrated in Figure 2.4 has planktonic (from 24 hours post fertilization (hpf) to 5 days post fertilization (dpf)) and benthic stages (from about 6 dpf).

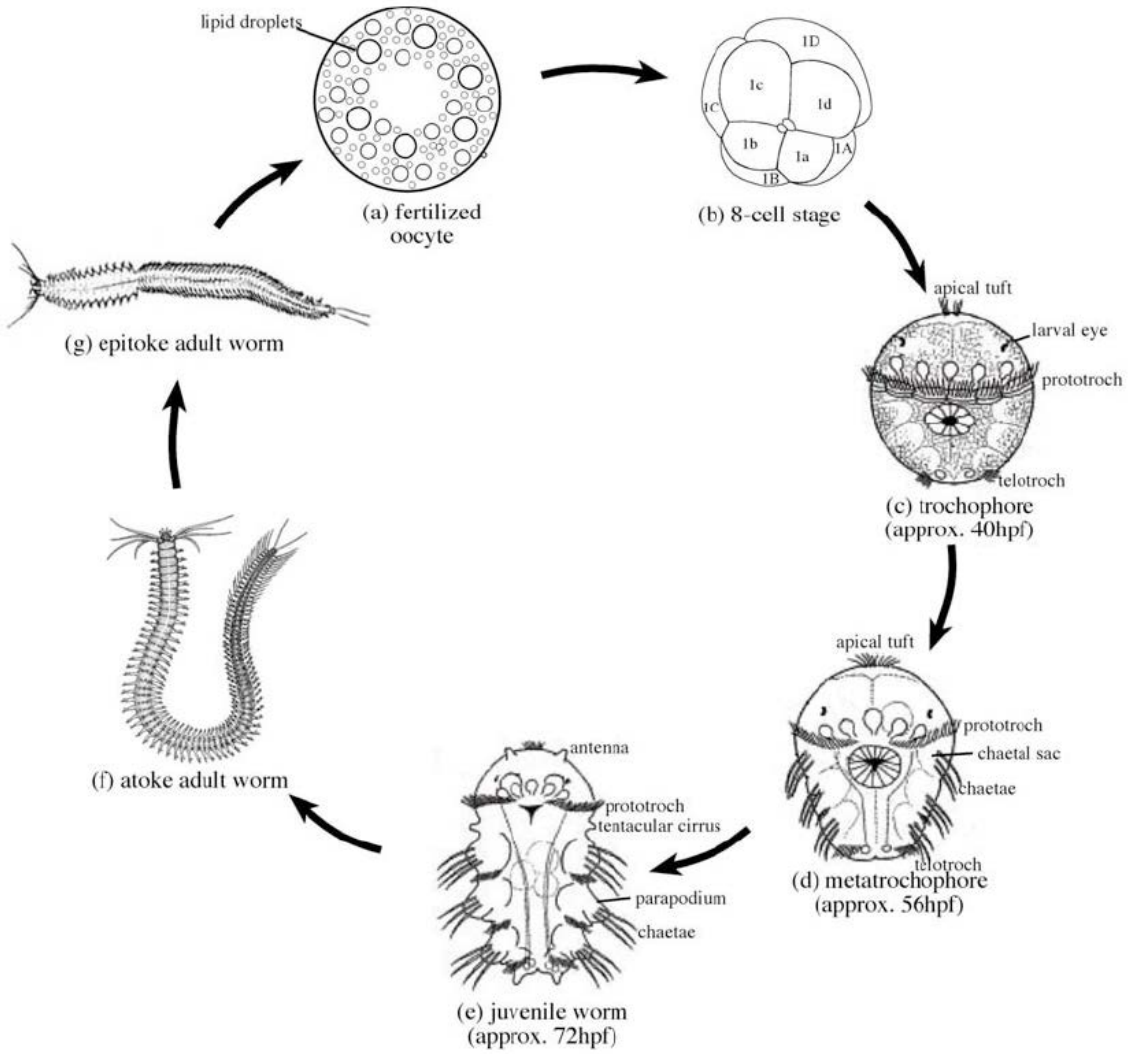

Figure 2.4 Life cycle of *P. dumerilii,* a meroplankton. The larvae from 24 hpf to around 6 dpf, are planktonic or freely swimming on the surface of the oceans, and during the later stages they transform into benthic habitat where they are crawling in the sea bed. The morphological changes that happen during different metamorphosing stages, help them in adapting to their respective habitats. Adapted from (Fischer and Dorresteijn, 2004) with permission from John Wiley and Sons.

2 Results

2.6 Tracking behavioral response of zooplankton in microfluidic devices

Two microfluidic devices were specifically designed for assaying zooplankton. The first device is for generating laminar flows. This device contains ten inlets for infusing chemically distinct conditions. Figure 2.5A-C shows the generation of ten laminar flow streams in a 4 x 4 mm chamber of the device with the larvae of *P. dumerilii*. A blue dye was used in every alternate stream for visualization. Every stream is 400 µm wide and the larvae are approx. 150 to 300 µm in length depending on the metamorphosing stage. A couple of larvae were able to crowd and stack themselves in one stream as visible in Figure 2.5C. The second device is for generating on-chip linear gradients. A "Christmas tree" gradient generator design proposed elsewhere (Jeon et al., 2000) is adapted for this purpose. Figure 2.5D-E shows the generation of a linear gradient in a 9 x 4 mm chamber. The volume that can be contained in each chamber is roughly 4 mm^3 and typically fifteen to twenty larvae were able to freely swim in one chamber all together.

For experiments, 5 dpf planktonic larvae and 9 dpf benthic larvae of *P. dumerilii* were used. The larvae were manually loaded into the chamber and were able to freely move within the chamber dimensions. Figure 2.5F shows the default distribution of the larvae when all streams contain natural sea water. Using automated tracking software, several individual and population specific behaviors were identified such as: the overall speed, (v), stream transition speed (v_{trans}), turning angle per second (θ), the average time of movement (τ_{mov}), number of individuals present in a stream over time ($d_{(x,t)}$), the overall distribution over time and the resulting stable distribution that is reached after an adaptation time (Figure 2.5A). These newly described, actively swimming zooplankton specific, behavioural parameters were used to evaluate the preferendum of these marine organisms.

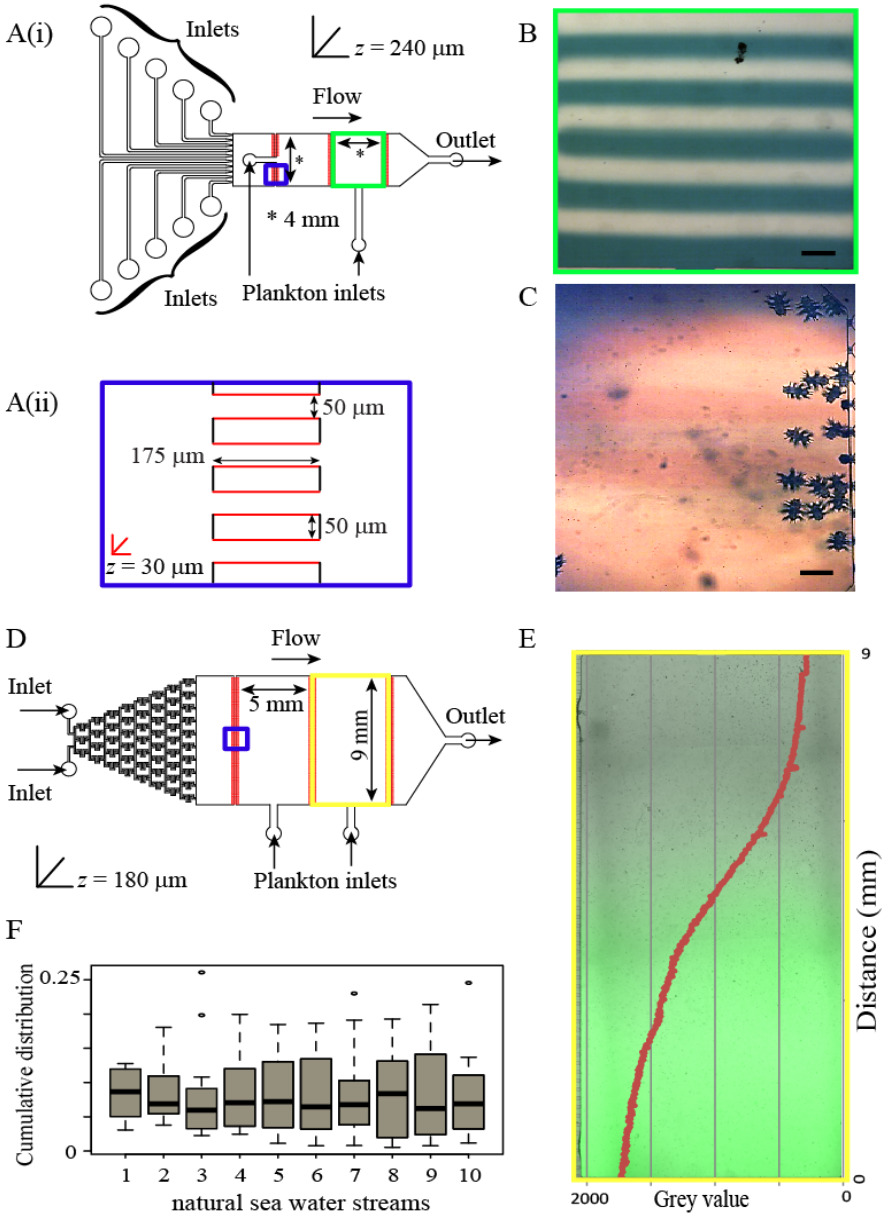

Figure 2.5 Microfluidic device geometry, flow profile and normal behaviour of *P.dumerilii* in the device. (A) Laminar flow device with ten inlets. A(i) The device has two 4 x 4 mm chambers that are 240 µm high and connected by shallow channels that are 30 µm in height as shown in A (ii). The two layer geometry is to prevent plankton from being flushed out of the device while allowing liquid flow. (B) Laminar flow profile as seen in one of the chambers of the device. A blue dye is used in every alternate stream for visualization. (C) *P. dumerilii* larvae (5 dpf) being exposed to streams containing natural sea water (NSW) with and without orange G (an acidic dye). (D) Gradient generator device with a Christmas tree gradient generator and two 9 x 4 chambers of 180 µm height. (E) Quantification of a linear fluorescein gradient produced using the device. (F) Default distribution of *P.dumerilii* in a microfluidic device while being exposed to identical, NSW conditions in all ten streams. Figures from (Ramanathan et al., submitted manuscript).

2.7 Response to pH changes

The preference of *P. dumerilii* to different pH to understand how sensitive or resilient this species is to ocean acidification was tested. When the larvae were exposed to different pH (pH 3 to 11) in the laminar flow device, different behavioral patterns could be observed depending on the location of the larvae in the chamber. In adverse pH, a 2.5 times higher stream transition speed was observed while in the preferred pH the transition speed and overall speed was lower because of the pausing behavior in these conditions. Furthermore, from experiments it was observed that animals tumble more in their preferred stream presumably because of their desire to stay in that limited region. Due to this, the turning angles were higher in these locations. However, in every experiment the stable distribution was achieved after 10 (+/- 7) seconds after the laminar flow was established Figure 2.6.

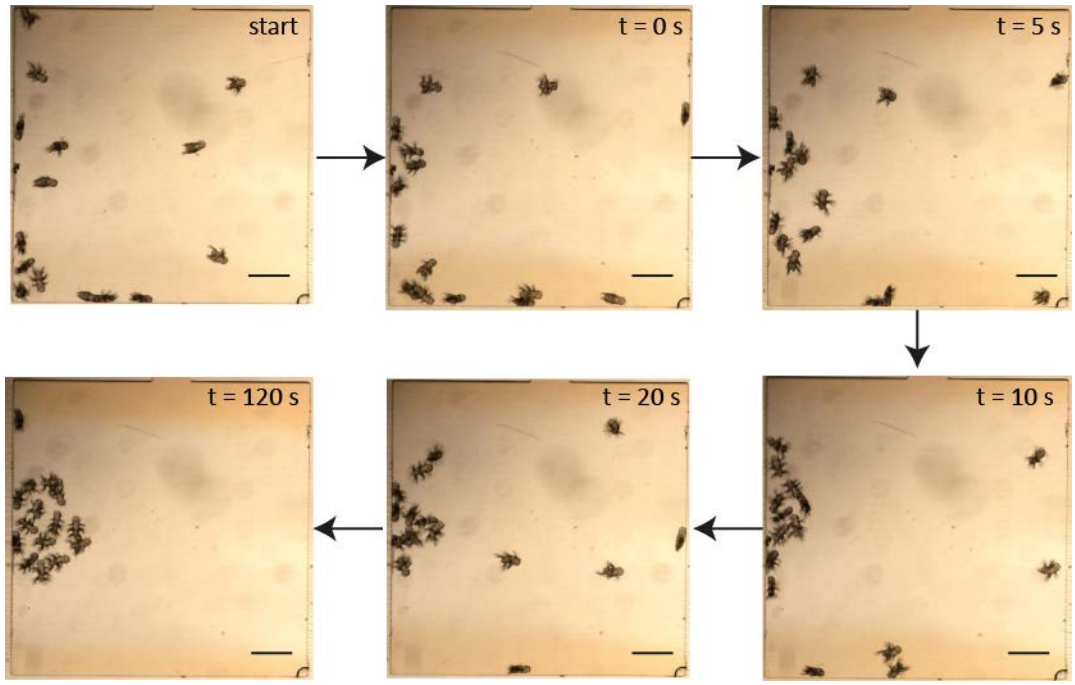

Figure 2.6 Time lapse image from an experiment exposing *P. dumerilii* larvae to different pH conditions (top to bottom: pH 3 to pH 11). pH 3 and pH 11 streams on top and bottom contain orange G as a dye to demarcate the initiation of laminar flow. Scale bars represent 400 µm.

With the cumulative distribution from ten experiments, a “comfort zone” or preferendum could be defined, which is the range of conditions for a given parameter for which the presence of specimens does not significantly deviate from the maximum recorded. This preferendum could

be further refined by taking into account the behaviour of the organism in this zone. For *P. dumerilii*, the preferendum of 5 dpf larvae was found to be between pH 6 and pH 8, and of 9 dpf larvae was between pH 5 and pH 9 (Figure 2.7). This was an unexpected, broad preferendum. Further experiments shifting the stream positions were done to confirm these results and to exclude any positional bias in the system. One of the reasons for the observed preference of *Platynereis* to acidic conditions could be because the lab cultures were originally collected in the vicinity of acid springs where *P. dumerilii* were reported to be found in very low pH (Cigliano et al., 2010).

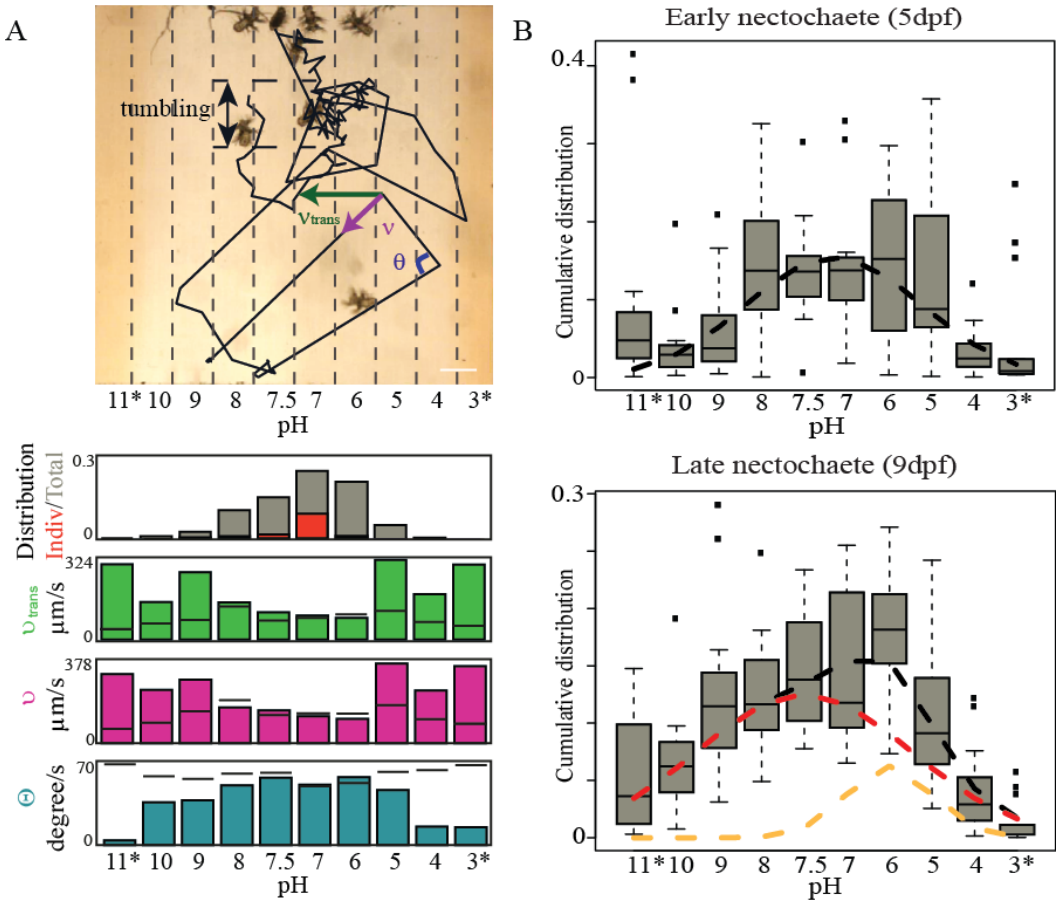

Figure 2.7 Behavioral response of *P.dumerilii* to pH changes. (A) Tracking of *P.dumerilii* inside the chamber. Stream transition speed (v_{trans}), overall speed (v) and turning angle (θ) are behavioural parameters that were assessed. From the distribution and the behaviour, the comfort zone can be evaluated. The black lines on the bar plots show the behaviour of *P. dumerilii* in a control experiment where they were exposed to only natural sea water. (B) Cumulative distribution of early (planktonic) and late (benthic) stage larvae. Black dotted line is the average of the distribution. Red dotted and orange dotted lines show two different populations. * represents streams with dye used to demarcate the initiation of laminar flow. Data from (Ramanathan et al., submitted manuscript).

In addition to the preferendum measurements, the analysis revealed that the distribution for the 9 dpf larvae fit as a bimodal distribution (Figure 2.7B) (best fitted by a mixture model of two Gaussians with a room-mean-square error (RMSE) of 49, compared to RMSE of 92 when fitting a single distribution). This means that the broadening of the preferendum was because of the existence of a sub-population that preferred more acidic conditions. These differences in preference could be because at 9 dpf the larvae transform into their benthic habitat and in the sea bed there are potentially more variations in pH than on the sea surface. So this shift in preferendum could indicate an adaptation benefit of the later stage larvae. Indeed the possibility of some genetic differences in these larvae could not be ruled out and hence further investigations are required to confirm the reasoning behind the preference for acidic conditions.

2.8 Response to salinity changes

Ocean salinity is another parameter that is being reduced because of global warming (Duplessy et al., 1992). The melting glaciers are diluting the oceans aside raising the sea levels. To estimate how this is affecting zooplankton, the gradient generator device was used to generate linear gradients of sodium chloride (NaCl). To be precise in the estimate, 5 dpf and 9 dpf *P. dumerilii* larvae were exposed to several gradient ranges: 30 to 50 g/l, 36 to 44 g/l and 38 to 42 g/l to get a good spatial resolution. By doing so, it was found that the larvae, regardless of the developmental stage, preferred more saline conditions between 34 and 42 g/l given that the surface salinity of the oceans around the world, excluding estuaries, range from 31 to 38 g/l (Reul et al., 2014). Also, *P. dumerilii* showed similar behavioral patterns to pH experiments: greater tumbling in the comfort zone and higher transition speed outside the comfort zone (Figure 2.8). However, for salinity there was no indication of any sub-populations.

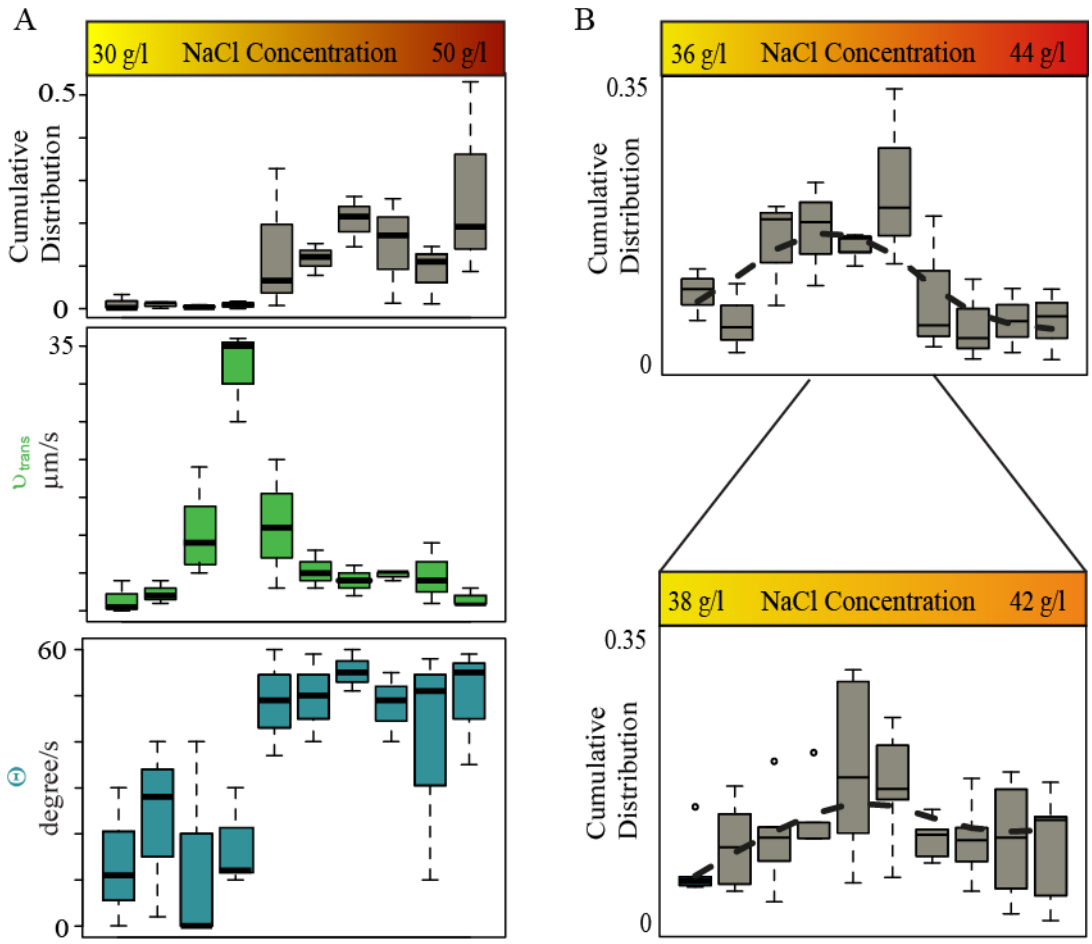

Figure 2.8 Behavioral response to salinity changes. (A) Response of *P. dumerilii* larvae exposed to an NaCl gradient (30 g/l to 50 g/l). Higher stream transition speed (v_{trans}) is observed at the edge of the comfort zone while the turning angles are higher in the comfort zone. (B) Narrowing the NaCl concentration gradient to resolve the preferendum better. This was done by consecutively narrowing the range based on the region where the highest slope in the distribution was observed. Data from (Ramanathan et al., submitted manuscript).

2.9 "Responsiveness"

The intensity of a behavioral response to a certain parameter (like pH or salinity) could reflect on the ecological importance of that parameter (Hay, 2009). This behavioral response can be quantified using the distributions from the above experiments. Mathematically, the highest slope in the distribution (inflection point) corresponds to the strongest change in behavioral response. The responsiveness is defined as the minimum change in concentration that is required to elicit a behavioral response. In order to determine this minimum molar concentration change, it is required to repeatedly zoom in into narrower concentration ranges to observe the changes in distribution until there is no significant change in the slope (Figure

2.9). For salinity changes, this was already observed in a concentration range between 36 - 44 g/l. This means that *P. dumerilii* can respond to changes in salinity as low as ~14 mM. For pH however, the changes in proton concentrations are much lower and *P. dumerilii* already responded to 1 µM change. This implies that *P. dumerilii* is much more sensitive to changes in pH than salinity.

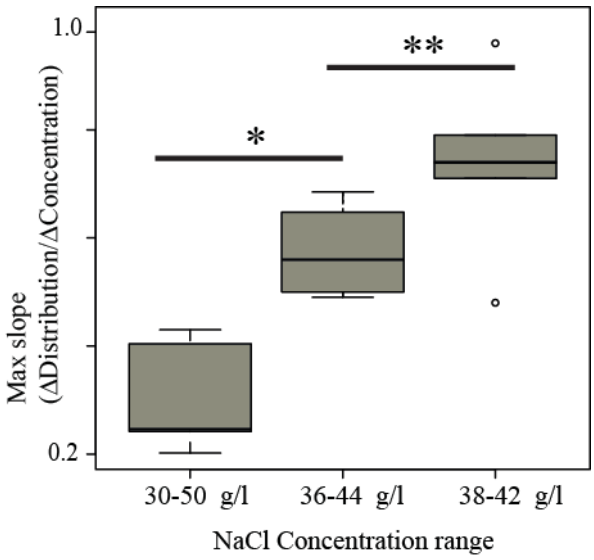

Figure 2.9 Estimating responsiveness. Boxplots show the highest slope of the distribution in different salt concentration ranges. Based on the p-values * > 0.05 and ** < 0.05 (Wilcoxon rank-sum test), the responsiveness for salinity changes is 36-44 g/l or ~14 mM change in concentration. Data from (Ramanathan et al., submitted manuscript).

2.10 Interspecies comparison

The microfluidic device described here is indeed also suitable to assess other marine plankton. To demonstrate the usability of the device for other marine plankton, the pH preference of an abundant holozooplankton: *Euterpina acutifrons* (a copepod species) was assessed. When *E. acutifrons* were exposed to different pH conditions (between pH 6 and pH 9) in the laminar flow device, they showed a much narrower preferendum than *P. dumerilii* (Figure 2.10). This could be because as a holozooplankton, *E.acutifrons* are not exposed to variations in pH in their natural environment unlike a meroplankton *P. dumerilii.* Moreover, *P. dumerilii* are known to adapt to chronic and elevated pH levels (Calosi et al., 2013). Interestingly, a similar behavioral pattern was observed for *E. acutifrons* in the microfluidic device (higher stream transition speed at the

edge of the comfort zone and higher turning angle within the comfort zone) as with *P. dumerilii* (Figure 2.10B). Experiments with several zooplankton species could give further insights on sensitive and resilient species to changing environmental condition.

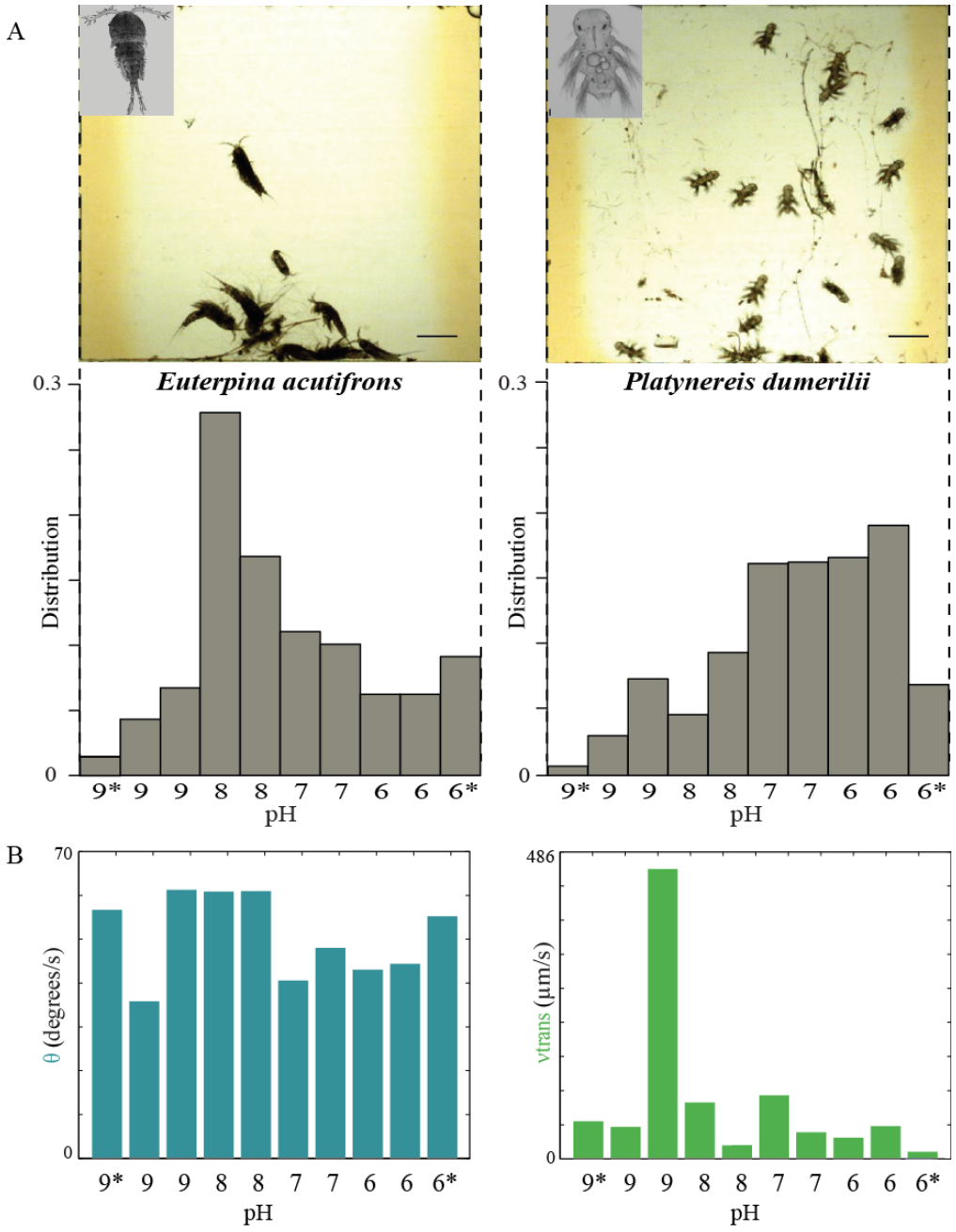

Figure 2.10 Comparing the pH preferenda of *E. acutifrons* and *P. dumerilii.* Two adjacent streams have the same pH to allow the larger *E. acutifrons* to fit in their preferred stream. (A) Distribution of the plankton in the device. (B) Variation of turning angle and stream transition speed of *E. acutifrons* in different pH. * represents streams with dye used to demarcate the initiation of laminar flow. Data from (Ramanathan et al., submitted manuscript).

2.11 Response to predator and prey (algal) smell

In addition to assessing responses to changes in environmental conditions, the response of zooplankton to predator and prey smell was also assessed. *P. dumerilii* is known to prey on different algae; however it is unclear which algae they prefer. Using the laminar flow device, 5 dpf larvae *P. dumerilii* was exposed to *Isochrysis* and *Dunaliella* microalgal extracts. The larvae showed a clear preference for *Dunaliella*. Similar experiments exposing *P. dumerilii* to water from a *Dicentrarchus labrax* (sea bass) tank was performed. *D. labrax* is one of the many predators of *P. dumerilii*. Within 2.5 minutes a stable distribution was achieved with all the larvae *of P. dumerilii* outside the stream containing the predator smell. However, the response time in this experiment was longer than in the pH experiment presumably because of the wider streams in these experiments compared to the pH experiment with ten streams which probably made the larvae unaware of the existence of a neighboring stream. Indeed, there could be other reasons to the observed delay in response such as the larvae were simply not as fast in responding to predator smell as to pH.

It is noteworthy that the experiments exposing *P. dumerilii* to predator smell was done using freshly collected field isolates from marine stations at Roscoff and Banyuls-sur-Mer. This experiment was performed to demonstrate the ability to perform microfluidic preferendum experiments in remote locations.

2.12 Identifying cell types involved in a certain sensory response

In a microfluidic device it is possible to track responses on an individual level and quantify them. This possibility can be favorably used to locate cell types responsible for sensing a certain parameter. To demonstrate this possibility, a specific cell type in the mouth region was located based on noelin expression (which is suggestive of olfactory function). When these ciliated cells in the foregut (indicated in Figure 2.11A) were ablated, a delay in the response was observed of ablated *P.dumerilii* to algal smell, in comparison to the non-ablated control individuals (Figure 2.11E). Indeed, their overall speed of movement remained the same, confirming that the delay in response was not due to physical impairments but because of the decreased ability to sense the smell. These experiments show the involvement of the ablated cells in sensing algal smell.

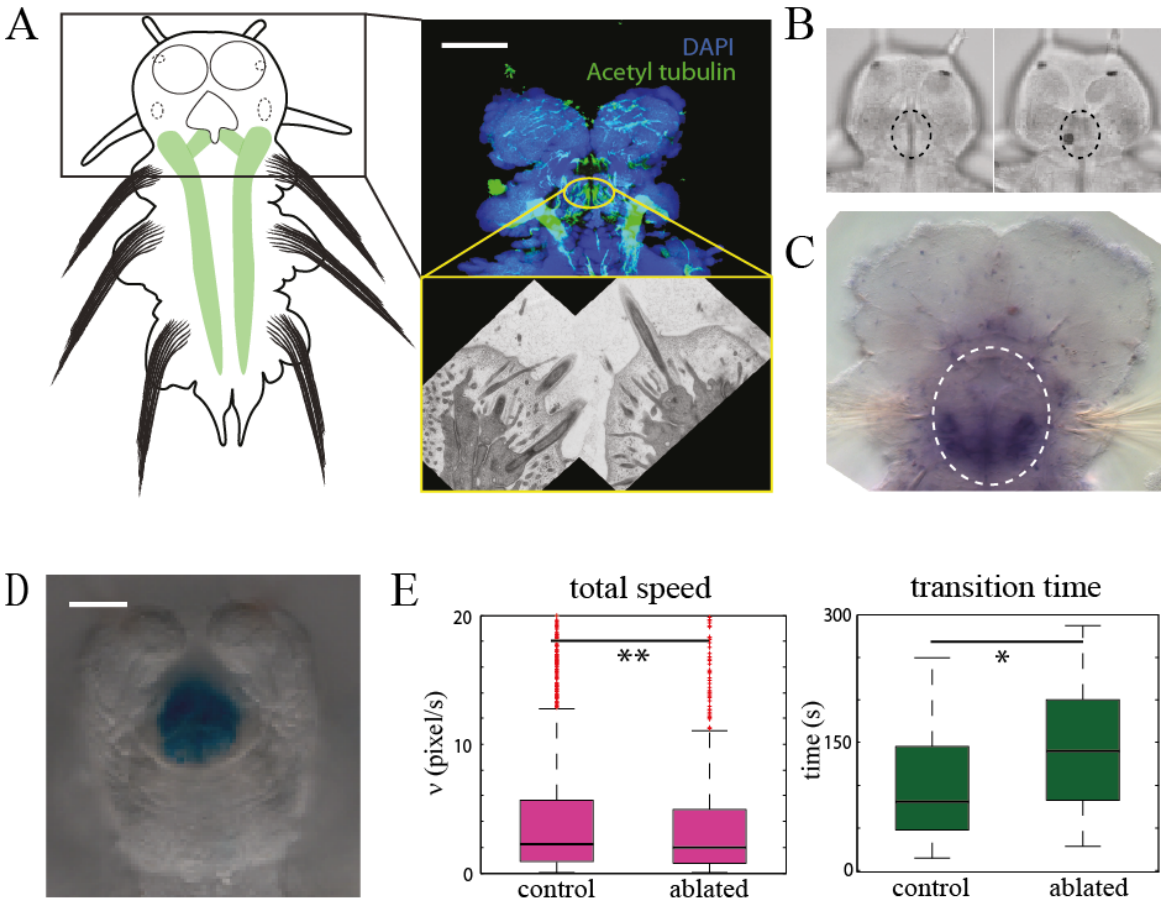

Figure 2.11 Identifying cells involved in sensing algal smell. (A) The ciliated cells in the foregut of *P. dumerilii* as visualized by confocal and transmission electron microscopy. (B) Ablation of these cells using a cold laser causes the targeted cells to disappear locally. Left image show 5 dpf larvae before ablation (circled region) and right is the same larvae after ablation (C) Expression of noelin in the ciliated cells suggesting a putative olfactory function of these cells. (D) Ability of the ciliated cells to trap particles shown by alcian blue staining. (E) Behaviour of control and ablated animals while being exposed to algal extracts of *Dunaliella* (preferred) and *Isochrysis*. P-values: * = 0.02 and ** > 0.1 (Wilcoxon rank-sum test). Scale bars represent 30 µm. Figures and data from (Ramanathan et al., submitted manuscript).

2 Discussion and future prospects

Using the specially devised microfluidic platform, the possibility of quantitatively estimating zooplankton preferenda to changing environmental and ecological conditions is demonstrated. Although most experiments in this work were done using *P. dumerilii* larvae, the platform and the basic behavioral characteristics may be applicable for other plankton species. For example, *Oxyrrhis marina,* a marine dinoflagellate showed a similar tumbling behavior when exposed to a chemoattractant (Seymour et al., 2010), suggesting the possibility that the behavioral parameters defined here could be universal for plankton. In addition, in the experiments with *E. acutifrons,* a tumbling behavior in the comfort zone and increased stream transition speed at the edge of the comfort zone was observed, which were similar behavioral patterns to *P. dumerilii* (Figure 2.10B). Although *E. acutifrons* uses appendages for locomotion and *P. dumerilii* uses cilia, this did not seem to change their behavioral pattern. These results indicate that regardless of the plankton species or their mode of locomotion, the behavioral parameters described here are applicable.

When exposed to different pH conditions, *P. dumerilii* and *E. acutifrons* were able to actively choose their preferendum. In experiments, *E. acutifrons* showed a narrower preferendum than *P. dumerilii.* Such experiments can help identify sensitive and resilient species to different changes. Thus far, these preferendum experiments on the species level in marine zooplankton were not demonstrated. Furthermore the ability to identify individual behavior in the device was useful to discover the existence of sub-populations that were previously unknown. With the use of valves in the microfluidic device, it might even be possible to isolate these sub-populations to further analyze them. Phenotypic sorting can allow identification of potential genetic variations that distinguish these individuals from the rest. This is also relevant in the evolutionary context to identify why a certain species has an advantage over the others. Several phenotypic sorting approaches using microfluidics have already been described in literature (Chung et al., 2008; Crane et al., 2009) and the integration of such functionalities into the present device might allow previously unprecedented analyses and discoveries.

Certainly, the ability to cope well with one parameter is not sufficient for the survival of species in a complex environment. Raise in CO_2 levels in the atmosphere is also influencing the surface temperature which in turn causes the addition of fresh waters from the melting glaciers into the

ocean. As a consequence, the salinity of the oceans are decreasing, and from the experiments *P. dumerilii* showed a clear preference to high salinity conditions, which suggests that, despite the high tolerance to pH drop, salinity changes might adversely affect the survival of *P. dumerilii.* Given that the salinity and pH of water bodies around the world are different, these effects might only affect the species locally, however, it is unclear how species interactions might be affected if local compositions change.

Zooplankton use chemical cues such as pheromones and kairomones to recognize mate (Snell and Morris, 1993), kin (Lazzaretto and Salvato, 1992), predator (Gutierrez et al., 2011), and prey (Heuschele and Selander, 2014). These ecological interactions mediated by chemical cues are necessary to understand and perceive how extinction of individual species can affect the overall ecosystem dynamics. For this purpose it is not just sufficient to measure the individuals' preferendum to changing environments but to also analyze the biotic interactions they have in their surroundings. The possibility to study interactions between zooplankton and other species, such as algae and predators, in the microfluidic device was demonstrated. These measurements mimic the "mesocosm" studies (section **2.3**) in a more controlled manner to give a broader understanding of species interaction networks.

Lastly, the possibility to do functional assays in the microfluidic device was shown. Since microfluidics allows tracking individuals at a high resolution, this allowed identifying differences in sensory response between experimentally-modified (ablated) and control plankton groups. This possibility allowed identifying cell types involved in sensing a certain stimulus. Such characterization on the cellular level further broadens the usability of the device.

In conclusion, taking advantage of the high spatial resolution offered by microfluidics, the possibility to make behavioral measurements of preferendum to different environmental and ecological conditions was demonstrated. In addition, the findings had a precision that allowed quantifying the minimum concentrations required for the microscopic plankton to elicit a response (responsiveness). These experiments can extend the "classical" ecological network reconstruction based on species abundance by providing information on actual responses (Aderhold et al., 2012).

Chapter 3

Generating combinatorial mixtures in droplets to assay stem cell niche

3 Introduction

Droplet-based microfluidic technology enables producing uniformly sized droplets at kilohertz frequencies (Park et al., 2011). This capability is especially attractive for HTS. Every droplet is comparable to a well in a microtiter plate in terms of isolation and uniqueness of samples it can contain. A single droplet can be of picoliter to nanoliter volume. This not only makes the reagent consumption lower but also reduces the number of cells or biological material required to attain a comparable density, making the platform suitable for assaying primary and rare samples. Thus far, the technology has been used mainly for screening biological entities like cells (Agresti et al., 2010), antibodies (El Debs et al., 2012), etc. where every droplet contained one biological entity. In this chapter, a novel droplet-based platform for HTS of compound combinations is described. In particular, here the platform is used to screen for compound cocktails triggering differentiation of mouse embryonic stem cells (mESC) to neuronal progenitors.

3.1 Stem cells

The innate ability of stem cells to self-renew and differentiate into different cell types is well recognized. Depending on their ability to differentiate into one or more cell lineages, stem cells are classified as totipotent, pluripotent or multipotent. Table 3.1 summarizes these differences and includes examples. Briefly, totipotent stem cells can give rise to a whole organism. A fertilized egg cell is an example of a totipotent cell. Pluripotent stem cells are immediate descendants from totipotent cells and have the ability to differentiate into all somatic cell types except placental tissues. Multipotent stem cells can only differentiate into cell types of one family. In principle, stem cells can proliferate indefinitely while retaining this potency (Gardner, 2002; Hima Bindu, 2011). This thesis focuses only on pluripotent stem cells.

Table 3.1 Comparison of different stem cell potencies

Potency	Explanation	Examples
Totipotency	A single cell that can give rise to an entire organism	Cell(s) in 1 to 3 day embryos
Pluripotency	Cells that can differentiate into all three germ layers and hence all cell types except placental tissues	Embryonic stem cells (ESC) forming the inner cell mass of the blastocyst stage or preimplantation embryos, Epiblast stem cells (EpiSC) from postimplantation embryos and artificially induced pluripotent stem cells (iPSC) derived from adult fibroblast
Multipotency	Cells that can differentiate into two or more cell types of their resident tissue kind	Mesenchymal stem cells (MSC) including: Hematopoietic stem cells (HSC), Neural stem cells (NSC) and other adult stem cells.

3.2 Pluripotent stem cells: past and present

Pluripotent stem cells are a unique resource that can, in theory, provide unlimited quantities of any somatic cell type *in vitro* (Evans and Kaufman, 1981; Martello and Smith, 2014; Yamanaka, 2012). In the 1950s pluripotency was discovered in subclones of cells isolated from testicular teratocarcinomas, a tumor containing multiple cell types including terminally differentiated structures like teeth and hair (Stevens Jr and Little, 1954). These pluripotent subclones of cells are called embryonal carcinoma (EC) cells (Kleinsmith and Pierce, 1964). Although EC cells are pluripotent they were found to be genetically abnormal (Papaioannou and Rossant, 1983). The challenge then was to get pluripotent cells without such abnormalities. Following this, around the 1980s, Martin and Evans found that these EC cells when cultured formed embryoid bodies (EB), a multicellular aggregate, and exhibited markers similar to embryonal identity (Martin, 1980, 1981; Martin and Evans, 1975). Consequently, in 1981 pluripotent ESCs directly from the inner cell mass (ICM) of blastocyst stage embryos were isolated (Figure 3.1) (Evans and Kaufman, 1981).

In the field of biology and medicine the assets of pluripotent stem cells are being used in developmental studies, disease modelling, pharmacological screening and cell therapy/organ

regeneration. Nonetheless there are ethical issues surrounding the use of human embryos and ESCs which hinder much of the progress in the field. The discovery of induced pluripotent stem (iPS) cells, where pluripotency is reprogrammed in adult fibroblast cells by genetically expressing four transcription factors (Oct4, Sox2, Klf4 and cMyc) revolutionized the field of stem cells (Figure 3.1) (Takahashi et al., 2007; Takahashi and Yamanaka, 2006; Yu et al., 2007). The creation of iPSCs not only negates all ethical issues but also alleviates the risk of immune rejection; since fibroblasts from the same patient can be used to reprogram pluripotency. However, there are still major impediments to their application in regenerative medicine, these include: difficulties in maintaining homogeneously undifferentiated stem cell cultures, directing differentiation into specific lineages at a high efficiency, and, eliminating potentially oncogenic transgenes when generating pluripotent stem cells (Yamanaka, 2012; Zhao et al., 2011). These difficulties can be overcome by the use of small molecules.

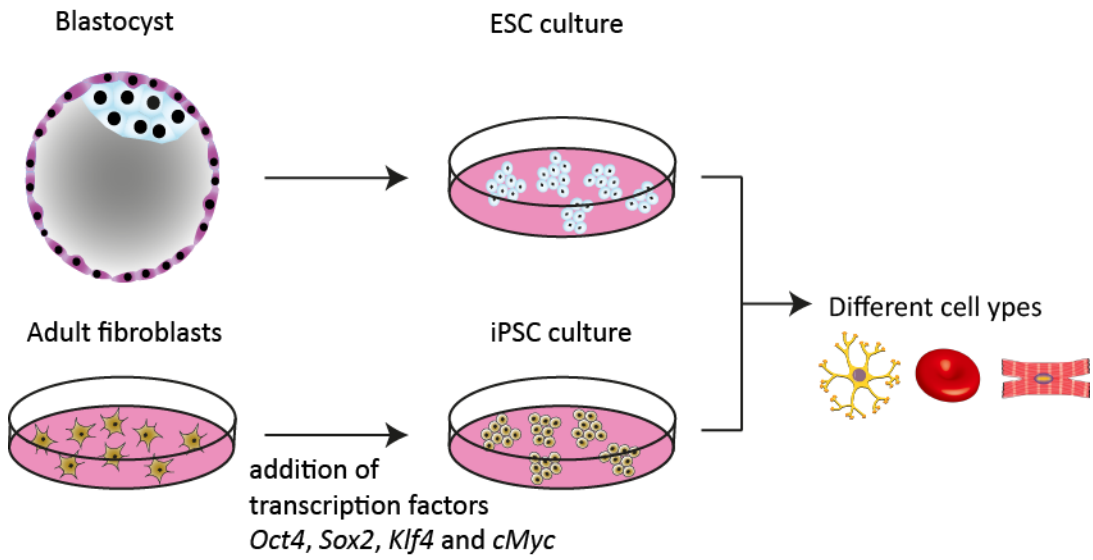

Figure 3.1 Generation of pluripotent stem cells. ESCs are derived from the inner cell mass (blue cells) of blastocyst stage embryos. iPSCs are reprogrammed cells that are made pluripotent by expressing four transcription factors (Oct4, Sox2, Klf4 and cMyc). Both pluripotent cells are capable of differentiating into different cell types.

Chemical screens have resulted in the identification of small molecule combinations that can maintain self-renewal (Ying et al., 2008), direct differentiation to a neuronal lineage (Ding et al., 2003), and chemically induce pluripotency (Hou et al., 2013). Yet, established protocols for efficient directed differentiation of every cell type continues to be refined. One reason for this is the lack of knowledge of underlying mechanisms involved in cell fate decisions. Most likely,

there is a complex interplay between pathways, and the desired effect can only be accomplished by using combinations of small molecules that act on different targets. This can be addressed by a chemical genetics approach.

3.3 Chemical genetics

Knowing the specific targets of a drug that induces a particular phenotype can be exploited to obtain insights into the underlying pathways. This concept is termed “chemical genetics” and although the effects are temporary, they are similar to conditional mutations on the genetic level (Mitchison, 1994; Schreiber, 1998). For instance, using known drugs with well characterized targets it is possible to uncover mechanisms involved in cell fate decisions by monitoring for the desired phenotype.

Indeed, this concept is used extensively to study antibiotic resistance mechanisms in bacteria (Walsh and Chang, 2006). Figure 3.2 illustrates the concept of chemical genetics. An additive effect means that there is no interaction between the pathways targeted by drugs X and Y (Figure 3.2A). For instance, if drug X can kill 10 % of the bacteria and if drug Y kills another 10 % then the effect observed while adding them together would be 20 % viability loss. On the other hand, an antagonistic or synergistic effect is observed when the pathways that the drugs act on interact, and either suppress (e.g. 5 % viability loss) or enhance (e.g. 90 % viability loss) the effect of each other respectively. With this information, it is possible to cluster different drugs into groups based on pure antagonistic or pure synergistic interactions when comparing any two groups as shown in Figure 3.2B. This classification further generates a system-level perspective of a drug network.

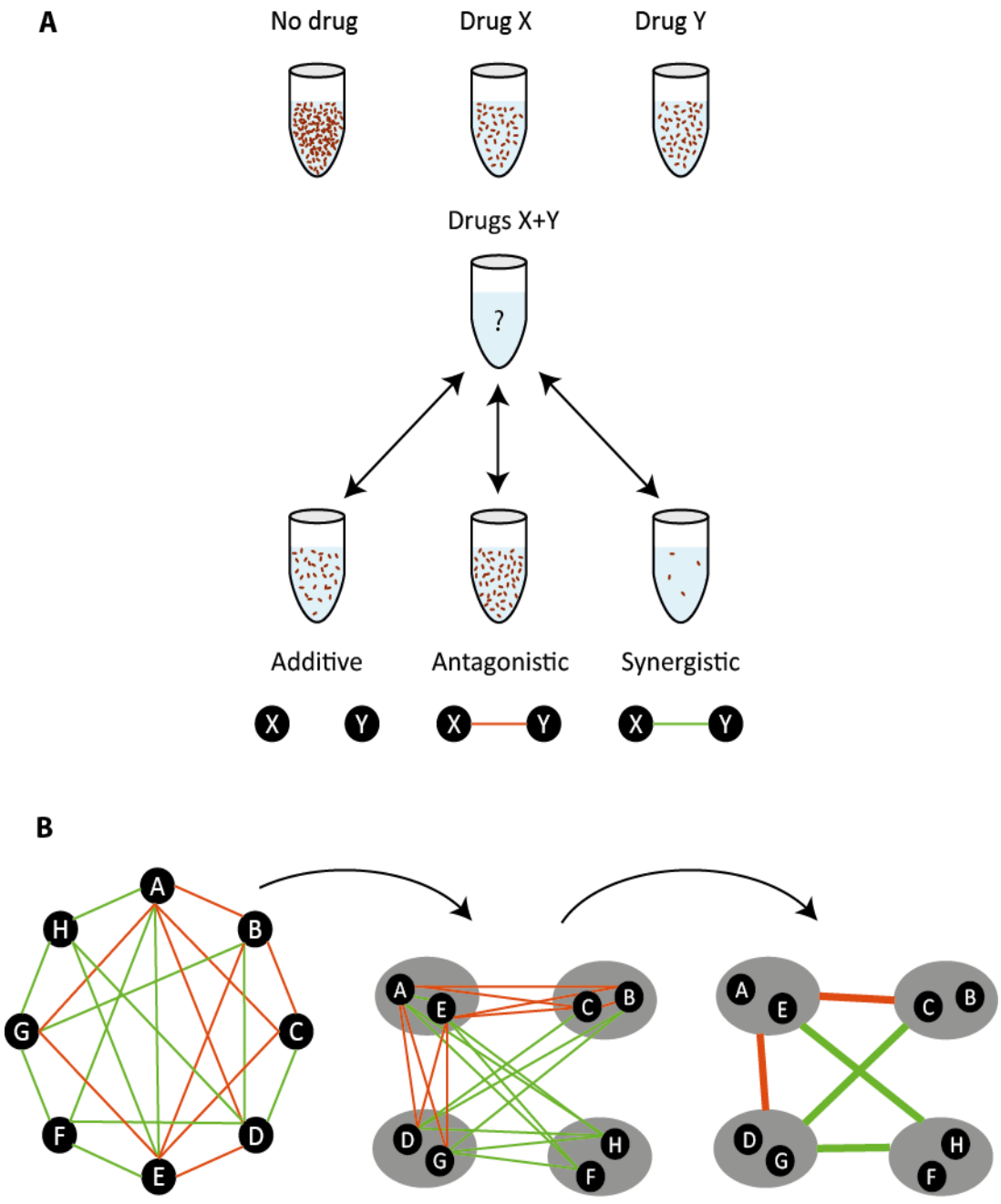

Figure 3.2 A chemical genetics approach. (A) Schematic showing the effects of drug X and Y individually and in combination. Additive effect means that the drugs target independent pathways. Antagonistic (red line) or synergistic (green line) effects result in either an increase or decrease to the additive effect observed. (B) Clustering of drugs into groups based on their effects. Classification of drugs (black circles) is done based on similar interactions with other classes of drugs. For instance, a group of drug acts purely synergistically (green line) or purely antagonistically (red line) with drugs in another group. Modified from (Yeh et al., 2006).

Furthermore, chemical perturbations, unlike genetic methods, allow a high degree of temporal control over protein functions. The effects of small molecules can be fine-tuned or reversed by

varying the concentrations. In addition, a single small molecule can modulate multiple targets in different pathways or within the same pathway (Xu et al., 2008). These factors are particularly interesting in stem cell biology. For example, it is well known that retinoic acid (RA) causes the differentiation of stem cells into neuronal lineage. The differentiation efficiency is shown to vary with different RA concentrations (Okada et al., 2004). However, it is reported that pharmacological interference of ERK and Wnt pathways blocked the differentiation even in the presence of retinoic acid (del Corral and Storey, 2004; Hirabayashi et al., 2004; Lu et al., 2009). One of the reasons could be that there is an active crosstalk between retinoic acid signaling, ERK and Wnt pathways. Thus identification of compounds that selectively interfere with cellular pathways gives insights about cell fate decision. Combinatorial perturbations with drugs can hence help in understanding the pathway interactome by revealing synergistic, antagonistic or additive effects between pathways (Yeh et al., 2006). Statistical models to identify these interactions have been previously described (Bliss, 1939; Loewe, 1928). Thus, chemical genetics allow dissecting complex cell-signaling pathways. Here a microfluidic technology was used to test for different combinations of small molecules, growth factors and proteins in a HTS approach while monitoring cell fate decision and thereby uncover the underlying mechanisms.

3.4 Why microfluidics for stem cell assays?

One of the challenges of culturing stem cells *in vitro* is the controlled expansion of the cells while maintaining homogeneity (Miyanari and Torres-Padilla, 2012). Previous studies have reported chromosomal abnormalities or DNA copy number variations in long-term cultivation of ESCs, iPSCs and MSCs (Laurent et al., 2011; Maitra et al., 2005; Närvä et al., 2010; Wang et al., 2013). For this reason, long-term passaging is not recommended for stem cells making it difficult to get the required billions of cells (~10,000 cells per well in a standard 384 well plate) for conventional, microtiter plate screening approaches (Ertl et al., 2014). One advantage of using microfluidics is the low cell number (down to 1 cell per droplet requirement because of working on a pico to nanoliter scale. This makes assays in microfluidics particularly more reliable for stem cells, because the results obtained from a single passage of cells have less variability. Additionally microfluidic systems consume lesser reagents, are inexpensive to work with, and can be fully automated as elaborated in the **General Introduction** section of this thesis.

3.5 Droplet-based small molecule combination screens

Microfluidics has been used for screening biological sample libraries such as cell libraries (Beneyton et al., 2014; Cao et al., 2012; El Debs et al., 2012). However, there is a lack of devices that allow screening using chemical libraries. Dose-response studies in droplets exist (Cao et al., 2012; Miller et al., 2012) where different concentrations of a chemical can be tested for their effects on cells, but these devices do not allow screening different chemicals and combinations of chemicals.

To our knowledge, the only existing small molecule combination HTS approach that can allow screening combinations of two or more compounds using droplet microfluidics was reported from Dr. Tza-Huei Wang's lab (Rane et al., 2014; Zec et al., 2012). In the latest report they elegantly demonstrated a 650 enzyme-substrate combination screen (Rane et al., 2014). However, screening of chemicals for their effect on mammalian cells adds additional difficulty because of the wetting caused by media proteins which can cause fusion or cross-contamination of chemicals between droplets (Figure 3.3). Although there are means of overcoming this problem to some extent (Subramanian et al., 2011), so far there is no HTS approach that allows co-encapsulating mammalian cells with small-molecule combinations. In this chapter, a novel approach that allows screening of small molecule combinations of entire libraries and a new barcoding strategy is shown. The system is further optimized to be used for screening small molecules inducing differentiation of mESCs to neuronal progenitors.

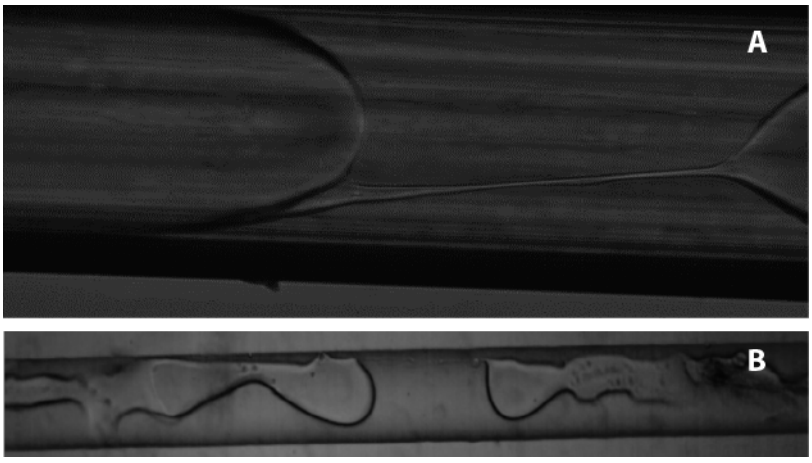

Figure 3.3 Cross-contamination due to wetting of plugs containing proteins. (A) Cross-contamination between two plugs inside tubing (B) Wetting in the drop-maker channel.

3 Results

3.6 A novel approach to generate binary barcoded droplets containing unique compositions using a braille display

A Braille display is a tactile writing aid used by the blind. In this project, a 64 pins braille display, as shown in Figure 3.4, is used and each pin can be individually actuated to move up or down. Here, this ability is made use of to open and close microfluidic channels thereby precisely controlling the flow of reagents. The concept of using a braille display to control liquid flow in microfluidics was previously demonstrated to generate different laminar flows (Gu et al., 2004). Here, the braille display was used to generate combinatorial mixtures in droplets.

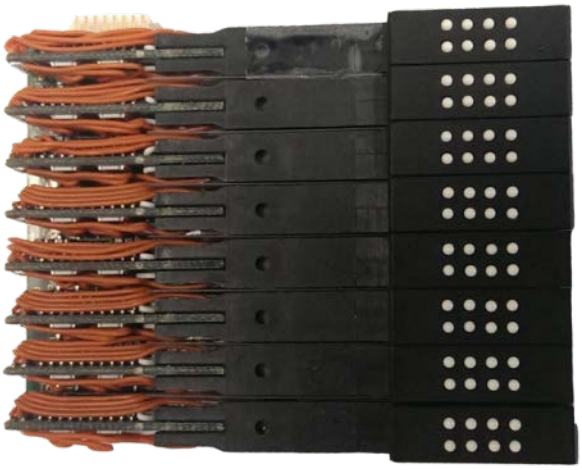

Figure 3.4 Braille display unit with 64 pins (white dots). Each of the pins can be individually actuated and used as a mechanical valve.

3.6.1 Working principle

A microfluidic chip for generating combinatorial mixtures was produced with the difference that the channels are closed off by bonding the chip to a thin polydimethylsiloxane (PDMS) membrane that is flexible, instead of a rigid glass as it is usually done. Thus when the chip is positioned on the braille display, the pins can deform the membrane to open and close the channels above as illustrated in Figure 3.5.

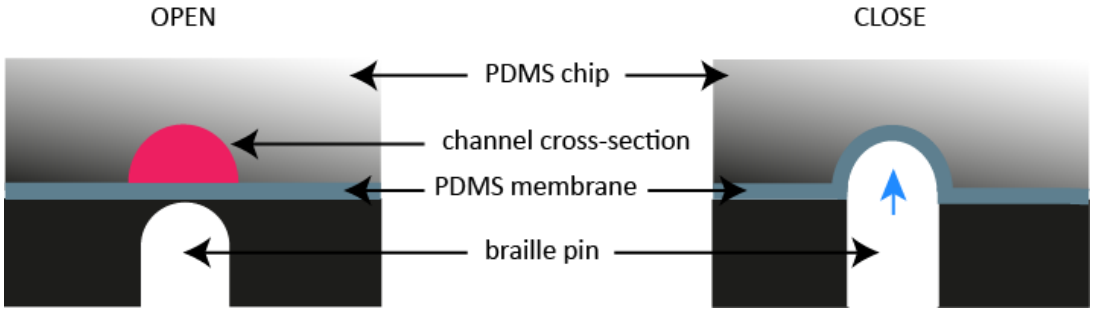

Figure 3.5 Open and closed valve configuration. The channel is aligned on the braille pin such that when the pin moves up, the membrane above it deforms and blocks the flow through the channel.

The 64 pins of the braille display are used to control 32 unique reagent inlets on a specifically designed microfluidic chip (Figure 3.6A) shows a 16 inlet half size version of the chip). Since the reagents are infused constantly using syringe pumps (Figure 3.6B), two pins are required to direct the flow to either the T-junction (where the droplets are produced) or to the waste outlet (marked with "W" in Figure 3.6A), to avoid pressure built-up in the system. At the T-junction the droplets are produced when the reagents (aqueous) come in contact with fluorinated oil (FC-40 + 0.5 % PFO). Perfluorooctanol (PFO) is used in the fluorinated oil as an anti-wetting agent. The flow rates are adjusted such that for each sample only a set number of droplets fuse to form a plug. To avoid further fusion between plugs, mineral oil was used as a spacer as it was previously reported to be effective in keeping plugs separate (Baraban et al., 2011). The result is the generation of a long array of plugs interspersed by mineral oil as illustrated in Figure 3.6A and Figure 3.6B.

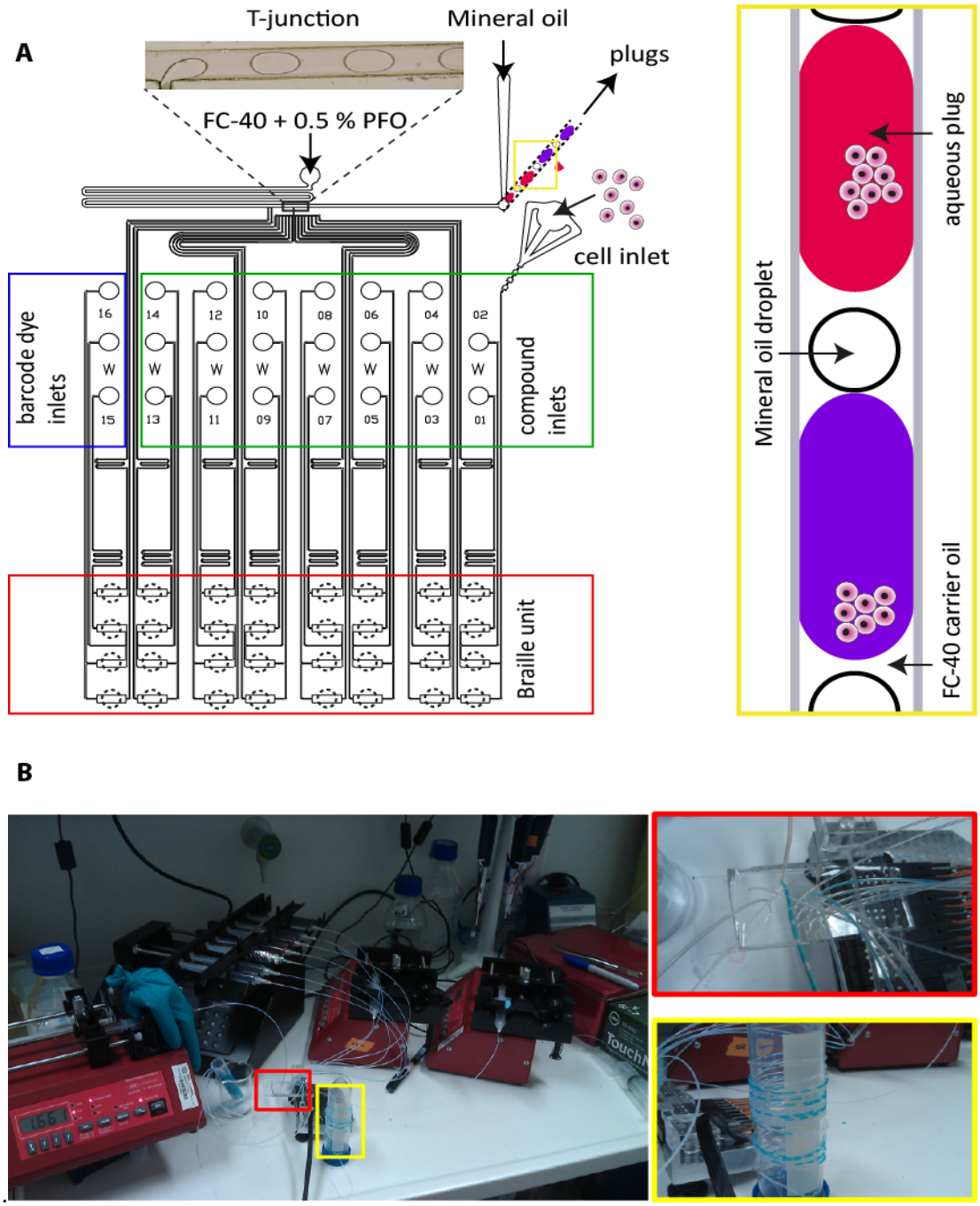

Figure 3.6 Experimental set-up. (A) Design of a 16 inlet microfluidic chip matching half of the braille unit (red box). Dotted circles show the position of the braille pins. Inlets 15 and 16 (blue box) are infused with two different concentrations of a fluorescent dye for barcoding. Inlet 02 is used for cells and has a different geometry to other inlets to prevent clumping of cells. All other inlets (green box) are used for infusing different compounds of interest. Circles marked with "W' are the waste outlets. Every two inlets share one waste outlet. Droplets are produced at the T-junction as shown. At the outlet where the droplets exit the chip into the tubing, several droplets fuse to form a plug and are interspersed by mineral oil droplets as shown in the schematic within the yellow box. (B) Entire experimental set-up along with the syringe pumps. Individual parts are zoomed in for a better view.

The braille system has the ability to generate uniform plugs of different compositions, which are represented by dyes in Figure 3.7A. Noticeably, there is cross-contamination in the plug between two colors (purple plug in Figure 3.7A), but this can be addressed by including replicates and excluding the cross contaminated first plug from the analysis.

Unique binary barcode plugs (blue plugs in Figure 3.7B) are produced before every new composition to make the compositions in every plug identifiable. These barcodes are nothing but plugs containing fluorescent dyes. Two different concentrations of the dyes are used to represent 0s and 1s in binary digits. A sequence of barcode plugs can thus be detected along with the fluorescent assay read-out and the compositions can be easily deciphered (Figure 3.7C).

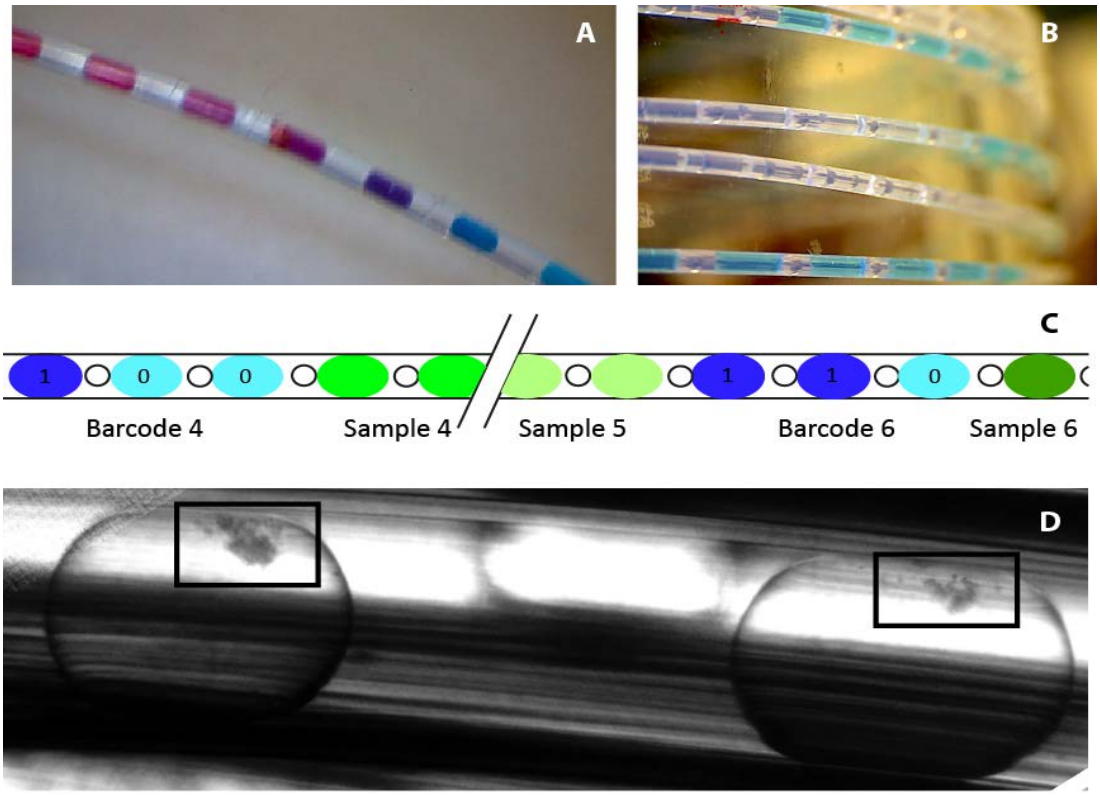

Figure 3.7 Plugs in tubing. (A) Plugs with different dyes to demonstrate the possibility of generating diversity in plugs on-demand. The purple plug in between blue and pink plugs is cross contaminated and can be excluded from analysis. (B) A reel of tubing containing a long train of different composition plugs identifiable by the blue barcode plugs. (C) An illustration of the binary barcode strategy. Samples (different shades of green plugs) are identified using barcodes (light and dark blue plugs). Barcodes are simply plugs with two different concentration of fluorescent dyes (indicated here as dark and light blue) to represent 0s and 1s in binary digits. (D) A magnified view showing cells (within black boxes) in plugs incubated in transparent and gas-permeable polytetrafluoroethylene (PTFE) tubing.

3.6.2 Generation, detection and analysis of small molecule mixtures

In a screen, two of the inlets are dedicated for the barcode dyes and one inlet is used for cells or other biological samples to be tested, leaving 29 inlets for chemicals or proteins. The number of combinations (*nCr*) that can be generated using these 29 compounds can be calculated using Equation 5.

$$nCr = \frac{n!}{r!(n-r)!} = \frac{n(n-1)(n-2)\ldots(n-r+1)}{r!} \qquad \rightarrow \text{Equation 5}$$

Where n is the total number of compounds and r is the maximum number of compounds mixed together in a plug. Therefore, with 29 compounds (n = 29) and pairs of compounds being mixed (r = 2), the total number of combinations that can be produced (*29C2*) is 406. Integration of the braille display with an autosampler, that is capable of sampling reagents from 96 well plates, can increase this sample number significantly. To enable this, one of the 29 inlets is connected to the output from the autosampler leaving 28 inlets on the braille display for other compounds. The resulting sample number is 406 + (96 x 28) = 3094 combinations. Besides, the autosampler is not limited to one 96 well plate. Therefore entire compound libraries can be fed into the autosampler and combined with compounds on the braille display, making the set-up scalable for higher sample numbers.

The train of plugs is automatically generated by sequentially executing the commands given by a software specifically designed in LabVIEW by Ramesh Utharala, EMBL to control the status of the 64 pins (Figure 3.8). Briefly, when the braille display is connected and initialized, the pins are maintained in an “all waste” configuration; meaning all the channels connecting to the drop maker/T-junction are closed off by the pins. Following this, the program uses preset commands to automatically generate combinations by opening and closing the assigned pins for a set duration. The graphical user interface shown in Figure 3.8 helps to preset the parameters like valve opening times, duration of oil flush in between two compositions, number of replicates per composition, etc.

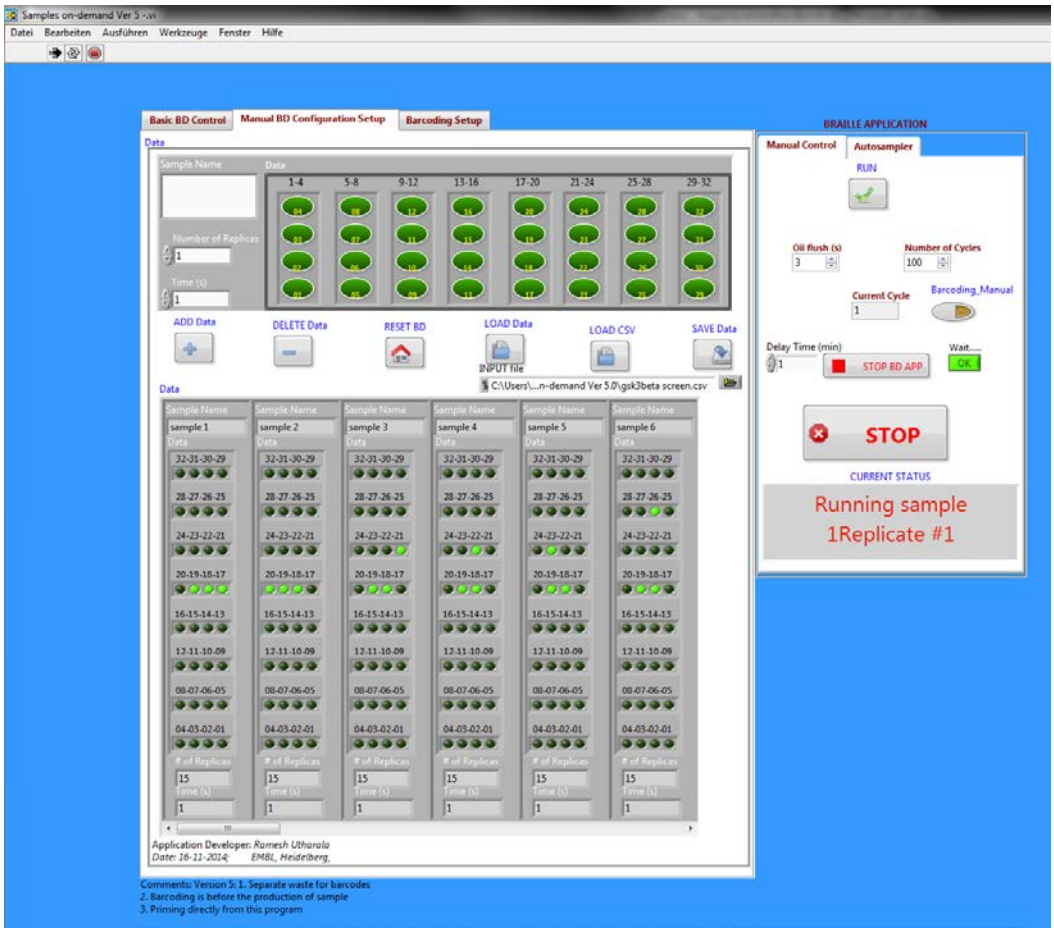

Figure 3.8 Graphical user interface of the program used to control pins on the braille display.

The plugs are then collected in the same order as they are produced, in a polytetrafluoroethylene (PTFE) tubing with an inner diameter of 600 µm. It is important to note that the length of the tubing has a significant effect on the plug production. Although long tubing can store more plugs, it also generates an equivalent back pressure. The back pressure was calculated using the Hagen-Poiseuille equation (Equation 6) which is generally only used for continuous flow but may serve as a rough estimate for the plugs.

$$\Delta P = \frac{8\mu LQ}{\pi r^4} \qquad \rightarrow \text{Equation 6}$$

Where ΔP is the pressure loss, μ the dynamic viscosity of the water in oil plugs, L the length of the tubing, Q the volumetric flow rate of plug production and r is the radius of the tubing (600/2 = 300 µm in this case). Inferring from this equation, the optimal length of the tubing (L) was estimated to be 6 meters with a negligible back pressure of 2.151 kPa (= 0.0215 bar) knowing that the flow rate (Q) is 1000 µl/h and viscosity (μ) of FC-40 oil is 4.1 mPa-s. Furthermore the 6

m of tubing were pre-filled with buffer plugs to avoid any further pressure differences while producing the experimental combinations. Indeed the tubing can be exchanged with new 6 m of tubing to allow storing more plugs.

The entire reel of tubing was then incubated for the assay duration in a 37 ºC and 5 % CO_2 incubation chamber with humidified atmosphere. PTFE is gas permeable making it suitable for cells (Figure 3.7D). Following this, the plugs were run through the readout spot, on which a laser beam was focused. The fluorescence intensities of the plugs were measured directly inside the transparent PTFE tubing. Photo multiplier tubes (PMT) amplify the emitted signal and these measurements were monitored using another LabView program developed by Ramesh Utharala, EMBL as shown in Figure 3.9. Every peak corresponds to a plug. The width of the peak indicates the plug length, and the amplitude of the signal corresponds to the fluorescence intensity of the plug. Since the microfluidics workstation enables the detection of three different fluorescent colors (red, green, blue) simultaneously, the barcode fluorescence can be recorded in parallel.

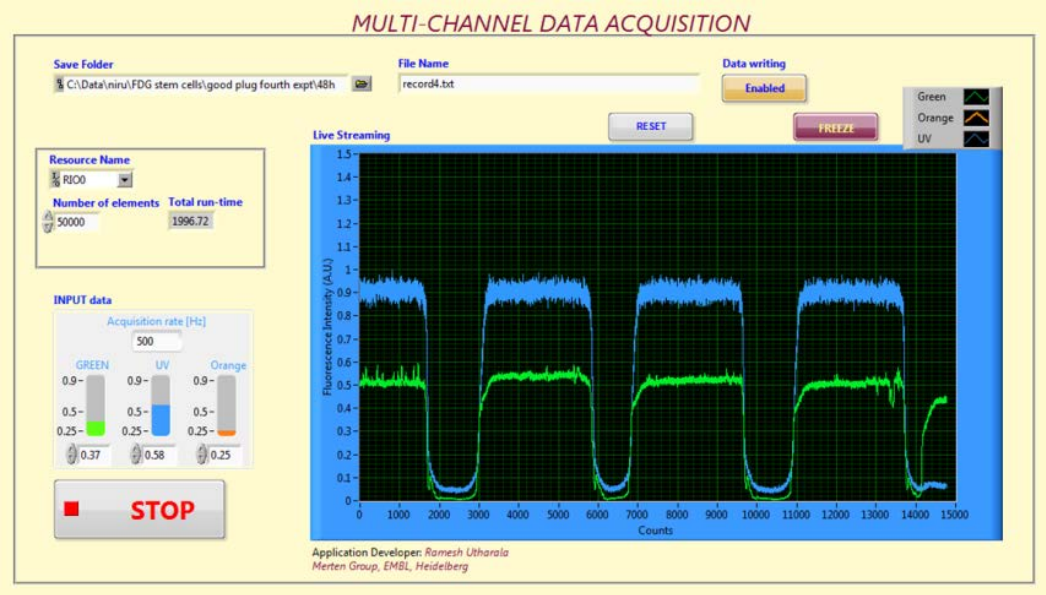

Figure 3.9 Data acquisition program. The program acquires fluorescence intensity values as the plug passes through the laser spot. Every peak corresponds to a plug. The amplitude of the peak correlates with the fluorescence intensity and the peak-width corresponds to the plug-width. Simultaneous recording of two different fluorescence channels (blue and green) is shown.

Finally, the recorded values are analyzed using a custom R package (BraDiPlus) with scripts specifically suited to analyze the data from plug-based screen. These scripts were written by

Federica Eduati, EMBL-EBI. The scripts are capable of reading the barcodes and selecting replicate sets of the same composition. It is then possible to compare the read-out signals between compositions to identify hits.

3.7 Application of the novel approach for stem cell differentiation screens

The usability of the newly developed approach to screen optimal protocols for directed differentiation of mESCs is described in this section.

3.7.1 Evaluating viability of mESCs in aqueous plugs

Although there are previous reports on stem cell survival in microcapsules made of hydrogels, all these assessments were done while soaking these microcapsules in fresh medium (Agarwal et al., 2013; Tumarkin et al., 2011). While this allows medium exchange, it is not suitable for screens with different medium compositions. Since the aim here was to generate chemical diversity in plugs to identify the optimal medium for differentiating stem cells, it is neither possible to soak these plugs in the same medium nor disturb the ordering of the barcoded plugs. As there is no report on survival of pluripotent stem cells in aqueous medium droplets, this was addressed first.

The survival kinetics of mammalian cell lines such as Jurkat and HEK 293 in droplets are documented elsewhere (Clausell-Tormos et al., 2008) (Figure 3.10A-B). It is evident from reported data (Figure 3.10A and B) that the Jurkat cells, which proliferate faster (doubling time 20.7 ± 2.2 hours (Schoene and Kamara, 1999)) than HEK 293 (doubling time 24 hours (Cervera et al., 2011)), also have a reduced survival time in 660 nanoliter plugs. For pluripotent mESCs the doubling time is 10-14 hours (Pauklin et al., 2011). When the same protocol was adapted for encapsulating 46c (Sox1-GFP) mESCs the percentage of surviving cells decreased to ~20 % after 24 hours incubation in plugs of the same cell density (Figure 3.10C). The survival rate was assessed by performing a flow cytometry and image based counting of cells recovered from plugs after staining with Calcein AM (live stain) and propidium iodide (PI, dead cell stain). Although this loss in survival percentage was expected from the rapid doubling time of mESCs, which perhaps depleted the limited medium nutrients and accumulated toxic metabolites, this rate did not increase by reducing the number of cells per plug. However the survival rate of

Jurkat cells linearly correlated with the cell density in the previous work (Clausell-Tormos et al., 2008)(Figure 3.10D). Trying different cell densities for mESCs resulted in a viability difference as shown in Figure 3.10E. The optimal cell density for encapsulating mESCs was found to be 3.5 million cells per ml. At this density the cells could be efficiently re-cultivated after recovering them from plug (Figure 3.10F). Too few or too many cells compromise survival of mESC in droplets. This finding is consistent with a recent report where Pettinato *et al*. tried to form EBs in microwells at different cell densities (Pettinato et al., 2014).

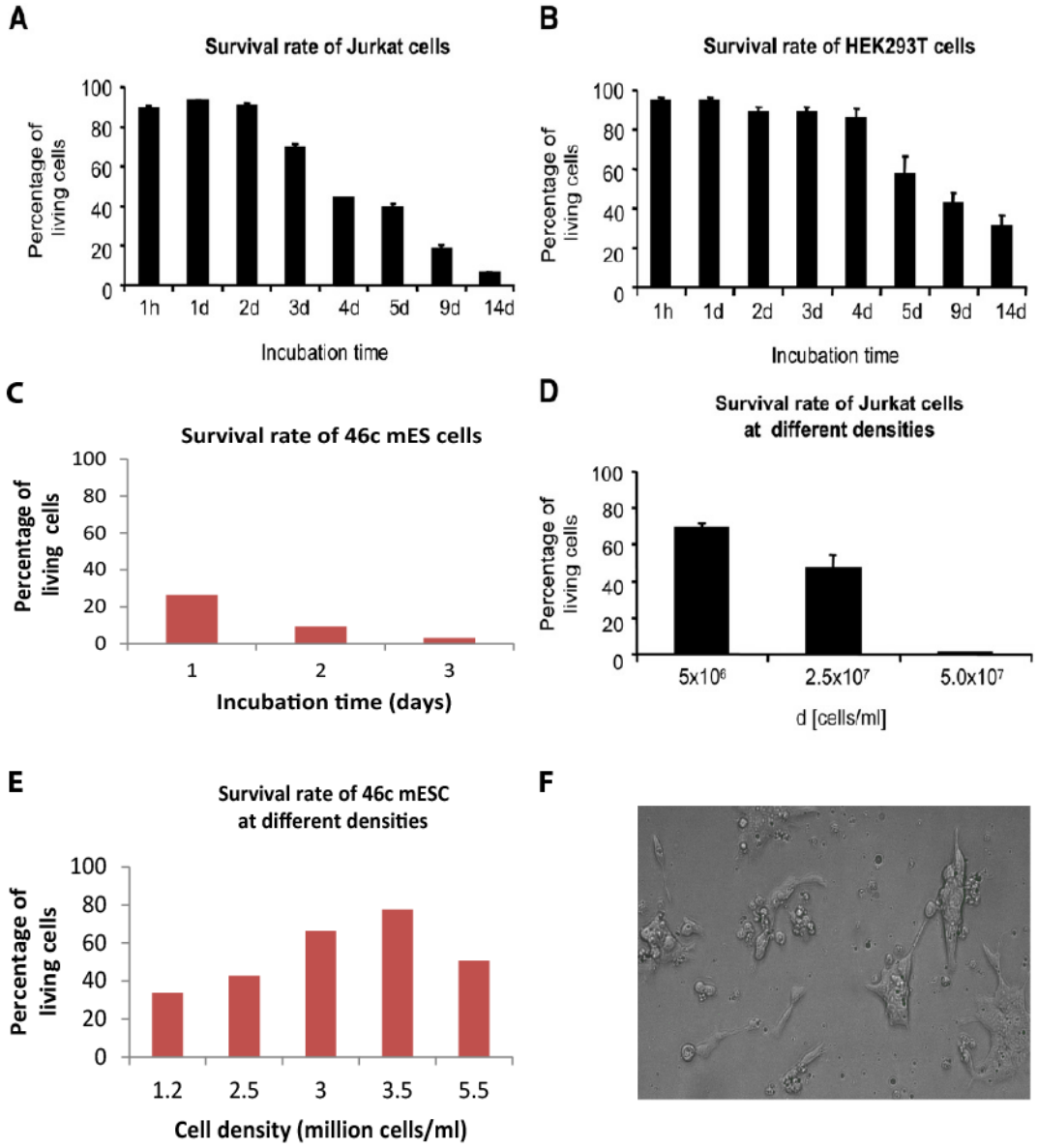

Figure 3.10 Survival kinetics of cells in plugs. (A) and (B) are survival rates of Jurkat cells and HEK 293T cells as reported elsewhere (Clausell-Tormos et al., 2008). (C) The survival rate of mESCs. (D) Correlation between cell density and cell viability as reported elsewhere (Clausell-Tormos et al., 2008). (E) Variation of survival at different cell densities

for mESCs. (F) The viability of cells recovered from plugs by re-cultivation. Data in A, B and D was reproduced from (Clausell-Tormos et al., 2008) with permission from *Elsevier.*

While monitoring the viability of 46c mESCs over time, a rapid decline in survival was observed after 24 hours. One of the major reasons for this loss of survival could be the acidification of the medium and depletion of glucose. For this reason it is advised to replenish the medium every 24 hours for mESCs (Smith, 1991). Moreover, it is known that ES cells predominantly rely on glycolysis for energy supply (Varum et al., 2011). Since the plugs are inaccessible to complete change of medium, an alternative solution of buffering the medium and adding more glucose was considered. The addition of 10 mM HEPES and 40 mM of glucose to the medium increased the survival to over 60 % after 48 hours (Figure 3.11A). However, after 72 hours the survival decreased to ~ 10 %.

To clarify that there is no difference in viability of the mESC in plugs based on their origin or genetic differences (Hughes et al., 2007), similar survival assessments were done for Sox1-βgeo mESCs generated from a different parental mouse line (C57BL/6) (Nishiguchi et al., 1998) than 46c mESCs (E14tg2a.IV) (Ying et al., 2003). No significant difference was observed in the survival of the two strains. Consequently, the maximum assay duration, using the above described optimization, for mESCs in isolated aqueous plugs is 48 hours.

Having quantified the survival, the effect of encapsulation on potency of pluripotent stem cells was assessed. For this, a mESC reporter line, with Rex1-GFP knock-in, generated by Wray J. and co-workers, was used (Wray et al., 2011). Rex1 is a self-renewal marker and the expression of Rex1-GFP in plug-recovered EBs after one and two days is shown in Figure 3.11B. This demonstrates that the mESCs in plugs are fully viable and retain their potency for up to 48 hours in plugs.

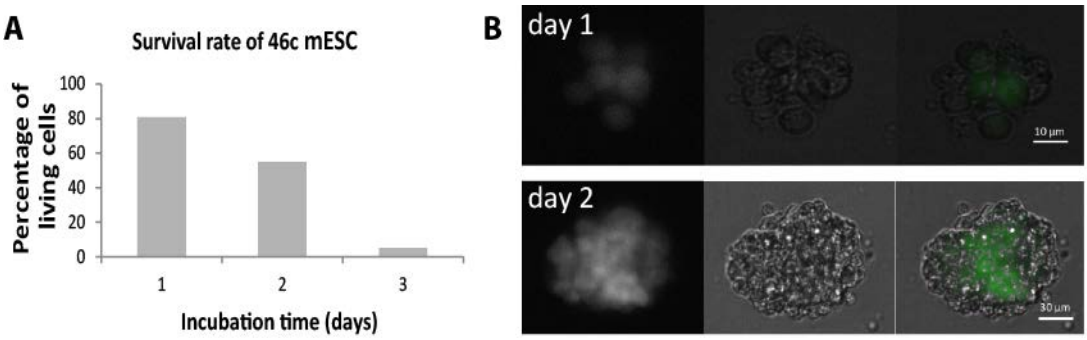

Figure 3.11 Long-term survival of mESCs. (A) Duration of survival of 46c mESC. (B) Rex1-GFP expression in embryoid bodies recovered from plugs after 1 day and 2 days. Scale bar represent 10 µm.

The viability could only be determined by recovering the EBs from plugs since the intracellular GFP signal can hardly be detected inside plugs. This is because the EBs can freely move in the plugs and do not necessarily pass the detection point at the exact same position. This causes artificial variations in the detected signal. To avoid this, Sox1-βgeo mESCs were used for the screens. This line produces β-galactosidase enzyme as a reporter upon *Sox1* induction. Substrates like X-gal or Fluorescein di-D-galactopyranoside (FDG) can be converted by this enzyme to produce a chromogenic or fluorogenic signal respectively. More specifically, in plugs FDG is used as a substrate and in the presence of β-galactosidase enzyme, FDG is hydrolyzed to fluorescein which then leaks from the cells into the plugs making the whole plug fluorescent. This reporter system, as illustrated in Figure 3.12, is better for detection within plugs.

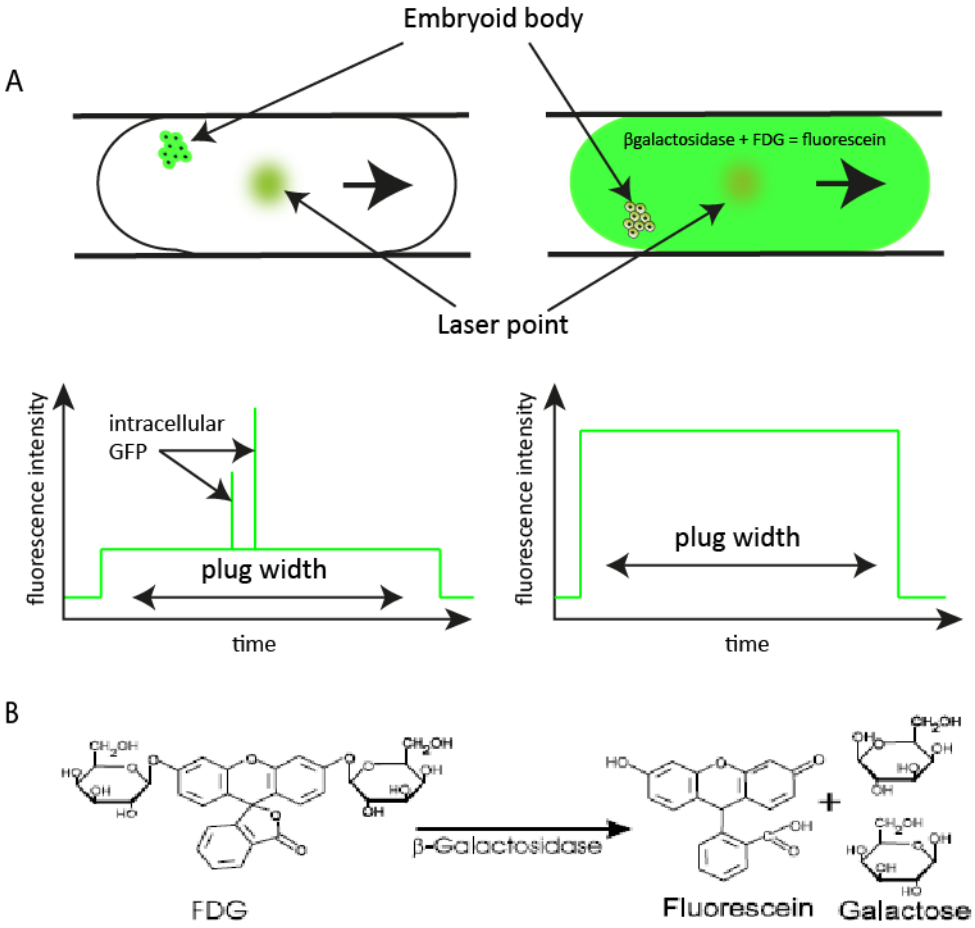

Figure 3.12 Fluorescence detection in plugs. (A) Intracellular GFP fluorescence (left) shows varying intensities based on the location of the cells within the plug. Assays generating an extracellular fluorescent product (Tatistcheff et al., 1993) are much more quantitative and reliable, because the fluorescence is uniform throughout the entire plug. (B) FDG hydrolysis. The β-galactosidase enzyme produced by the cell, converts the FDG to fluorescein which makes the whole plug fluorescent.

3.7.2 Differentiation of mESCs in aqueous plugs

The most commonly used protocol for mESCs differentiation into neuronal progenitors is using N2B27 serum-free medium developed by Ying and co-workers (Ying et al., 2003). Using this protocol, the differentiation of 46c mESCs to neuronal progenitors takes 4 days at an efficiency of around 80 % in monolayer cultures (Figure 3.13B) (Ying et al., 2003). This was monitored by the expression of Sox1-GFP where Sox1 is an early marker for neuronal lineage (Pevny et al., 1998). Figure 3.13 shows the kinetics of differentiation in monolayers based on the GFP reporter expression. While the efficiency of differentiation in the N2B27 protocol was unmatched, a couple of years later Abranches E. *et al.* published a new protocol for faster and more efficient

(60 % after 3 days) medium composition (RHB-A medium) for differentiating 46c mESC to Sox1 positive neural progenitors (Abranches et al., 2009). The newly described approach can be used to screen for optimal differentiation protocols that can induce detectable differentiation already after 48 hours. Firstly, a small molecule that can potentially influence neuronal differentiation was identified from literature (Lu et al., 2009).

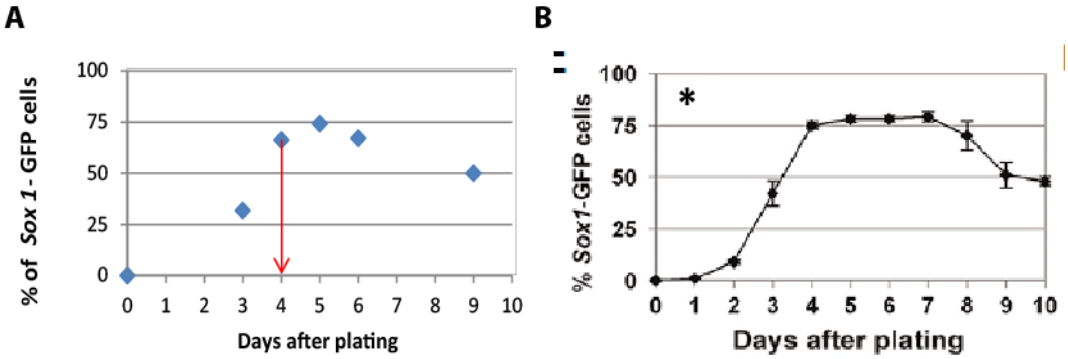

Figure 3.13 Kinetics of differentiation of 46c mESC to Sox1 positive neuronal progenitors. (A) Detectable differentiation was observed after 4 days of incubation in N2B27 medium. After 4 days the Sox1 expression reduces as the cells proceed to neural fate. (B) Data from Ying et al. showing the same kinetics. *Reproduced with permission from Nature Publishing Group.*

All-trans retinoic acid (RA), is a morphogen with pleiotropic actions and is known to promote differentiation into neuronal lineage (Lu et al., 2009; Maden, 2007) as measured by Sox1 expression. While the differentiation efficiency is a function of RA amount (Okada et al., 2004), here, with Sox1-βgeo cells, β-galactosidase reached detectable levels, evaluated by X-gal conversion and microscopy, 48 hours after RA addition (10^{-8} M in N2B27 medium) (Figure 3.14A-C), thereby showing differentiation of the cells within the time window during which they are viable in plugs. Subsequently, a two condition screen was performed to show feasibility of mESC differentiation in plugs. Plugs were generated with (+) and without (-) RA, and measurements of fluorescein intensity were performed in 16x 20 replicate plugs for each condition after 64 hours and 85 hours. While there was no significant difference between the sample groups at 64 hours Figure 3.14D(i), the prolonged conversion of FDG into fluorescein at 85 hours Figure 3.14D(ii) resulted in a well pronounced and significant (P=0.0013) difference between samples with and without RA.

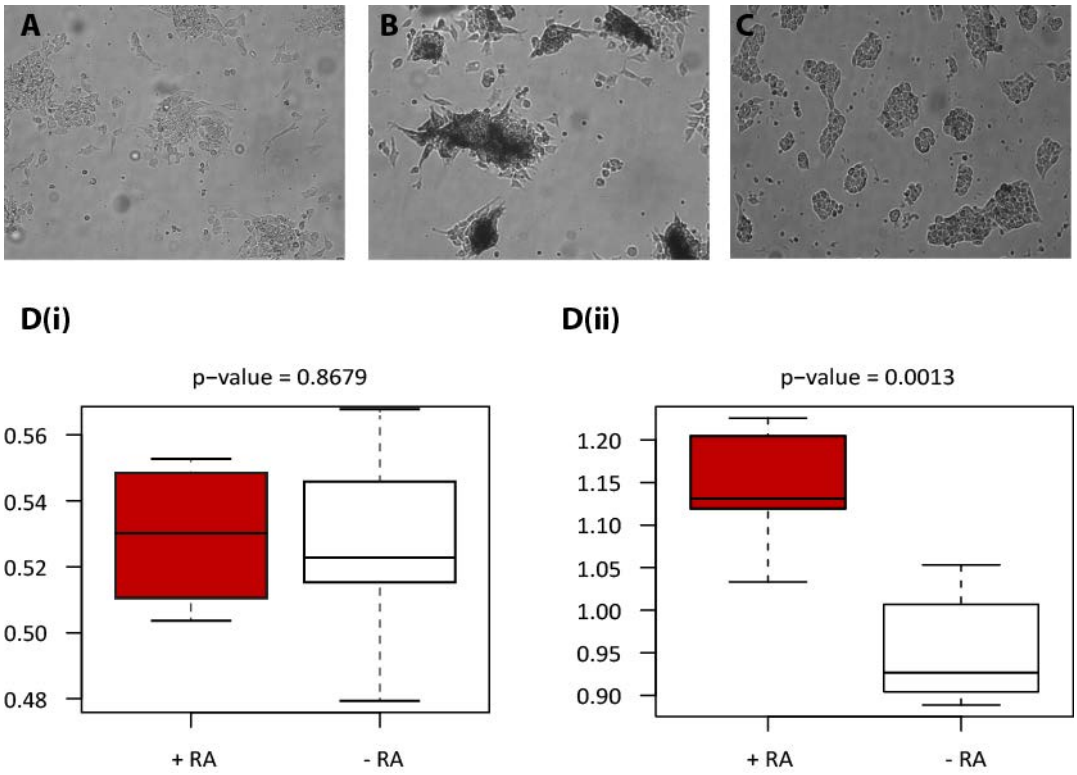

Figure 3.14 Differentiation of Sox1-βgeo mESC to neuronal progenitors. (A) and (B) X-gal stained cells cultivated for two days in N2B27 medium with 10^{-8}M RA. (A) 46c mESCs taken as a negative control. (B) Sox1-βgeo mESCs stained for the expression of β-galactosidase. (C) Sox1-βgeo mESCs in the self-renewing medium and hence shows no staining with X-gal. (D) The outcome from a two condition screen in plugs with Sox1-βgeo mESCs. +RA is N2B27 medium with 10^{-8}M RA and -RA is N2B27 medium without any RA. The fluorescence intensity is shown on the y-axis D(i) Measurement after 64 hours and D(ii) after 85 hours. The difference between the two conditions is clearly significant after 85 hours. p-values are as indicated.

The combination of the mESC being viable and fully potent in plugs for a time window that allows the pronounced detection of neuronal lineage markers, ultimately shows the suitability of microfluidics for stem cell differentiation screens. The further use of the binary barcodes to trace sample identity, renders this approach suitable for high-throughput combination studies with large chemical compound libraries.

3 Discussion and future prospects

A novel approach for HTS of optimal neuronal differentiation protocols for pluripotent mESCs has been established. The possibility of generating combinatorial diversity in droplets with binary barcodes and the ability to screen for molecules inducing differentiation of mouse

embryonic stem cells has been demonstrated. While the approach may be suitable for use with other stem cells, the niche environment of every stem cell type is unique (Scadden, 2006) and the system has to be optimized accordingly. For example, EB formation that occurs naturally in droplets is typical for assessing ESC and iPSCs differentiation; however, this is not the case for MSCs. Most MSCs fate choices depend on the ECM or substrate properties (Engler et al., 2006). Although gelation of entire droplets is possible (Agarwal et al., 2013; Tumarkin et al., 2011), and can closely mimic the ECM, this is technically challenging in the approach described here. One of the reasons being the increase in the overall back-pressure while collecting the plugs in a 6 m long tubing, due to the high viscosity of hydrogels. Another reason is wetting caused by hydrogels that could potentially cross-contaminate samples. An alternative that can overcome the problems with gelation while supporting MSC differentiation is to co-encapsulate beads coated with ECM materials along with MSCs in droplets. Although the entire plug remains aqueous the MSCs can adhere to these beads which support their differentiation. This method for MSCs can help to assess what factors apart from the ECM play a role in fate decision.

Aside differentiation, other stem cell assays, like organ development, could potentially also be monitored using the novel microfluidic approach described here. Studies have reported the formation of 3D structures called organoids when MSCs like intestinal crypt stem cells are cultured without a niche or substrate (Sato et al., 2009). Intestinal organoids can self-assemble and form entire crypts with villus and lumen. Organoids of stomach (Barker et al., 2010), colon (Sato et al., 2011), pancreas (Huch et al., 2013a) and liver (Huch et al., 2013b) have also been reported. Such 3D organoids are being used to understand the formation of entire organs and serve as disease models (Shamir and Ewald, 2014). These organoids are able to originate from individual stem cells, and hence can simply be formed by encapsulating single cells in plugs. However, for all these assays, the major limitation in using droplet-based approaches is the duration of survival of stem cells in droplets. For instance, intestinal organoids take two weeks to develop (Sato et al., 2009).

Since the maximum assay duration in plugs with the optimized protocol described here for mESCs is 48 hours, the number of possible assays that can be performed in this time window is restricted. Indeed stem cells, depending on their origin, also differ in their energy metabolism which is an important parameter for their survival (Rafalski et al., 2012). This parameter can be adjusted further to extend their survival in droplets, however, these alterations have to be

within physiological limits. Heavily changing the stem cell energy metabolism by altering the surrounding glucose or oxygen levels also interferes with fate decisions (Teslaa and Teitell, 2015; Xu et al., 2013).

A 48 hour window can still allow assaying stem cells for optimal differentiation protocols. As described in this chapter, the differentiation of mESC to neuro-ectodermal progenitors normally takes four days to attain over 75 % differentiation with the standard N2B27 protocol (Ying et al., 2003), however, by adding 10^{-8} M RA to the medium, detectable differentiation could already be observed after two days (Figure 3.14). In this particular case, RA is known to target multiple pathways (Lu et al., 2009) and hence this sole molecule can efficiently direct differentiation to Sox1+ neuro-ectoderm. Similarly, for endoderm (Li et al., 2011) and mesoderm (Torres et al., 2012) lineages, combinations of small molecules, protein and growth factors are already being explored to increase differentiation efficiency. For instance, from the study performed by Li et al. it is proven that chemical activation of canonical Wnt signaling pathway by lithium chloride (LiCl) could synergize with Activin A-mediated Nodal signaling pathway to promote induction of definitive endoderm (DE) cells, and inhibition of Bmp4 signaling by Noggin along with Activin A/LiCl further improved the efficiency of DE cell differentiation. It is clear that combination screens are necessary for investigating stem cell differentiation and so far the progress is impeded by the lack of robust and high-throughput tools. Although, the droplet-based microfluidic platform only allows limited survival, many stepwise differentiation protocols are described in literature (Kanke et al.; Li et al., 2003). Hence, the assay duration might not necessarily be a limiting factor as long as suitable early lineage markers can be identified.

Furthermore, pluripotent epiblast stem cells (EpiSC) are gaining attention because of the molecular and phenotypic similarity between mouse EpiSC and human ESC (Jang et al., 2014; Najm et al., 2011; Tesar et al., 2007). Screening with these mouse cells might make the results directly adaptable to human stem cells. These mouse EpiSCs derived from post implantation epiblast embryos are in a ‘primed’ state for differentiating, hence, unlike ‘naïve’ state mESCs they are capable of differentiating faster into the germ layers. This means that screening with EpiSCs might allow assessing more lineage marker expression within the 48 hour time window.

In conclusion, the droplet-based combinatorial screening platform described in this chapter has been optimized for assaying stem cell niches to find optimal differentiation protocols that can

potentially be useful for regenerative medicine. Additionally, the screen results can also be used to understand underlying mechanisms of fate decisions which are useful to refine protocols. For example, RA is known to target multiple pathways. One way to know which among the various targets is essential for neurogenesis is by combining RA with specific inhibitors of the target receptors. For this, a selection of compounds from the Food and Drug Administration approved Prestwick library can be used, that are known kinase inhibitors of signaling pathways involved in neurogenesis. Indeed the screen results obtained from the novel platform have to be validated in regular tissue culture, however the platform can tremendously decrease the time, cost and sample requirement for a preliminary screen.

Chapter 4

Semi-compartmentalization

4 Introduction

The previous chapters describe development and application of single-phase and two-phase microfluidic platforms. Despite the many advantages of the individual formats, there are some limitations to using them for cell-based assays which are discussed in this chapter, where a novel approach combining the advantages of single-phase and two-phase microfluidic platforms is presented.

4.1 Need for an approach combining single- and two-phase microfluidics

For cell-based screening assays, droplet microfluidics offers high-throughput and compartmentalization possibilities. However, survival of cells inside droplets is limited to a few days depending on the cell type, because of the inability to renew medium in droplets and remove the toxic metabolites secreted by the cells in droplets (Clausell-Tormos et al., 2008). In addition to this, droplets do not allow any assays that require washing steps, such as immunofluorescence assays. Furthermore, high-resolution imaging in droplets is not easily possible because cells in droplets randomly float into and out of the focal plane. Although these limitations do not exist in single-phase perfusion microfluidic systems where cells are fully accessible, single-phase microfluidics cannot match the throughput offered by droplets systems. To overcome the individual limitations of the two systems, an approach was devised as described here, for combining the individual advantages.

4.2 Working Principle

The novel approach takes advantage of the permeability of PDMS (the material of which microfluidic devices are produced) to chemicals. Studies describing the absorption and diffusion of chemicals (Toepke and Beebe, 2006) and biologically active compounds (Regehr et al., 2009) into PDMS have already been described elsewhere (Figure 4.1). Wang *et al.* found that the absorption of a molecule into PDMS depends on the partition coefficient ($\log P$) (Wang et al., 2012), as measure of lipophilicity of that molecule. As shown in the equation below, $\log P$ is the ratio of concentrations of solute in octanol (a non-polar solvent) to distilled water (Equation 7).

$$\log P = \log\left(\frac{[solute]octanol}{[solute]dH2O}\right) \qquad \rightarrow \text{Equation 7}$$

Wang *et al.* estimated that molecules with $\log P$ values lower than 2.47 show less than 10 % absorption into PDMS, while at $\log P$ values higher than 2.62, more than 90 % absorption occurs (Wang et al., 2012). Indeed for many cell based assays this absorption is unacceptable. Much literature exists to prevent this absorption by various surface treatments (Lei et al., 2011; Roman and Culbertson, 2006; Roman et al., 2005); however, the novel approach described here takes advantage of this phenomenon.

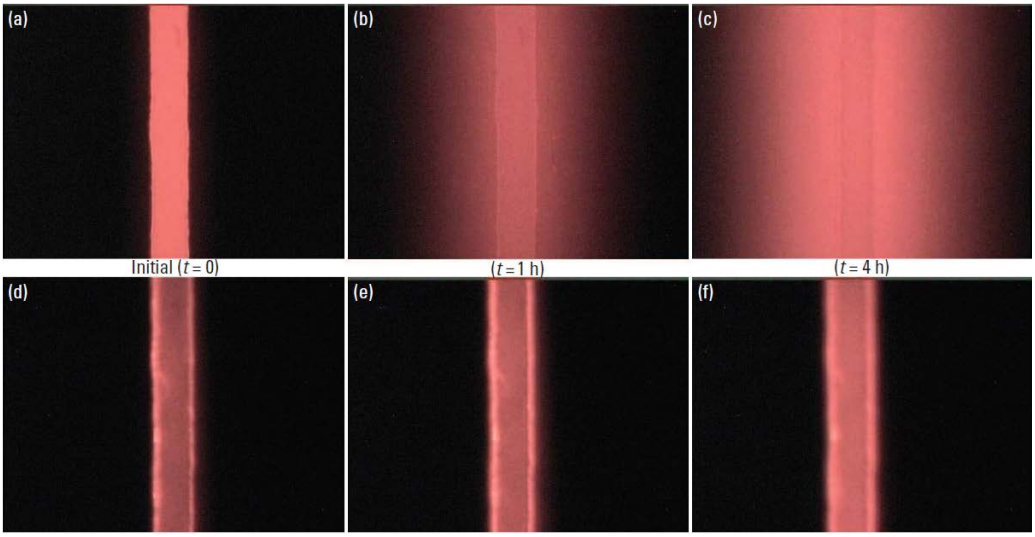

Figure 4.1 Rhodamine B diffusion into PDMS. (a-c) diffusion into untreated PDMS. (d-f) Sol-gel treatment of PDMS (PDMS-SiO_2) prevented this diffusion. Reproduced from (Mukhopadhyay, 2007) with permission from ACS.

The absorption by PDMS is used here to locally expose cells to different concentration of drugs. In more detail, chemically distinct drugs in isolation and in combination can be compartmentalized as plugs using the braille display as described in chapter 3. Instead of co-encapsulating the cells, the cells are seeded in close vicinity to the plugs, making the cells accessible to perfusion. This can be done by either seeding the cells in a separate neighboring channel, or by growing them over the plug channel separated by a membrane (detailed in section **4.3**). Since in this new approach, the compounds in the plug compartments are allowed to diffuse out of the plug, through the PDMS, to reach the cells, it was termed: "semi-compartmentalization". The ability of compounds to diffuse into plugs has already been demonstrated by Shim and co-workers (Shim et al., 2011), and a similar principle is employed here.

4 Results

4.3 Microfluidic chip design

The semi-compartmentalization approach can be implemented in two ways:

1. The parallel channel method allows culturing cells as a continuous stretch inside a channel, that runs parallel to the channel containing the array of plugs with different compounds (Figure 4.2A). The two channels are separated by a PDMS channel wall of 100 µm thickness through which the compounds diffuse and locally form a gradient over the cells. In this method, although the cells are accessible to washing and perfusion, there can be no flow in the cell channel during compound exposure. This is because flow will cause cross-contamination and disrupt the local gradients of compounds. No perfusion implies that there can be no medium renewal during compound exposure. To still allow supply of nutrients, a third channel was designed close to the cell channel through which fresh medium was infused constantly, thus allowing the media components to diffuse to the cells (Figure 4.2C).

2. The membrane method allows simply culturing cells on top of a PDMS membrane that is used to seal the channel containing the array of compound plugs (Figure 4.2B). The microfluidic chip design (Figure 4.2D) in this method, merely has one single serpentine channel and instead of sealing off the channel with glass, as done in the traditional chip fabricating procedure, a thin (100 – 150 µm) PDMS membrane is used. The membrane allows diffusion of the plugs and spotting of drug gradients which locally influence the cells above. Since in this method the cells are exposed to the exterior, the culturing can be performed similar to conventional tissue culture (Figure 4.2B).

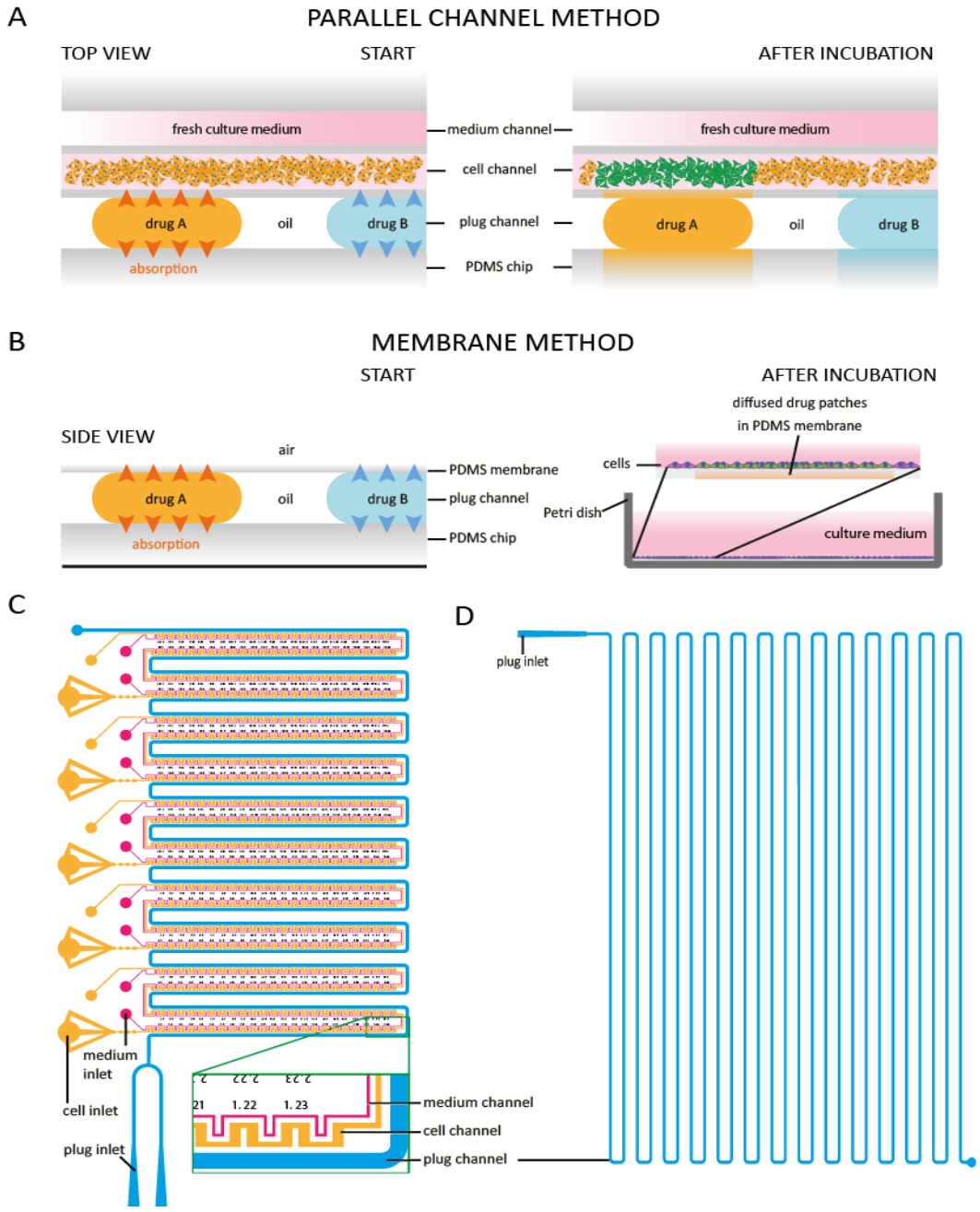

Figure 4.2 Semi-compartmentalization experimental design. (A) The parallel channel method, where one channel hosts the plugs containing drugs and the other channel hosts the cells. The drugs diffuse through the channel walls and reach the cells. (B) The membrane method, where the cells are seeded on a membrane above the channel containing the plugs. The cells on top of the membrane are exposed to the exterior and can be cultured similar to conventional tissue culture procedures. (C) Design of the parallel channel chip with channel functions as indicated in the zoom in. (D) Design of the chip for the membrane approach with just a long serpentine plug channel. Data published in (Eicher et al., 2015).

4.4 Assessing diffusion of drugs

As described above, diffusion of compounds through PDMS depends on the partition coefficient (Wang et al., 2012). PDMS being hydrophobic (Bodas and Khan-Malek, 2006) absorbs compounds with high partition coefficients. The higher the $\log P$ value the greater the absorption. The average $\log P$ value of drugs was determined as 1.80 by Lipinski and co-workers (Lipinski et al., 2012). However, other studies reported $\log P$ values of drugs close to 2.5 for synthetic oral drugs (Proudfoot, 2005) and 3.1 to 3.4 for industrial collections (Macarron et al., 2011). In order to make our approach compatible with drugs having different properties, two fluorescent dyes, Nile red ($\log P$ = 5) and fluorescein ($\log P$ = -0.67) with partition coefficients covering the entire spectrum of drugs, were chosen for experimenting as representatives.

Fluorescein, being strongly hydrophilic, showed no absorption into PDMS while Nile red quickly (within seconds) got absorbed into PDMS. This indicated that treating the PDMS to make it more hydrophilic and less hydrophobic was required to promote the absorption of fluorescein while dampening the absorption of Nile red. Typically, oxygen-plasma treatment, which is also used for bonding PDMS to glass to produce a chip, renders the channels hydrophilic (Bodas and Khan-Malek, 2006). However, the duration of the treatment was short (1 minute) which only made the channel walls hydrophilic. Increasing the duration of treatment to 3 hours at full power, made the whole chip hydrophilic and to maintain this hydrophilicity and dampen excess diffusion, the chip was kept soaked overnight at 65 ^{o}C in phosphate buffer saline (PBS) prior to experiments.

To test the absorption and diffusion of the fluorescent dyes after plasma treatment, a simple set-up was designed. This set-up had a source well on a PDMS slab where the dye was added and three sink wells around it containing distilled water (dH_2O) (Figure 4.3A). The diffusion of the fluorescent dye was measured by comparing the intensity of fluorescence in the source and sink wells at the start and end of the experiment. As shown in Figure 4.3 (B and C), the plasma treatment promoted the diffusion of hydrophilic fluorescein (10 µM) while dampening the diffusion of hydrophobic Nile red (150 µM).

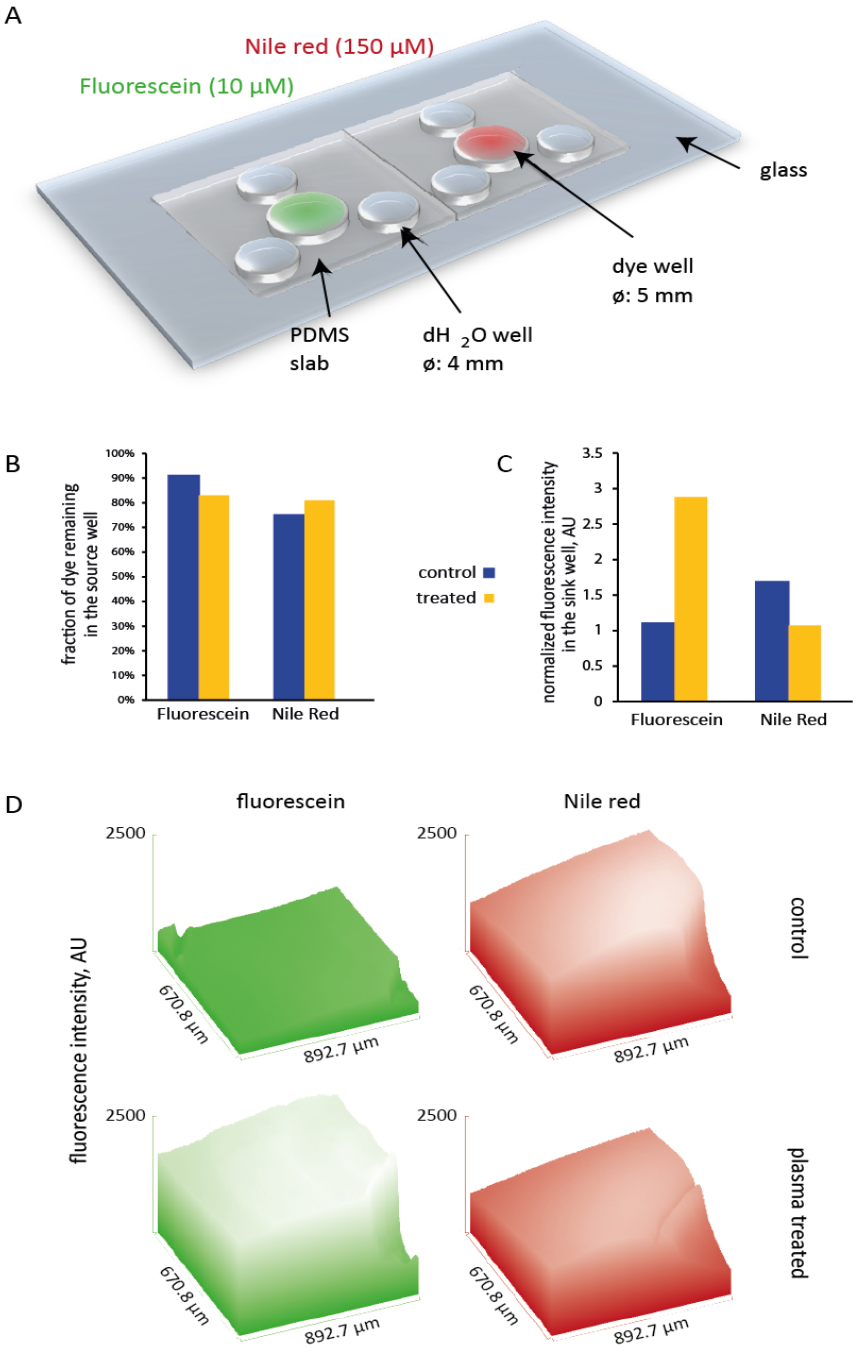

Figure 4.3 Diffusion of fluorescent dyes altered by plasma treatment. (A) The test set-up with a source well containing the dye and three sink wells at equal distance (1 mm) around it containing dH_2O. (B-C) Plate reader measurement of the fluorescence remaining in the source well (B) and diffused into the sink well (C). (D) Surface plot micrographs (generated using ImageJ) of source well walls facing the sink wells after incubation. Data published in (Eicher et al., 2015).

To demonstrate the diffusion of drugs, two drug molecules were chosen: tetracycline ($\log P$ = 0.62) and minocycline ($\log P$ = 2.12) with different partition coefficients. Minocycline is a derivative of tetracycline and hence structurally closely related. To test the diffusion of these two drugs a simple set-up with PDMS wells sealed by a membrane was used. The set-up was plasma treated and soaked as stated above, however, unlike for fluorescent dyes where a sink well can be used to assess the diffusion, here drug inducible cellular GFP expression was used to determine if and how much diffusion occurred. The HeLa TRex™ cells used for these experiments express GFP upon induction by tetracycline (Castello et al., 2012). Since minocycline is a derivative of tetracycline, both the drugs can induce GFP expression in HeLa cells. The set-up is designed such that the cells were seeded on the reverse side of the membrane to where the drug was spotted to measure diffusion through the membrane. Figure 4.4 (A and B) shows a schematic of the set-up and the expression of GFP in cells upon exposure to different concentration of tetracycline and minocycline.

When a similar diffusion experiment was mimicked in a parallel channel chip with the plug channel simply replaced by a loop that can be filled, diffusion of the drugs could be observed. In addition, this experiment showed a gradient of GFP expression along the length of the channel (Figure 4.4C). This demonstrated that the semi-compartmentalization approach is useful to not only study the effect of drugs but potentially also allows monitoring the drug affect at different concentrations.

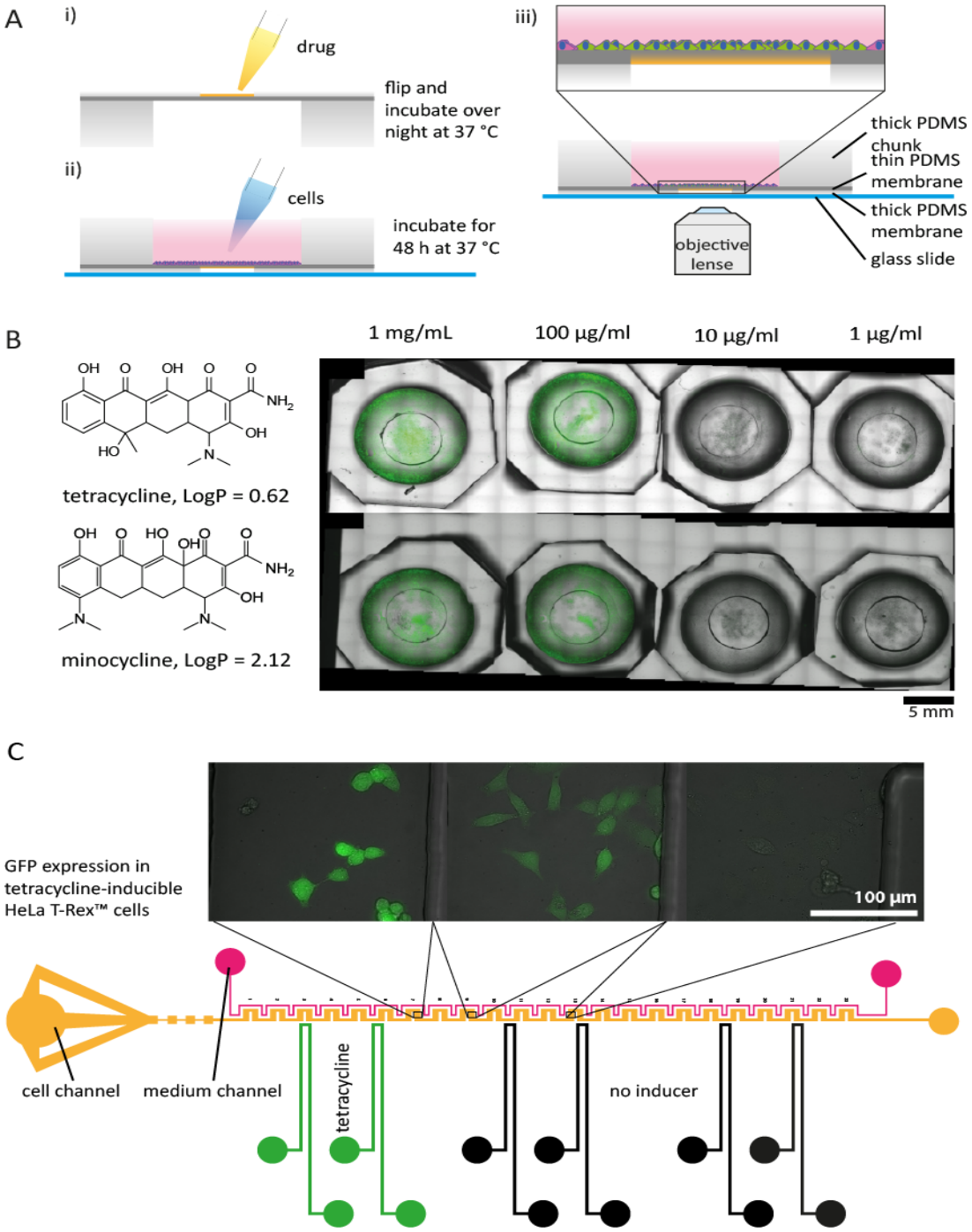

Figure 4.4 Diffusion of drugs through PDMS shown by induction of GFP in HeLa TRex™ cells. (A) Schematic of the experimental set-up. (i) The drug was dispensed into the smaller of the two wells separated by a membrane and incubated overnight at 37 °C. (ii) In the following day cells were seeded into the larger well and incubated. (iii) After 48 hours the cells were imaged using a fluorescence microscope. (B) Difference in GFP expression between cells incubated with the two drugs: tetracycline and minocycline at different concentrations. (C) A similar induction experiment with tetracycline performed in a representative parallel channel chip with the plug channel replaced by a loop for easier handling. Data published in (Eicher et al., 2015).

4.5 Troubleshooting culturing cells on PDMS

Microfluidic devices fabricated with PDMS are gas permeable and biocompatible. Several perfusion microfluidics have been demonstrated for culturing cells (Huang et al., 2013; Hung et al., 2005) and are also commercially available (ibidi® flow chambers). However, in our parallel channel approach, since the gradients are passive and can be washed away by flow, the cells have to be cultured in static medium conditions without the possibility of medium renewal. Nonetheless, the integration of a third channel (as explained in section **4.3** and Figure 4.2C) with a constant medium flow, and immersing the entire chip in medium (Figure 4.5), sustained the cells with the diffused medium nutrients but the cells showed a tendency to migrate towards the medium flow inlet (data not shown). This migration of cells is not desirable for our assay because of the different compound gradients at different position of the chip. From the direction of migration, it was reasoned that this could be because of depletion of gas or nutrients along the serpentine delay line. To avoid this, several medium inlets were integrated in the design.

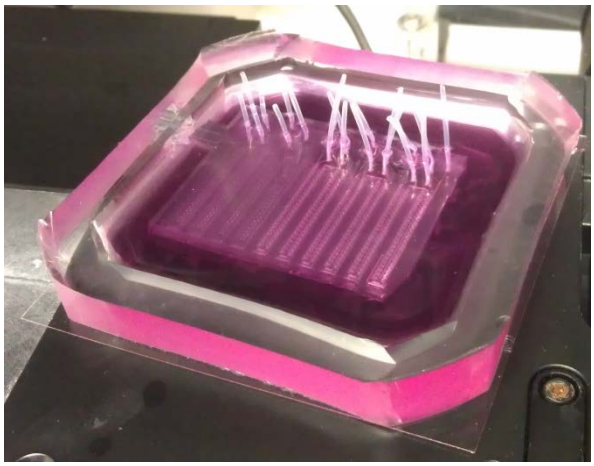

Figure 4.5 A fully set-up semicompartmentalization chip immersed in media. The short tubing inserted in some of the inlets was to prevent medium entry into the plug channel.

Assays for up to 48 hours could still be demonstrated, however, for long-term assays, the membrane method was more reliable. Furthermore, immunostaining experiments involving several washing steps might generate shear forces causing detachment and loss of cells when cultured inside channels. Hence all further experiments were performed by the membrane method.

4.6 Localized perturbation of cell population with tetracycline

To demonstrate the possibility of using the membrane method for locally perturbing cells with different drugs, the same HeLa TRex^{TM} cells as above were used. However, the cells were cultured on the PDMS membrane instead of inside a channel (see section 4.3). Using the braille display, plugs of tetracycline (1 mg/ml) were produced and loaded into the serpentine channel shown in Figure 4.6A. A blue dye was added to the plugs to clearly visualize them. Once the entire channel was filled with nicely spaced tetracycline plugs, the channels were sealed with liquid PDMS that solidified in the inlet crevice. This sealing prevented evaporation and movement of plugs. This whole set-up was incubated in 37 ^{o}C overnight to facilitate absorption and diffusion.

Following this, the plugs were all flushed out with oil. Then the chip was flipped and placed on a tissue culture dish. A dense suspension of HeLa TRex cells were seeded on the chip and the cells were incubated at 37 ^{o}C in a humidified atmosphere with 5 % CO_2. After 48 hours, the chip was flipped again with the cell side placed on a glass coverslip for imaging. An image of the whole chip is displayed in Figure 4.6B. It is evident from the image that there is local induction of GFP within the cell population (Figure 4.6C). Comparing the position of the plugs with the GFP expression it was confirmed that the GFP expressing cells co-localized with the position of the plugs (Figure 4.6D). Furthermore, based on the spacing of the plugs, the areas of GFP expression were clearly separated, proving that no significant level of cross-contamination occurred. Figure 4.6D shows an overlay of the plugs with the cells.

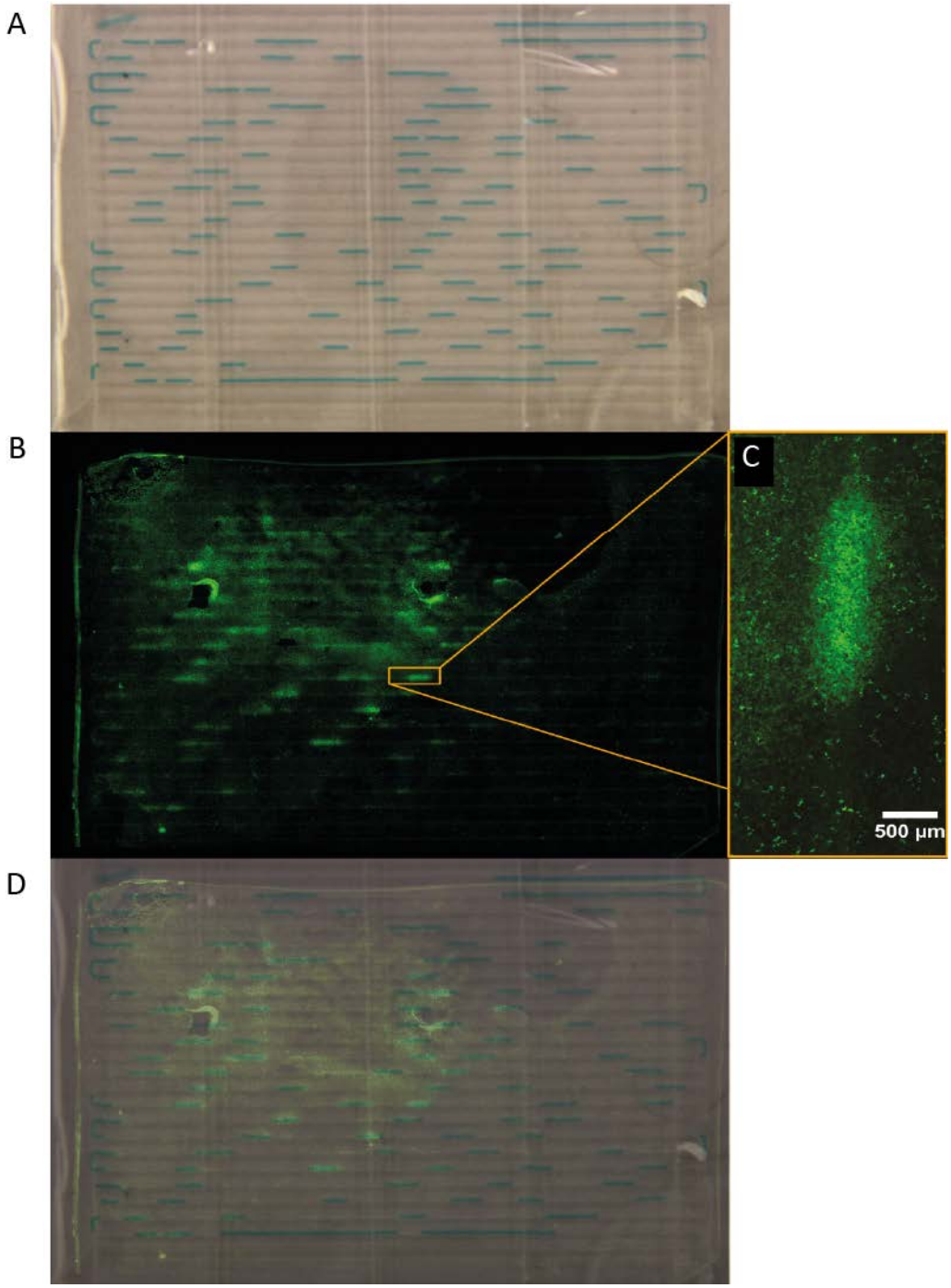

Figure 4.6 Localized induction of GFP expression using the membrane method. (A) Position of the plugs in the serpentine channel after sealing them. (B) Fluorescence image of the entire chip with cells expressing GFP (C) Zoomed in view of an area on the chip where there is local induction of GFP expression. (D) Overlay to compare the regions of GFP expression with the location of plugs.

4 Discussion and future prospects

A novel approach for cell-based drug screening is demonstrated. The approach uses fewer cells than a conventional microtiter plate screen. The approach should also allow high content screening, given the high magnification that can be achieved as suggested in Figure 4.6C. Furthermore since the cells are freely accessible, immunostaining experiments with several washing procedures are potentially possible thereby circumventing the individual limitations of droplet-based and perfusion systems. However, the novel approach exploits absorption of PDMS as a means of locally delivering drugs to sub populations of cells. Since diffusion through a material like PDMS depends on the partition coefficient of the molecule (Wang et al., 2012), not all molecules diffuse at the same rate. For this reason, Upadhyaya S. and Sevaganpathy R. used a microfluidic device sealed with a nanoporous membrane through which drugs can diffuse and locally induce cells above the membrane (Upadhyaya and Selvaganapathy, 2010). However, the throughput (in terms of the number of unique drugs that can be screened at a time) offered by this system is limited to the number of channels that can be embedded under the nanoporous membrane (four channels were reported). In order to increase this throughput, droplet microfluidics was integrated. Since droplets are aqueous phase (containing the drugs) in oil carrier phase, a hydrophobic surface (such as PDMS) is necessary to produce and maintain the droplets without cross-contamination. Nonetheless, plasma treatment allowed the PDMS to be made hydrophilic, while the channel walls containing the plugs could be maintained as hydrophobic by silane (SiO_2) treatment. This enhanced the diffusion of hydrophilic drugs and dampened the diffusion of hydrophobic drugs.

Thus, the experiments reported in this chapter reveal that although absorption and diffusion of compounds vary based on the physical properties, it is possible to alter the diffusion by various chemical treatments of the chip. For a large-scale screening it would also be possible to separate drugs based on their partition coefficients (available in chemical databases) and treat the PDMS chip accordingly.

Chapter 5

General Conclusions

In this thesis, novel devices based on single and two-phase microfluidics are described for biological applications. For preferendum and chemotaxis experiments, single phase microfluidics have tremendous advantages over other approaches for both cell-based and organism-based assays. These advantages include the possibility to: (1) produce both spatial and temporal gradients with sub-cellular precision and (2) expose cells and organisms to different conditions simultaneously. Together, these can be used to mimic natural dynamic environments in unprecedented ways and allow, in combination with time-lapse imaging, the examination of individual as well as group behavior in response to multiple chemical conditions. These features are used here to analyze for the first time, the ecological preferendum of zooplankton - a vital player in the marine food web. For actively swimming zooplankton, that are capable of choosing their preference, a method that allows exposing them to different conditions through which they can freely move and choose is required. So far, the possibility to produce layered water with several different conditions through which zooplankton can swim and choose had not been demonstrated. Here, microfluidics was used to not only perform preferendum measurements to environmental parameters but also to study biotic interactions.

In addition, the portability of microfluidic devices allowed performing experiments in remote marine stations at Roscoff and Banyuls-sur-Mer. This possibility is especially useful because not all plankton species can be transported as fully viable to laboratories. Further, until very recently (22nd May 2015), only about 11,000 of the approx. 150,000 plankton species were documented (de Vargas et al., 2015) and many are yet to be discovered. Hence, there are no established culturing conditions for most of the plankton species. For these reasons, the ability to perform preference measurements directly in remote locations makes microfluidics an attractive tool for marine ecology studies.

Furthermore, the possibility of phenotypic sorting, by only integrating minor modifications in the design of the presented device, can potentially allow isolating specimen of interest for further sequencing analysis. One way of achieving this is to separate the two 4 x 4 mm chambers in the existing design (Figure 2.5A) into several sub-chambers that can allow hosting one plankton per sub-chamber. Since the laminar flow is established perpendicular to the chamber divisions, the plankton in every chamber can still move laterally within the flow gradient to choose their preference. It is also possible to individually load and recover plankton using a micropipette from the chamber, as documented in this thesis. However,

the throughput of this method is limited by the number of parallel sub-chambers that can be designed in one device, since diffusion occurs when laminar streams travel together over long distances (see section **1.2**). Another way of achieving the isolation of specimen without compromising throughput is by the integration of valves. For instance, the 4 x 4 mm chamber of the existing design can be modified to have ten outlets matching the ten inlets. A valve (like the braille valve described in **Chapter 3**) can be integrated at each outlet which, in the "closed" position, only allows the flow of liquid while the plankton is prevented from being washed away. The valves can then be controllably opened after a stable distribution of plankton is achieved in the chamber, and plankton of interest can be isolated, fixed and taken to laboratories for further genetic analysis.

Droplet (Plug) microfluidics, in contrast, has the potential of generating individual micro compartments at a kilohertz frequency (Park et al., 2011). These systems are useful for HTS approaches and a fully integrated microfluidic system that allows the generation of barcoded combinatorial mixtures in water-in-oil plugs is described here. Additionally, the possibility to screen for specific phenotypic effects of these combinatorial mixtures on stem cells (such as: neuronal differentiation) is shown. A preliminary two condition screen, with and without RA, demonstrates the usability of the system for screens with stem cells. Nonetheless, by using all the 29 inlets in the braille display, 406 pairs of combinatorial mixtures can be generated as explained previously in section **3.1.2**. It is important to note that this can be achieved with just the braille display without any additional equipment. Together with an autosampler the throughput can be further increased by feeding in compounds from 96 well plates into one of the inlets on the braille chip. In a proof of principle experiment, Federica Eduati, EMBL-EBI and Ramesh Utharala, EMBL have used the coupled system and generated 206 different sample combinations for a screen with mammalian cancer cells (unpublished data). The number of combinations that can be generated using this approach can be further increased, by feeding entire chemical libraries, from several 96 well plates, using the autosampler. In the field of stem cells, the possibility for such HTS approaches is attractive for applications in regenerative medicine. Chemical perturbation approaches for differentiation and generation of iPSCs are often favored over transgene approaches (Hou et al., 2013). One reason for this is the potential oncogenicity of transgene methods (Zhao et al., 2011) that hinders application in regenerative medicine. The current method used for such HTS, involves microtiter plates. Given that a maximum of 100 cells are required per plug generated using a microfluidic

device, in the traditional method, the cell requirement is at least 10 folds higher even when using 1536-well plates (Griner et al., 2014). In fact due to technical difficulties such as sample evaporation and cross-contamination because of bridging between wells (Dove, 1999), 1536-well plates are not as widely used as 384 or 96 well plates for screening, and the latter require even larger cell numbers and reagent volumes. To achieve the population sizes necessary for HTS in microtiter plates, excessive cell proliferation beforehand which might contribute to the accumulation of mutations, particularly in rare stem cell samples. Thus, two of the main limitations of current HTS approaches on cell cultures are overcome with the microfluidic approach presented here.

Aside the stem cell screening applications to our microfluidic system, the ability to use primary tumor cells from patient biopsies allows screening for personalized medicine. In addition to this, small-molecule combinatorial screens are vastly performed for identifying efficient antibiotic combinations to prevent multiple drug resistance (Aaron et al., 2000; Tateda et al., 2006). Such screens can be performed in microfluidics with the infectious strains from the patient. These are just a couple of examples to suggest the broader applicability of our system. However, one limitation of the droplet microfluidic system is the impracticality of the droplet to medium renewal which can limit survival of the biological sample. Although drop manipulations as described in section **1.3** are possible, staining experiments involving several washing steps to mark a certain phenotype remain to be demonstrated.

With the semi-compartmentalization approach discussed in **Chapter 4**, a part of the drawbacks of droplets are circumvented. Since the approach allows assaying with freely accessible cells, there is no survival issue but the approach can only be used with adherent cells. Furthermore, since the cells are cultivated as a monolayer on a PDMS membrane and then locally (a subpopulation of cells) exposed to drugs; there can be interactions between neighboring populations of cells. While this might be undesirable for some applications, these interactions between neighboring populations can be employed to study cell-cell communications like paracrine signaling.

In conclusion, novel microfluidic devices have been devised for different applications in biology. Firstly, making use of the behavior of miscible liquids in microfluidic device, it was possible to generate laminar co-flows of different sea water conditions, such as different

pH and salinity. This possibility enabled exposing marine zooplankton to different conditions through which they can freely move and choose. By this marine zooplankton were exposed to different conditions through which they can freely move and choose their preferred environment. Based on their choices, a preferendum was estimated which can increase our understanding on how environmental changes can affect the zooplankton communities. Secondly, the possibility to generate combinatorial mixtures in droplets at a high-throughput was demonstrated for cell-based chemical screening assays. In addition, the ability to use the novel approach for screening with rare cells like stem cells has been demonstrated. Although such chemical screens are already performed in microtiter plates, microfluidics allow using significantly low cell numbers and reagent volumes. Lastly, an approach that allows cell-based screening while enabling high content screening with freely accessible cells has been reported. On the whole, in this thesis, microfluidics has been used for a variety of biological applications which suggests the broad applicability of the device. However, in the present state, microfluidics still requires validations of results using conventional methodologies such as microtiter plate for cell-based screening.

Chapter 6

Materials & Methods

6 Materials and Methods

6.1 Microfluidic device fabrication

Standard soft-lithography technique (Brittain et al., 1998; Qin et al., 1998) using polydimethylsiloxane (PDMS; Sylgard 184 silicone elastomer kit, Dow Corning Corp.) was used to fabricate all microfluidic devices in this thesis.

6.1.1 Designing using AutoCAD and photomask printing

All microfluidics devices used in this thesis were designed using computer aided design software called AutoCAD (Autodesk Inc.). The designs were either drawn based on pre-existing devices in the lab or literature or newly conceived to suit the purpose. These designs were then sent to an external company (Selba S.A., Versoix Switzerland) for printing a photomask. The photomasks have a high resolution of 25400 dpi and are printed on transperancy sheets. Depending on the requirement they are printed either as positive (clear background, dark design) or negative (dark background, clear design) mask.

6.1.2 Mold manufacturing

Molds for microfluidic devices were prepared from the photomask using photolithography. For producing molds with square channel geometry, a negative photomask and SU-8 photoresist (MicroChem Corp., Newton MA) was used and for round geometry a positive photomask and AZ®40XT photoresist (MicroChemicals GmbH, Ulm) was used. In this thesis, only the Braille chip required round channels to allow proper closing of channels using the round braille pins, for all other applications, a negative photomask and SU-8 photoresist was used. For SU-8 photoresist, depending on the desired height of the channel, different viscosity of the photoresist was used. For example, SU-8 2075 is used to attain a channel depth ranging from 75 to 150 µm). Once the choice of photoresist is made, about 5 ml of the resist is poured on a heat dried silicon wafer (3 or 4 inches; Siltronix, France or Silicon Materials, Germany). The resist is then uniformly spread on the silicon wafer using a spin coater. For positive photoresists mainly, an additional adhesion promotor (Ti prime; Micro Chemicals GmbH) was spin coated prior to coating with resist. After spin coating of the resist a series of soft-baking procedures at different temperatures are followed. The duration of the baking is dependent on the height of the channels aimed for. The

information on temperatures and duration were followed from the manufacturer's manual. Following the soft baking, the photomask is placed on the resist and exposed to ultra violet (Wang et al.) light using a mask aligner (Karl Suss MA45) for about 90 to 120 seconds. Photo-crosslinking occurs at regions exposed to the UV (for negative photoresist) thereby transferring the pattern on the photomask to the resist. The photomask was then removed and can be reused to make more molds of the same pattern. The cross-linking of the resist was completed by another series of post-baking procedures in the suggested temperatures and times from the manual. Finally, the wafers were developed using mr-Dev 600 (micro resist technology GmbH, Berlin) for negative photoresist and AZ 726 MIF developer (AZ electronic materials GmbH, Germany) for positive photoresist. This step removes all non-cross-linked photoresist leaving the structure of the channel behind. Lastly, a hard baking procedure was performed at around 150 ^{o}C. This step solidifies the structure on the mold and in the case of positive photo resist, this final heating step allows the photoresist to reflow and soften their edges making the structures rounded.

Silanization of the mold using trichloromethylsilane (TCMS) (abcr GmbH & Co. KG, Germany) prevented the structures on the mold from being destroyed while producing PDMS chips. This was done by simply placing a drop of the chemical next to the mold in a closed glass Petri dish for an hour. The height of the attained structures was either measured using a Surface Profiler Profilometer (Faulhaber) (for structures < 110 µm) or a regular wide field microscope (for structures > 110 µm).

6.1.3 Casting PDMS on molds

Finished molds were placed on plastic Petri dishes and filled with freshly prepared and degassed PDMS mixture. For chips a 10:1 ratio of elastomer PDMS:curing agent was used. All air bubbles were degassed using a vacuum desiccator and the dishes with the mold and the PDMS mixtures were baked in a 65 ^{o}C oven overnight (or for a minimum 4 hours).

6.1.4 Producing PDMS membranes

Membranes of PDMS were made using a 20:1 mixture of degassed PDMS mixture. A transparency sheet (1/8th of a standard A4 size) was used to spin coat the PDMS mixture into a uniform sheet. A speed of 700 rpm for 30 s was used on the spin coater as a standard procedure for making membranes of the same thickness.

6.1.5 Assembling a microfluidic chip

To assemble a chip for experiments, the cast PDMS was cut using a scalpel and peeled off the mold. Thus the PDMS retains the channel structures on one side. Access holes are punched using biopsy punches (Harris Unicore) all the way through the structures to the other side making it possible to access the channels after they are sealed. Different sizes of biopsy punches exists depending on the size of the tubing used for experiments (see section x). Pressurized air from an air gun and sticky tape was used to remove any unwanted particles from the PDMS. The chip was then completed by covalent bonding of PDMS (on the structured side) to a glass (Menzel Gläser, Thermo Fisher Scientific Inc., Germany) or a PDMS membrane. The bonding was achieved by exposing the surfaces that needed to be bonded to oxygen plasma generated using a plasma oven (Femto, Diener electronic GmbH & Co. KG, Germany), and then bringing them in contact with each other. The plasma treatment for producing chip was usually done for 1 minute at 2.5 V in the presence of oxygen. To facilitate boding without any delamination, the chip was placed in the 65 ^{o}C oven or hotplate for at least 1 minute.

6.1.6 Treating channel surfaces

For experiments with two phase microfluidics, a hydrophobic channel surface is required. Two methods were followed to treat surfaces. The first method involved purging the channel with a 1 % solution of 1H,1H,2H,2H,-perfluorooctyltrichlorosilane (abcr GmbH & Co. KG, Germany) in Novec^{TM} 7500 oil (3M Company, St. Paul MN), and rinsing it with pure Novec^{TM} 7500 oil. Alternatively, Aquapel (Autoserv, Germany) was used in some experiments instead of the 1 % silane solution.

6.2 Allied equipment

6.2.1 PTFE Tubing

Polytetrafluotoethylene (PTFE) tubing (Adtech Polymer Engineering Ltd, UK and APT Advanced Polymer Tubing GmbH, Germany) were used in all experiments. Tubing were used to connect the syringes via needles (Becton, Dickinson and Company) to the chip inlets, for the outlets and for connecting any two points in a chip setup. Different tubing diameters and thicknesses were used based on the purpose. For example, TW24 tubing

with the big inner diameter (ID) of 0.59 mm was used for infusing cells into chip for encapsulation. The range of tubing used in this work can be found in the table below.

Adtech name	APT name/AWG size	Specifications (ID; OD; wall thickness in mm)
UT3	P1000,30x0,101	0.3; 0.4; 0.10
UT6	P1000,60x0,101	0.6; 0.8; 0.10
HW30	AWG30S	0.32; 0.76; 0.23
TW24	AWG24T	0.59; 1.06; 0.25

6.2.2 Syringe pumps

For all experiments in this work, fluids are infused into the microfluidic device at specific flow rates using positive displacement syringe pumps (Harvard apparatus, Holliston MA or World Precision Instruments, Sarasota FL).

6.2.3 Braille display

The braille display used in Chapter 3 and 4 is made by KGS Corporation, Japan. To adapt the braille for our experiments, our in-house mechanical workshop built a metal case and a chip holder made of transparent Plexiglas® (to allow aligning braille pins to the chip) to grip the chip in position above the pins as shown in Figure 6.1.

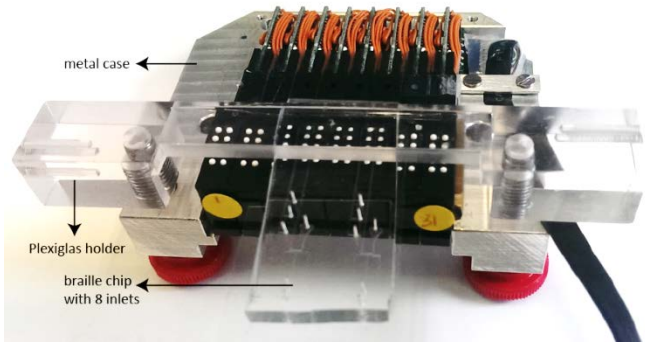

Figure 6.1 Braille display with a microfluidic chip

6.2.4 Autosampler

For initial semi-compartmentalization experiments, plugs were generated using an autosampler (Dionex UltiMate® 3000 Analytical Autosampler WPS-3000 SL, Thermo Fisher Scientific Inc.) instead of a braille display, as described by Clausell-Tormos and co-workers.

(Clausell-Tormos et al., 2010). For future experiments using the braille display to generate combinations in plus, the throughput can be increased by integrating the autosampler.

6.2.5 Microscopy and Spectroscopy

6.2.5.1 Microscope and Camera

Standard inverted light microscope (Eclipse Ti-S, Nikon GmbH, Germany) was used for imaging inside microfluidic devices. A halogen fiber illuminator (Nikon Intensilight C-HGFI, Nikon GmbH, Germany) was used as a fluorescence light source in fluorescence microscopy. Images were recorded using a CCD camera (Hamamatsu ORCA-05G, Hamamatsu Photonics Deutschland GmbH, Germany) for long exposure times. For high speed, color recordings with short exposure times of drop generation etc. a Motion BLITZ® EoSens® mini1 camera from Mikrotron GmbH., Germany was used. A custom setup of µManager program (http://www.micromanager.org (Edelstein et al., 2010)) was used to control microscope components, such as stage controller (Prior ProScan III, Prior Scientific GmbH, Germany), fluorescence and bright field shutters and CCD camera.

A USB microscope (dnt DigiMicro scale) was used in some experiments as a handy microscope For example, for zooplankton chemotaxis experiments; these portable microscopes allowed making experiments in remote locations at marine stations where there are no regular microscopes available.

6.2.5.2 Optical setup for plug measurements

For spectroscopic plug measurements, a customized optical setup was built as depicted in Figure 6.2. The setup comprises of a vibration-reduced/free breadboard fitted next to the standard inverted microscope. Several dichroic mirrors and photomultiplier tubes (PMTs) are aligned on the breadboard which focusses and detects the laser signals respectively from three different lasers. The wavelengths of the lasers are 375 nm, 488 nm and 561 nm. Simultaneous excitation and detection with all three lasers and PMTs is possible allowing three different assay read-outs.

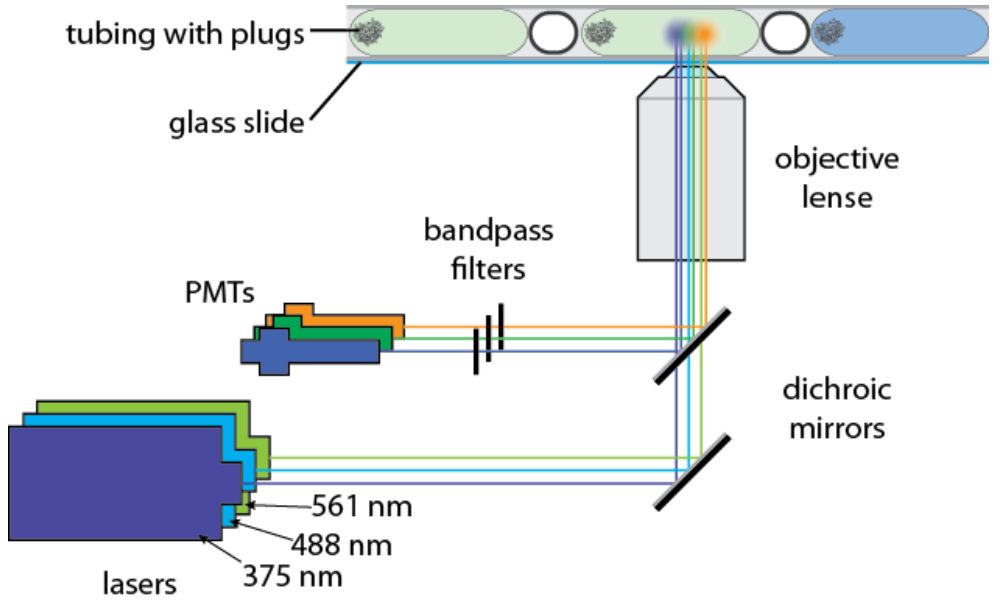

Figure 6.2 Optical setup for fluorescence readout from plugs. Reproduced from Eicher D., 2014 PhD thesis.

6.3 Software

6.3.1 Software for data acquisition and analysis of zooplankton chemotaxis experiments

A screenshot freeware: Auto screen capture 2.0.5 (http://www.softpedia.com/get/Multimedia/Graphic/Graphic-Capture/Auto-Screen-Capture.shtml) was used to capture images every second. These Images (around 300 frames) were cropped and pre-rotated using ImageMagick software (http://www.imagemagick.org/). The tracking of moving objects was done using the motion tracker add-on (http://www.anc.ed.ac.uk/demos/tracker/) for MATLAB 2010, using the following mixture model parameters: alpha 0.1, rho 0.01, background_thresh 0.95. Because the software tends to lose track of animals that remain at a given position for longer periods of time, a custom script was written that iteratively merges trajectories if the animal position at the ends of two trajectories was within 135µm distance. For a recording of the 300 frames (5 minutes), the average track length was 2.5 min, with at least half of the tracks going through at least 50% of the total recording time. In cases where the tracking software lost an animal (e.g., due to animals clustering together), it started a new track and the centroid positions could be determined again. This increases the number of tracks recorded per device, but usually this does not exceed 1.5 times the animal count. Using regular seawater in all ten streams, we have acquired the 'normal' behavioral

repertoire of our animals (Figure 2.5F). Doing so, a cumulative 'random' distribution of animals in the device was obtained and used this distribution as the null-hypothesis for the statistical tests of deviation.

6.3.2 Software for controlling braille display, plug data acquisition and analysis

To control braille display and record data from the plug measurements, a custom software using Lab View was designed by Ramesh Utharala, EMBL. The recordings using this Multi-channel data acquisition program were made with a frequency of hundreds of Hz. Further analysis of the data was done using R with the custom scripts (BraDiPlus package) from Federica Eduati, EMBL-EBI. The package allowed semi-automated data analysis of the raw fluorescence intensity measurements. Based on the visual representation of the fluorescence measured, thresholds have to be set to define the plug sizes and distance between plugs (since these parameters vary between experiments). This further allowed the program to automatically identify and label plugs/peaks and allows further evaluations by isolating different samples and their replicates.

6.3.3 Image analysis for semi-compartmentalization experiments

All image analysis in Chapter 4 were done using FIJI (Fiji is just ImageJ). For a view of the whole chip, several images recorded in a predefined grid with 20 % overlap between frames, were stitched together by using the "Grid/collection stitching" plugin as published elsewhere (Preibisch et al., 2009).

6.4 Protocols for Chapter 2

6.4.1 Plankton breeding

P. dumerilii breeding and preparation was accomplished according to the standard culturing protocol described elsewhere (Fischer and Dorresteijn, 2004). Lab cultures of *P. dumerilii* from the Arendt lab at EMBL, Heidelberg were used for these experiments. For initiating a batch, a male and a female swarming epitokes (mature adult worms) were collected and spawned in a dish to release the eggs which were subsequently fertilized by the sperms. The dish was then maintained at 18 ˚C and exposed to 16 hours of light and 8 hours of darkness to initiate embryogenesis and development. *Tetraselmis marina*, a sessile

green flagellate that can be grown under bright, daylight-type artificial illumination was provided as food source during breeding.

6.4.2 Preparation of pH, saline and algal extracts

The different pH solutions were made by adjusting the pH of sea water using hydrochloric acid (HCl) as an acid and sodium hydroxide (NaOH) as alkali base. The pH values were measured using a regular benchtop pH meter (Sartorius PB11 with glass electrode). For preparing different salt concentrations, sea water was diluted in a ratio of 1:2 with distilled water and then added NaCl to obtain different concentrations (0.75x to 1.25x or 30 g/l to 50 g/l NaCl). Since the sea water is already rich in its salt content, diluting it and then adding NaCl allowed us to control the molar changes of NaCl. Finally, microalgae extracts were prepared by filtering the algae cultures using a 0.22 µm filter and then UV treating the extract for 10 minutes to avoid algal filament formation and proliferation in long term experiments.

6.4.3 Laser ablations

Ablations were done using a Zeiss FluoView 1000 cold laser. During this step, fifteen to twenty larvae were kept in 7.5% magnesium chloride ($MgCl_2$) solution to impede muscle movements. A 40x objective was used and the target cells in the mouth were ablated using multiple one second laser pulses (to avoid cavitation) until the morphology (cell outlines) changed and the tissue ‘caved in’. Animals were used for microfluidic experiments on the same day.

6.4.4 Chemotaxis experiments

Prior to all chemotaxis experiments, the microfluidic chip was made air-free by immersing the entire chip in sea water and degassing it in a vacuum desiccator for at least 15 minutes. Experiments using the laminar flow were performed using a flow rate of 400 µl/h per stream or 4000 µl/h overall, and experiments to generate linear gradients using the gradient generator device were performed at an overall flowrate of 200 µl/h. 5 ml syringes filled air-free with different solutions (example different pH) were connected to the inlets on the device using 22G needles and TW24 tubing. Plankton larvae were manually loaded into the chip through the assigned inlets using a 200 µl micropipette. After fifteen to twenty larvae were loaded, the inlets were tightly sealed using board pins. Larvae were

exchanged between experiments by simply using the micropipette to suck out the existing larvae and adding fresh ones.

6.5 Protocols for Chapter 3

6.5.1 Mouse embryonic stem cell culturing and differentiation

The 46c mESCs were obtained from the authors and cultured and differentiated as described by Ying and co-workers (Ying et al., 2003). Similarly, Sox1-βgeo cells were obtained from Episkopou's lab currently in Imperial College, London and cultured based on their published protocol (Nishiguchi et al., 1998). All mESCs were cultured in 0.1 % gelatin coated dishes with Glasgow minimum essential medium (GMEM; GIBCO Life Technologies) containing 10 % fetal bovine serum (FBS; Sigma-Aldrich) and 100U/ml leukemia inhibitory factor (LIF; produced in-house in the protein expression and purification (PEP) core facility, EMBL) after thawing for at least two passages. Eventually, to culture mESCs for microfluidic experiments, the stem cells grown in 2i+LIF conditions on 0.1 % gelatin coated dishes. The 2i+LIF medium contains: Dulbecco's modified Eagle medium F12 (DMEM/F12; GIBCO Life Technologies), 2.5 ml N2 supplement (Life Technologies), 5 ml B27 supplement (-Vitamin A) (Life Technologies), 5 ml L-Glutamine (Sigma-Aldrich), 3 µl of β-mercaptoethanol (Sigma-Aldrich), 3 µM MEK pathway inhibitor (PD0325901; Reagents Direct), 1 µM GSK 3β inhibitor (CHIR99021; Reagents Direct) and 100U/ml LIF.

The cells were passaged using Stem Pro® Accutase® (Life Technologies) every two days and the medium was renewed daily to propagate the cells in culture. The regular culturing conditions are 37 ^{o}C, 5 % CO_2 and water saturated atmosphere. To monitor their pluripotency, a flow cytometer (BD LSRFortessa^{TM}) analysis with Oct4 antibody (Santa Cruz) was performed every three months.

For differentiation to neuro ectodermal progenitors, the 2i and LIF components were removed from the above medium and the cells were cultured in the DMEM/F12 medium supplemented with N2 and B27 (+Vitamin A) supplements (referred to as: N2B27 medium). The Vitamin A in the B27 supplement is an inducer of differentiation into neuroectodermal progenitors. After 6 days, to continue differentiating the cells into neurons, the cells have to be transferred into laminin coated dishes as described by (Ying et al., 2003).

6.5.2 Stem cell encapsulation into plugs

For encapsulation, mESCs were harvested using Accutase®, neutralized with serum medium and washed with PBS. The cells were then pelleted and re-suspended in fresh N2B27 medium without Vitamin A (basal medium) containing 10 mM HEPES, 40 mM glucose and 0.1 % xanthan gum (Sigma-Aldrich). The xanthan gum is used to keep the cells in suspension in the syringe while encapsulating. This purpose of xanthan gum was previously described for flow cytometry experiments (Freyer et al., 1989) and adapted here. The cell suspension was then passed through a 41 µm Steriflip® nylon net filter (Merck Millipore) to remove any cell clumps. Finally, after counting the cells, 3 million cells/ml were loaded in a 5 ml syringe and a 22G needle with TW24 tubing was used to inject the cells into the braille chip for encapsulation.

6.5.3 Estimating viability of cells recovered from droplets

To evaluate the number of viable cells after a certain period of incubation in plugs, the plugs were first collected in a 15 ml falcon tube. Since the plugs are not stabilized, they fuse when in contact with each other. To the collected emulsion, 10 ml of fresh medium was added and kept upright for 3 minutes. This period allows phase separation of oil from the media. Since the oil is has a higher density than the media, the oil sinks down faster leaving the cells and the media in the supernatant. From this supernatant, 8 ml was carefully pipetted out into a fresh falcon tube without touching the oil phase below. This 8 ml of media with the cells were then spun down at 1200 rpm for 5 minutes causing the cells to pellet. The cells were then washed and trysinized in a 37 ^{o}C water bath to allow individualizing the cells from embryoid bodies that form in plugs. These cells were then stained with Calcein AM (live stain; Invitrogen) and propidium iodide PI (dead stain; Sigma-Aldrich) and counted using a flow cytometer to estimate the percentage of viable cells. In parallel, the stained cells were also manually counted under a microscope to obtain a more accurate measure.

6.5.4 Combinatorial plug production and incubation

Freshly filled 5 ml syringes with the reagents to be screened (such as retinoic acid and other chemicals), are placed on syringe pumps and “primed”: i.e. the pumps are switched to pumping mode until liquid reaches the edge of the tubing connected to the syringe. For these syringes HW30 and 27G needles were used. After priming, the tubing were

connected in the chip inlets and the chip is positioned on the Braille display. The reagent pumps and the pump hosting the cell suspension were all switched to pumping mode at a flow rate of 1000 µl/h. The Lab View program controls the Braille pins which then regulate the flow of liquid either to the T-junction or to the waste outlet. At the T-junction there is a constant flow (200 µl/h) of Fluorinert® FC-40 (Sigma-Aldrich) with 0.5 % 1H,1H-perfluorooctanol (PFO; abcr GmbH & Co. KG, Germany). Further at the exit of the T-junction there is a constant infusion (75 µl/h) of mineral oil (Sigma-Aldrich), this causes the generated plugs at the T-junction to be interspersed by mineral oil. Finally, 6 m long UT6 tubing wound around a 1 l Schott glass bottle or a 50 ml falcon tube was used to collect the generated plugs and store them in the same order as they are produced. The reek of tubing with the plugs were sealed with sticky tape and incubated in a 37 ^{o}C, 5 % CO_2 containing humidified incubation chamber for the assay period.

6.5.5 Plug read-out

For measuring the plugs, one end of the tubing (about 10-15 cm of the end) was fixed on the microscope stage with the end itself placed in a waste collection tube. The other end was connected to a syringe containing pure FC-40 oil. The plugs were slowly moved over the microscope point of focus by infusing the oil at a flow rate of 750 µl/h. The measurements were recorded using the Lab View program described before.

6.6 Protocols for Chapter 4

6.6.1 HeLa TRex^{TM} cell culture

The engineered HeLa cells were obtained from the Hentze group at EMBL, Heidelberg (Castello et al., 2012). These cells were cultured in DMEM medium (GIBCO; Life Technologies) with 4.5 g/l glucose, 10 % FBS and 1 % sodium pyruvate (Sigma-Aldrich). The selection antibiotics: 100 µg/ml hygromycin (Sigma-Aldrich) and 10 µg/ml blasticidin (Sigma-Aldrich) were for at least two passages before using them for microfluidic experiments. The cells were split using Trypin-EDTA (Sigma-Aldrich), neutralized with medium and washed with PBS. Pelleting of cells were done at 1000 rpm for 5 mins and cultured in tissue culture flasks (Nunc^{TM} Thermo Scientific). The cells were split every three days upon attaining 80 % confluency and cultured at 37 ^{o}C, 5 % CO_2 and humidified

atmosphere. To induce GFP expression in culture 1 µg/ml of tetracycline hydrochloride (Sigma-Aldrich) was used.

6.6.2 Plug production and loading for semi-compartmentalization

Plugs containing different drugs were generated in a similar manner as described in **section 6.5.3** but no mineral oil is used in this experiment. The serpentine plug hosting channel was silanized as explained in **section 6.1.6**. To allow loading of plugs directly into the serpentine channel from the braille chip, UT3 tubing was connected from the braille chip outlet to the semi-compartmentalization chip. Instead of connecting the tubing through access hole from the top (as usually done), here the connection to the serpentine channel is made through the side. To allow this, instead of punching an access hole while assembling the chip, the chip was cut at the channel edge allowing the tubing to be inserted through the side (in between the membrane and the chip). This is necessary to prevent plug breakup while being loaded into the chip.

For some initially experiments however, the autosampler was used to produce the plugs (see **section 6.2.4**). The autosampler produced plugs into UT3 tubing which could be connected to the serpentine channel as stated above. FC-40 containing 1.5 % PEG-PFPE amine block copolymer (Raindance; custom synthesized from Sigma-Aldrich) was used as a carrier phase for these experiments.

6.6.3 Seeding cells on chip

The chip was sterilized by exposing the assembled chip to UV for about an hour prior to all experiments. Before seeding the cells inside channels, the channels were washed several times with PBS to remove any leeched un-polymerized PDMS. For some experiments the channels were coated with fibronectin (Sigma-Aldrich) by infusing a 0.1 % solution of fibronectin overnight at a flow rate of 75µl/h in 4 ^{o}C cold room. For the membrane method this coating was easier and done by simply pouring a 0.1 % solution on the membrane and keeping it in a 4 ^{o}C fridge. Seeding of cells was done using a syringe containing a very dense suspension (~5 x 10^{6} cells/ml) of cells into the channel. For the membrane method the cells were simply pipetted onto the membrane and incubated. In entire setup was incubated in a 37 ^{o}C incubator containing 5 % CO_2 and humidified atmosphere for the assay duration.

6.7 Microtiter plate reader measurements

All microtiter plate reader measurements in this thesis were carried out in a Tecan Safire (Tecan Group Ltd., Switzerland) plate reader.

6.8 Flow cytometry

Quantification experiments for counting the number of GFP positive, Calcein and PI stained or antibody stained cells, were done using a BD LSRFortessa^{TM} flow cytometer. The machine is equipped with 5 lasers: 355 nm, 405 nm, 488 nm, 561 nm and 640 nm, for simultaneous measurements of different readout signals.

List of Abbreviations

CPR	Continuous Plankton Recorder
DE	Definitive endoderm
DEP	Dielectric properties
dpf	Day post fertilization
EB	Embryoid body
EC	Embryonal carcinoma
ECM	Extra cellular matrix
ESC	Embryonic stem cell
EpiSC	Epiblast stem cell
FDG	Fluorescein di-β-D-galactopyranoside
FFF	Field flow fractionation
GFP	Green fluorescent protein
HEK 293	Human Embryonic kidney cell
HEPES	4-(2-hydroxyethyl)-1-piperazineethanesulfonic acid
hpf	Hours post fertilization
HSC	Hematopoietic stem cell
HTS	High-throughput screening
ICM	Inner cell mass
iPSC	Induced pluripotent stem cell
LOC	Lab-on-a-chip
mEF	Mouse embryonic fibroblast
mESC	Mouse embryonic stem cell
MSC	Mesenchymal stem cell
NSC	Neural stem cell
NSW	Natural sea water
PDMS	Polydimethylsiloxane
PFO	Perfluorooctotanol
PI	Propidium iodide
PMT	Photo multiplier tube
PTFE	Polytetrafluoroethylene
RA	Retinoic acid

Bibliography

Aaron, S.D., Ferris, W., Henry, D.A., Speert, D.P., and MacDonald, N.E. (2000). Multiple Combination Bactericidal Antibiotic Testing for Patients with Cystic Fibrosis Infected with Burkholderia cepacia. American Journal of Respiratory and Critical Care Medicine *161*, 1206-1212.

Abate, A.R., Hung, T., Mary, P., Agresti, J.J., and Weitz, D.A. (2010). High-throughput injection with microfluidics using picoinjectors. Proceedings of the National Academy of Sciences *107*, 19163-19166.

Abranches, E., Silva, M., Pradier, L., Schulz, H., Hummel, O., Henrique, D., and Bekman, E. (2009). Neural Differentiation of Embryonic Stem Cells <italic>In Vitro</italic>: A Road Map to Neurogenesis in the Embryo. PLoS ONE *4*, e6286.

Aderhold, A., Husmeier, D., Lennon, J.J., Beale, C.M., and Smith, V.A. (2012). Hierarchical Bayesian models in ecology: Reconstructing species interaction networks from non-homogeneous species abundance data. Ecological Informatics *11*, 55-64.

Agarwal, P., Zhao, S., Bielecki, P., Rao, W., Choi, J.K., Zhao, Y., Yu, J., Zhang, W., and He, X. (2013). One-step microfluidic generation of pre-hatching embryo-like core-shell microcapsules for miniaturized 3D culture of pluripotent stem cells. Lab on a chip *13*, 4525-4533.

Agresti, J.J., Antipov, E., Abate, A.R., Ahn, K., Rowat, A.C., Baret, J.-C., Marquez, M., Klibanov, A.M., Griffiths, A.D., and Weitz, D.A. (2010). Ultrahigh-throughput screening in drop-based microfluidics for directed evolution. Proceedings of the National Academy of Sciences *107*, 4004-4009.

Ahn, K., Agresti, J., Chong, H., Marquez, M., and Weitz, D.A. (2006). Electrocoalescence of drops synchronized by size-dependent flow in microfluidic channels. Applied Physics Letters *88*, 264105.

Albrecht, D.R., and Bargmann, C.I. (2011). High-content behavioral analysis of Caenorhabditis elegans in precise spatiotemporal chemical environments. Nature methods *8*, 599-605.

Allen, M.R., Frame, D.J., Huntingford, C., Jones, C.D., Lowe, J.A., Meinshausen, M., and Meinshausen, N. (2009). Warming caused by cumulative carbon emissions towards the trillionth tonne. Nature *458*, 1163-1166.

Anna, S.L., Bontoux, N., and Stone, H.A. (2003). Formation of dispersions using “flow focusing” in microchannels. Applied physics letters *82*, 364-366.

Anthony, K.R., Kline, D.I., Diaz-Pulido, G., Dove, S., and Hoegh-Guldberg, O. (2008). Ocean acidification causes bleaching and productivity loss in coral reef builders. Proceedings of the National Academy of Sciences *105*, 17442-17446.

Au, A.K., Lai, H., Utela, B.R., and Folch, A. (2011). Microvalves and micropumps for biomems. Micromachines *2*, 179-220.

Auroux, P.-A., Iossifidis, D., Reyes, D.R., and Manz, A. (2002). Micro total analysis systems. 2. Analytical standard operations and applications. Analytical chemistry *74*, 2637-2652.

Baraban, L., Bertholle, F., Salverda, M.L.M., Bremond, N., Panizza, P., Baudry, J., de Visser, J.A.G.M., and Bibette, J. (2011). Millifluidic droplet analyser for microbiology. Lab on a chip *11*, 4057-4062.

Baret, J.-C., Miller, O.J., Taly, V., Ryckelynck, M., El-Harrak, A., Frenz, L., Rick, C., Samuels, M.L., Hutchison, J.B., and Agresti, J.J. (2009). Fluorescence-activated droplet sorting (FADS): efficient microfluidic cell sorting based on enzymatic activity. Lab on a chip *9*, 1850-1858.

Barker, N., Huch, M., Kujala, P., van de Wetering, M., Snippert, H.J., van Es, J.H., Sato, T., Stange, D.E., Begthel, H., and van den Born, M. (2010). Lgr5+ ve stem cells drive self-renewal in the stomach and build long-lived gastric units in vitro. Cell stem cell *6*, 25-36.

Beare, D., McQuatters-Gollop, A., van der Hammen, T., Machiels, M., Teoh, S.J., and Hall-Spencer, J.M. (2013). Long-term trends in calcifying plankton and pH in the North Sea. PloS one *8*, e61175.

Beebe, D.J., Mensing, G.A., and Walker, G.M. (2002). Physics and applications of microfluidics in biology. Annu Rev Biomed Eng *4*, 261-286.

Behrenfeld, M.J., O/'Malley, R.T., Siegel, D.A., McClain, C.R., Sarmiento, J.L., Feldman, G.C., Milligan, A.J., Falkowski, P.G., Letelier, R.M., and Boss, E.S. (2006). Climate-driven trends in contemporary ocean productivity. Nature *444*, 752-755.

Beneyton, T., Coldren, F., Baret, J.-C., Griffiths, A.D., and Taly, V. (2014). CotA laccase: high-throughput manipulation and analysis of recombinant enzyme libraries expressed in E. coli using droplet-based microfluidics. Analyst *139*, 3314-3323.

Blaxter, J.H., Douglas, B., Tyler, P.A., and Mauchline, J. (1998). The Biology of Calanoid Copepods: The Biology of Calanoid Copepods, Vol 33 (Academic Press).

Bliss, C. (1939). The toxicity of poisons applied jointly1. Annals of applied biology *26*, 585-615.

Bodas, D., and Khan-Malek, C. (2006). Formation of more stable hydrophilic surfaces of PDMS by plasma and chemical treatments. Microelectronic Engineering *83*, 1277-1279.

Brittain, S., Paul, K., Zhao, X.-M., and Whitesides, G. (1998). Soft lithography and microfabrication. Physics World *11*, 31-36.

Brody, J.P., Yager, P., Goldstein, R.E., and Austin, R.H. (1996). Biotechnology at low Reynolds numbers. Biophys J *71*, 3430-3441.

Caldeira, K., and Wickett, M.E. (2003). Oceanography: anthropogenic carbon and ocean pH. Nature *425*, 365-365.

Caldeira, K., and Wickett, M.E. (2005). Ocean model predictions of chemistry changes from carbon dioxide emissions to the atmosphere and ocean. Journal of Geophysical Research: Oceans (1978–2012) *110*.

Calosi, P., Rastrick, S.P., Lombardi, C., de Guzman, H.J., Davidson, L., Jahnke, M., Giangrande, A., Hardege, J.D., Schulze, A., and Spicer, J.I. (2013). Adaptation and acclimatization to ocean acidification in marine ectotherms: an in situ transplant experiment with polychaetes at a shallow CO2 vent system. Philosophical Transactions of the Royal Society of London B: Biological Sciences *368*, 20120444.

Cao, J., Kursten, D., Schneider, S., Knauer, A., Gunther, P.M., and Kohler, J.M. (2012). Uncovering toxicological complexity by multi-dimensional screenings in microsegmented flow: modulation of antibiotic interference by nanoparticles. Lab on a chip *12*, 474-484.

Carrel, A. (1912). PURE CULTURES OF CELLS. The Journal of Experimental Medicine *16*, 165-168.

Castello, A., Fischer, B., Eichelbaum, K., Horos, R., Beckmann, B.M., Strein, C., Davey, N.E., Humphreys, D.T., Preiss, T., and Steinmetz, L.M. (2012). Insights into RNA biology from an atlas of mammalian mRNA-binding proteins. Cell *149*, 1393-1406.

Cervera, L., Gutiérrez, S., Gòdia, F., and Segura, M.M. (2011). Optimization of HEK 293 cell growth by addition of non-animal derived components using design of experiments. BMC Proceedings *5*, P126-P126.

Chiu, D.T., Jeon, N.L., Huang, S., Kane, R.S., Wargo, C.J., Choi, I.S., Ingber, D.E., and Whitesides, G.M. (2000). Patterned deposition of cells and proteins onto surfaces by using three-dimensional microfluidic systems. Proceedings of the National Academy of Sciences *97*, 2408-2413.

Christopher, G., Bergstein, J., End, N., Poon, M., Nguyen, C., and Anna, S.L. (2009). Coalescence and splitting of confined droplets at microfluidic junctions. Lab on a chip *9*, 1102-1109.

Chung, C., and Burdick, J.A. (2008). Engineering cartilage tissue. Advanced drug delivery reviews *60*, 243-262.

Chung, K., Crane, M.M., and Lu, H. (2008). Automated on-chip rapid microscopy, phenotyping and sorting of C. elegans. Nature methods *5*, 637-643.

Cigliano, M., Gambi, M., Rodolfo-Metalpa, R., Patti, F., and Hall-Spencer, J. (2010). Effects of ocean acidification on invertebrate settlement at volcanic CO2 vents. Marine Biology *157*, 2489-2502.

Clausell-Tormos, J., Griffiths, A.D., and Merten, C.A. (2010). An automated two-phase microfluidic system for kinetic analyses and the screening of compound libraries. Lab on a chip *10*, 1302-1307.

Clausell-Tormos, J., Lieber, D., Baret, J.-C., El-Harrak, A., Miller, O.J., Frenz, L., Blouwolff, J., Humphry, K.J., Köster, S., and Duan, H. (2008). Droplet-based microfluidic platforms for the encapsulation and screening of mammalian cells and multicellular organisms. Chemistry & biology *15*, 427-437.

Crane, M.M., Chung, K., and Lu, H. (2009). Computer-enhanced high-throughput genetic screens of C. elegans in a microfluidic system. Lab on a chip *9*, 38-40.

Csete, M. (2005). Oxygen in the cultivation of stem cells. Annals of the New York Academy of Sciences *1049*, 1-8.

De Menech, M., Garstecki, P., Jousse, F., and Stone, H. (2008). Transition from squeezing to dripping in a microfluidic T-shaped junction. journal of fluid mechanics *595*, 141-161.

de Vargas, C., Audic, S., Henry, N., Decelle, J., Mahé, F., Logares, R., Lara, E., Berney, C., Le Bescot, N., Probert, I.*, et al.* (2015). Eukaryotic plankton diversity in the sunlit ocean. Science *348*.

del Corral, R.D., and Storey, K.G. (2004). Opposing FGF and retinoid pathways: a signalling switch that controls differentiation and patterning onset in the extending vertebrate body axis. Bioessays *26*, 857-869.

Ding, S., Wu, T.Y., Brinker, A., Peters, E.C., Hur, W., Gray, N.S., and Schultz, P.G. (2003). Synthetic small molecules that control stem cell fate. Proceedings of the National Academy of Sciences of the United States of America *100*, 7632-7637.

Doney, S.C., Ruckelshaus, M., Emmett Duffy, J., Barry, J.P., Chan, F., English, C.A., Galindo, H.M., Grebmeier, J.M., Hollowed, A.B., and Knowlton, N. (2012). Climate change impacts on marine ecosystems. Annual review of marine science *4*, 11-37.

Dove, A. (1999). Drug screening-beyond the bottleneck. Nature biotechnology *17*, 859-864.

Duplessy, J.-C., Labeyrie, L., Arnold, M., Paterne, M., Duprat, J., and van Weering, T.C. (1992). Changes in surface salinity of the North Atlantic Ocean during the last deglaciation.

Edelstein, A., Amodaj, N., Hoover, K., Vale, R., and Stuurman, N. (2010). Computer control of microscopes using μManager. Current protocols in molecular biology, 14.20. 11-14.20. 17.

Edwards, M., and Richardson, A.J. (2004). Impact of climate change on marine pelagic phenology and trophic mismatch. Nature *430*, 881-884.

Eicher, D., Ramanathan, N., and Merten, C.A. (2015). Soft compartmentalization: Combining droplet-based microfluidics with freely accessible cells. Engineering in Life Sciences.

El Debs, B., Utharala, R., Balyasnikova, I.V., Griffiths, A.D., and Merten, C.A. (2012). Functional single-cell hybridoma screening using droplet-based microfluidics. Proceedings of the National Academy of Sciences *109*, 11570-11575.

Engler, A.J., Sen, S., Sweeney, H.L., and Discher, D.E. (2006). Matrix Elasticity Directs Stem Cell Lineage Specification. Cell *126*, 677-689.

Ertl, P., Sticker, D., Charwat, V., Kasper, C., and Lepperdinger, G. (2014). Lab-on-a-chip technologies for stem cell analysis. Trends in biotechnology *32*, 245-253.

Evans, M.J., and Kaufman, M.H. (1981). Establishment in culture of pluripotential cells from mouse embryos. nature *292*, 154-156.

Fabry, V.J., Seibel, B.A., Feely, R.A., and Orr, J.C. (2008). Impacts of ocean acidification on marine fauna and ecosystem processes. ICES Journal of Marine Science: Journal du Conseil *65*, 414-432.

Fischer, A., and Dorresteijn, A. (2004). The polychaete Platynereis dumerilii (Annelida): a laboratory animal with spiralian cleavage, lifelong segment proliferation and a mixed benthic/pelagic life cycle. Bioessays *26*, 314-325.

Freyer, J.P., Fillak, D., and Jett, J.H. (1989). Use of xantham gum to suspend large particles during flow cytometric analysis and sorting. Cytometry *10*, 803-806.

Gardner, R.L. (2002). Stem cells: potency, plasticity and public perception. Journal of Anatomy *200*, 277-282.

Gobaa, S., Hoehnel, S., Roccio, M., Negro, A., Kobel, S., and Lutolf, M.P. (2011). Artificial niche microarrays for probing single stem cell fate in high throughput. Nat Meth *8*, 949-955.

Griner, L.A.M., Guha, R., Shinn, P., Young, R.M., Keller, J.M., Liu, D., Goldlust, I.S., Yasgar, A., McKnight, C., and Boxer, M.B. (2014). High-throughput combinatorial screening identifies drugs that cooperate with ibrutinib to kill activated B-cell–like diffuse large B-cell lymphoma cells. Proceedings of the National Academy of Sciences *111*, 2349-2354.

Gu, H., Malloggi, F., Vanapalli, S.A., and Mugele, F. (2008). Electrowetting-enhanced microfluidic device for drop generation. Applied Physics Letters *93*, 183507.

Gu, W., Zhu, X., Futai, N., Cho, B.S., and Takayama, S. (2004). Computerized microfluidic cell culture using elastomeric channels and Braille displays. Proceedings of the National Academy of Sciences of the United States of America *101*, 15861-15866.

Guo, M.T., Rotem, A., Heyman, J.A., and Weitz, D.A. (2012). Droplet microfluidics for high-throughput biological assays. Lab on a chip *12*, 2146-2155.

Gutierrez, M., Gagneten, A., and Paggi, J. (2011). Behavioural responses of two cladocerans and two copepods exposed to fish kairomones. Marine and Freshwater Behaviour and Physiology *44*, 289-303.

Han, M., Gao, X., Su, J.Z., and Nie, S. (2001). Quantum-dot-tagged microbeads for multiplexed optical coding of biomolecules. Nat Biotechnol *19*, 631-635.

Hansen, C.L., Classen, S., Berger, J.M., and Quake, S.R. (2006). A Microfluidic Device for Kinetic Optimization of Protein Crystallization and In Situ Structure Determination. Journal of the American Chemical Society *128*, 3142-3143.

Hattori, K., Sugiura, S., and Kanamori, T. (2011). Microenvironment array chip for cell culture environment screening. Lab on a chip *11*, 212-214.

Hay, M.E. (2009). Marine chemical ecology: chemical signals and cues structure marine populations, communities, and ecosystems. Annual Review of Marine Science *1*, 193.

Hays, G.C., Richardson, A.J., and Robinson, C. (2005). Climate change and marine plankton. Trends in Ecology & Evolution *20*, 337-344.

Heuschele, J., and Selander, E. (2014). The chemical ecology of copepods. Journal of Plankton Research *36*, 895-913.

Hima Bindu, A. (2011). Potency of Various Types of Stem Cells and their Transplantation. Journal of Stem Cell Research & Therapy.

Hirabayashi, Y., Itoh, Y., Tabata, H., Nakajima, K., Akiyama, T., Masuyama, N., and Gotoh, Y. (2004). The Wnt/β-catenin pathway directs neuronal differentiation of cortical neural precursor cells. Development *131*, 2791-2801.

Hoegh-Guldberg, O., and Bruno, J.F. (2010). The Impact of Climate Change on the World's Marine Ecosystems. Science *328*, 1523-1528.

Hoegh-Guldberg, O., Mumby, P., Hooten, A., Steneck, R., Greenfield, P., Gomez, E., Harvell, C., Sale, P., Edwards, A., and Caldeira, K. (2007). Coral reefs under rapid climate change and ocean acidification. science *318*, 1737-1742.

Hou, P., Li, Y., Zhang, X., Liu, C., Guan, J., Li, H., Zhao, T., Ye, J., Yang, W., Liu, K., *et al.* (2013). Pluripotent stem cells induced from mouse somatic cells by small-molecule compounds. Science *341*, 651-654.

Houghton, R.A., Hackler, J.L., and Cushman, R.M. (2001). Carbon flux to the atmosphere from land-use changes: 1850 to 1990 (Carbon Dioxide Information Center, Environmental Sciences Division, Oak Ridge National Laboratory).

Huang, S.-B., Wang, S.-S., Hsieh, C.-H., Lin, Y.C., Lai, C.-S., and Wu, M.-H. (2013). An integrated microfluidic cell culture system for high-throughput perfusion three-dimensional cell culture-based assays: effect of cell culture model on the results of chemosensitivity assays. Lab on a chip *13*, 1133-1143.

Huch, M., Bonfanti, P., Boj, S.F., Sato, T., Loomans, C.J., van de Wetering, M., Sojoodi, M., Li, V.S., Schuijers, J., and Gracanin, A. (2013a). Unlimited in vitro expansion of adult bi-potent pancreas progenitors through the Lgr5/R-spondin axis. The EMBO journal *32*, 2708-2721.

Huch, M., Dorrell, C., Boj, S.F., van Es, J.H., Li, V.S., van de Wetering, M., Sato, T., Hamer, K., Sasaki, N., and Finegold, M.J. (2013b). In vitro expansion of single Lgr5+ liver stem cells induced by Wnt-driven regeneration. Nature *494*, 247-250.

Hughes, E.D., Qu, Y.Y., Genik, S.J., Lyons, R.H., Pacheco, C.D., Lieberman, A.P., Samuelson, L.C., Nasonkin, I.O., Camper, S.A., and Van Keuren, M.L. (2007). Genetic variation in C57BL/6 ES cell lines and genetic instability in the Bruce4 C57BL/6 ES cell line. Mammalian Genome *18*, 549-558.

Huh, D., Leslie, D.C., Matthews, B.D., Fraser, J.P., Jurek, S., Hamilton, G.A., Thorneloe, K.S., McAlexander, M.A., and Ingber, D.E. (2012). A human disease model of drug toxicity-induced pulmonary edema in a lung-on-a-chip microdevice. Science translational medicine *4*, 159ra147.

Huh, D., Matthews, B.D., Mammoto, A., Montoya-Zavala, M., Hsin, H.Y., and Ingber, D.E. (2010). Reconstituting Organ-Level Lung Functions on a Chip. Science *328*, 1662-1668.

Hung, P.J., Lee, P.J., Sabounchi, P., Lin, R., and Lee, L.P. (2005). Continuous perfusion microfluidic cell culture array for high-throughput cell-based assays. Biotechnology and bioengineering *89*, 1-8.

Ingber, D.E. (2006). Cellular mechanotransduction: putting all the pieces together again. The FASEB journal *20*, 811-827.

Irimia, D., Geba, D.A., and Toner, M. (2006). Universal microfluidic gradient generator. Analytical chemistry *78*, 3472-3477.

Jang, H.J., Kim, J.S., Choi, H.W., Jeon, I., Choi, S., Kim, M.J., Song, J., and Do, J.T. (2014). Neural stem cells derived from epiblast stem cells display distinctive properties. Stem Cell Research *12*, 506-516.

Jeon, N.L., Baskaran, H., Dertinger, S.K., Whitesides, G.M., Van De Water, L., and Toner, M. (2002). Neutrophil chemotaxis in linear and complex gradients of interleukin-8 formed in a microfabricated device. Nature biotechnology *20*, 826-830.

Jeon, N.L., Dertinger, S.K., Chiu, D.T., Choi, I.S., Stroock, A.D., and Whitesides, G.M. (2000). Generation of solution and surface gradients using microfluidic systems. Langmuir *16*, 8311-8316.

Kanke, K., Masaki, H., Saito, T., Komiyama, Y., Hojo, H., Nakauchi, H., Lichtler, Alexander C., Takato, T., Chung, U.-i., and Ohba, S. (2014). Stepwise Differentiation of Pluripotent Stem Cells into Osteoblasts Using Four Small Molecules under Serum-free and Feeder-free Conditions. Stem Cell Reports *2*, 751-760.

Kann, L.M., and Wishner, K. (1995). Spatial and temporal patterns of zooplankton on baleen whale feeding grounds in the southern Gulf of Maine. Journal of Plankton Research *17*, 235-262.

Kleinsmith, L.J., and Pierce, G.B. (1964). Multipotentiality of single embryonal carcinoma cells. Cancer research *24*, 1544-1551.

Larsch, J., Ventimiglia, D., Bargmann, C.I., and Albrecht, D.R. (2013). High-throughput imaging of neuronal activity in Caenorhabditis elegans. Proceedings of the National Academy of Sciences *110*, E4266-E4273.

Laurent, L.C., Ulitsky, I., Slavin, I., Tran, H., Schork, A., Morey, R., Lynch, C., Harness, J.V., Lee, S., and Barrero, M.J. (2011). Dynamic changes in the copy number of pluripotency and cell proliferation genes in human ESCs and iPSCs during reprogramming and time in culture. Cell stem cell *8*, 106-118.

Lazzaretto, I., and Salvato, B. (1992). Cannibalistic behaviour in the harpacticoid copepod Tigriopus fulvus. Marine Biology *113*, 579-582.

Lee, C.-C., Sui, G., Elizarov, A., Shu, C.J., Shin, Y.-S., Dooley, A.N., Huang, J., Daridon, A., Wyatt, P., Stout, D.*, et al.* (2005). Multistep Synthesis of a Radiolabeled Imaging Probe Using Integrated Microfluidics. Science *310*, 1793-1796.

Lee, J., Cuddihy, M.J., and Kotov, N.A. (2008). Three-dimensional cell culture matrices: state of the art. Tissue engineering Part B, Reviews *14*, 61-86.

Lee, K.Y., and Mooney, D.J. (2001). Hydrogels for tissue engineering. Chem Rev *101*, 1869-1879.

Lee, W., Walker, L.M., and Anna, S.L. (2009). Role of geometry and fluid properties in droplet and thread formation processes in planar flow focusing. Physics of Fluids (1994-present) *21*, 032103.

Lei, Y., Liu, Y., Wang, W., Wu, W., and Li, Z. (2011). Studies on Parylene C-caulked PDMS (pcPDMS) for low permeability required microfluidics applications. Lab on a chip *11*, 1385-1388.

Li, F., He, Z., Li, Y., Liu, P., Chen, F., Wang, M., Zhu, H., Ding, X., Wangensteen, K.J., Hu, Y.*, et al.* (2011). Combined activin A/LiCl/Noggin treatment improves production of mouse embryonic stem cell-derived definitive endoderm cells. Journal of cellular biochemistry *112*, 1022-1034.

Li, H., Roblin, G., Liu, H., and Heller, S. (2003). Generation of hair cells by stepwise differentiation of embryonic stem cells. Proceedings of the National Academy of Sciences *100*, 13495-13500.

Lindsey, R., and Scott, M. (2010). Importance of phytoplankton. NASA Earth Observatory, http://earthobservatorynasagov/Features/Phytoplankton/page2php.

Lipinski, C.A., Lombardo, F., Dominy, B.W., and Feeney, P.J. (2012). Experimental and computational approaches to estimate solubility and permeability in drug discovery and development settings. Advanced drug delivery reviews *64*, 4-17.

Liu, J., Hansen, C., and Quake, S.R. (2003). Solving the "World-to-Chip" Interface Problem with a Microfluidic Matrix. Analytical Chemistry *75*, 4718-4723.

Loewe, S. (1928). Die quantitativen probleme der pharmakologie. Ergebnisse der Physiologie *27*, 47-187.

Lu, J., Tan, L., Li, P., Gao, H., Fang, B., Ye, S., Geng, Z., Zheng, P., and Song, H. (2009). All-trans retinoic acid promotes neural lineage entry by pluripotent embryonic stem cells via multiple pathways. BMC cell biology *10*, 57.

Lucchetta, E.M., Lee, J.H., Fu, L.A., Patel, N.H., and Ismagilov, R.F. (2005). Dynamics of Drosophila embryonic patterning network perturbed in space and time using microfluidics. Nature *434*, 1134-1138.

Macarron, R., Banks, M.N., Bojanic, D., Burns, D.J., Cirovic, D.A., Garyantes, T., Green, D.V., Hertzberg, R.P., Janzen, W.P., and Paslay, J.W. (2011). Impact of high-throughput screening in biomedical research. Nature reviews Drug discovery *10*, 188-195.

Maden, M. (2007). Retinoic acid in the development, regeneration and maintenance of the nervous system. Nature Reviews Neuroscience *8*, 755-765.

Maitra, A., Arking, D.E., Shivapurkar, N., Ikeda, M., Stastny, V., Kassauei, K., Sui, G., Cutler, D.J., Liu, Y., and Brimble, S.N. (2005). Genomic alterations in cultured human embryonic stem cells. Nature genetics *37*, 1099-1103.

Marcus, J.S. (2006). Single cell gene expression analysis using microfluidics. PhD thesis Calif Inst Tech, 165 pp.

Marcus, J.S., Anderson, W.F., and Quake, S.R. (2006). Microfluidic Single-Cell mRNA Isolation and Analysis. Analytical Chemistry *78*, 3084-3089.

Marland, G., Brenkert, A., and Olivier, J. (1999). CO 2 from fossil fuel burning: a comparison of ORNL and EDGAR estimates of national emissions. Environmental Science & Policy *2*, 265-273.

Martello, G., and Smith, A. (2014). The nature of embryonic stem cells. Annual review of cell and developmental biology *30*, 647-675.

Martin, G.R. (1980). Teratocarcinomas and mammalian embryogenesis. Science *209*, 768-776.

Martin, G.R. (1981). Isolation of a pluripotent cell line from early mouse embryos cultured in medium conditioned by teratocarcinoma stem cells. Proceedings of the National Academy of Sciences *78*, 7634-7638.

Martin, G.R., and Evans, M.J. (1975). Differentiation of clonal lines of teratocarcinoma cells: formation of embryoid bodies in vitro. Proceedings of the National Academy of Sciences *72*, 1441-1445.

Marx, V. (2013). Where stem cells call home. Nature Methods *10*, 111-115.

Matebr, R.J., and Hirst, A.C. (1999). Climate change feedback on the future oceanic CO2 uptake. Tellus B *51*, 722-733.

Mayola, A., Irazoki, O., Martínez, I.A., Petrov, D., Menolascina, F., Stocker, R., Reyes-Darias, J.A., Krell, T., Barbé, J., and Campoy, S. (2014). RecA Protein Plays a Role in the Chemotactic Response and Chemoreceptor Clustering of <italic>Salmonella enterica</italic>. PLoS ONE *9*, e105578.

McDonald, J.C., and Whitesides, G.M. (2002). Poly(dimethylsiloxane) as a material for fabricating microfluidic devices. Acc Chem Res *35*, 491-499.

Meier, M., Lucchetta, E.M., and Ismagilov, R.F. (2010). Chemical stimulation of the Arabidopsis thaliana root using multi-laminar flow on a microfluidic chip. Lab on a chip *10*, 2147-2153.

Miller, O.J., El Harrak, A., Mangeat, T., Baret, J.-C., Frenz, L., El Debs, B., Mayot, E., Samuels, M.L., Rooney, E.K., and Dieu, P. (2012). High-resolution dose–response screening using droplet-based microfluidics. Proceedings of the National Academy of Sciences *109*, 378-383.

Mitchison, T.J. (1994). Towards a pharmacological genetics. Chemistry & biology *1*, 3-6.

Miyanari, Y., and Torres-Padilla, M.-E. (2012). Control of ground-state pluripotency by allelic regulation of Nanog. Nature *483*, 470-473.

Mukhopadhyay, R. (2007). When PDMS isn't the best. Analytical chemistry *79*, 3248-3253.

Najm, F.J., Zaremba, A., Caprariello, A.V., Nayak, S., Freundt, E.C., Scacheri, P.C., Miller, R.H., and Tesar, P.J. (2011). Rapid and robust generation of functional oligodendrocyte progenitor cells from epiblast stem cells. Nat Meth *8*, 957-962.

Närvä, E., Autio, R., Rahkonen, N., Kong, L., Harrison, N., Kitsberg, D., Borghese, L., Itskovitz-Eldor, J., Rasool, O., and Dvorak, P. (2010). High-resolution DNA analysis of human embryonic stem cell lines reveals culture-induced copy number changes and loss of heterozygosity. Nature biotechnology *28*, 371-377.

Nishiguchi, S., Wood, H., Kondoh, H., Lovell-Badge, R., and Episkopou, V. (1998). Sox1 directly regulates the γ-crystallin genes and is essential for lens development in mice. Genes & Development *12*, 776-781.

Okada, Y., Shimazaki, T., Sobue, G., and Okano, H. (2004). Retinoic-acid-concentration-dependent acquisition of neural cell identity during in vitro differentiation of mouse embryonic stem cells. Developmental biology *275*, 124-142.

Papaioannou, V., and Rossant, J. (1983). Effects of the embryonic environment on proliferation and differentiation of embryonal carcinoma cells. Cancer surveys *2*, 165-183.

Park, S.-Y., Wu, T.-H., Chen, Y., Teitell, M.A., and Chiou, P.-Y. (2011). High-speed droplet generation on demand driven by pulse laser-induced cavitation. Lab on a chip *11*, 1010-1012.

Pauklin, S., Pedersen, R.A., and Vallier, L. (2011). Mouse pluripotent stem cells at a glance. Journal of cell science *124*, 3727-3732.

Pettinato, G., Wen, X., and Zhang, N. (2014). Formation of Well-defined Embryoid Bodies from Dissociated Human Induced Pluripotent Stem Cells using Microfabricated Cell-repellent Microwell Arrays. Sci Rep *4*.

Pevny, L.H., Sockanathan, S., Placzek, M., and Lovell-Badge, R. (1998). A role for SOX1 in neural determination. Development *125*, 1967-1978.

Poulet, S., and Ouellet, G. (1982). The role of amino acids in the chemosensory swarming and feeding of marine copepods. Journal of Plankton Research *4*, 341-361.

Preibisch, S., Saalfeld, S., and Tomancak, P. (2009). Globally optimal stitching of tiled 3D microscopic image acquisitions. Bioinformatics *25*, 1463-1465.

Proudfoot, J.R. (2005). The evolution of synthetic oral drug properties. Bioorganic & medicinal chemistry letters *15*, 1087-1090.

Qin, D., Xia, Y., Rogers, J.A., Jackman, R.J., Zhao, X.-M., and Whitesides, G.M. (1998). Microfabrication, microstructures and microsystems. In Microsystem technology in chemistry and life science (Springer), pp. 1-20.

Rafalski, V.A., Mancini, E., and Brunet, A. (2012). Energy metabolism and energy-sensing pathways in mammalian embryonic and adult stem cell fate. Journal of cell science *125*, 5597-5608.

Ramanathan, N., Simakov, O., Merten, C.A., and Arendt, D. (submitted manuscript). Ocean on a chip: Quantifying preferences and responsiveness of marine zooplankton to changing environmental conditions.

Rane, T.D., Zec, H.C., and Wang, T.-H. (2014). A Barcode-Free Combinatorial Screening Platform for Matrix Metalloproteinase Screening. Analytical chemistry.

Rawlinson, K., Davenport, J., and Barnes, D. (2004). Vertical migration strategies with respect to advection and stratification in a semi-enclosed lough: a comparison of mero-and holozooplankton. Marine Biology *144*, 935-946.

Rayleigh, L. (1879). On the capillary phenomena of jets. Paper presented at: Proc R Soc London.

Regehr, K.J., Domenech, M., Koepsel, J.T., Carver, K.C., Ellison-Zelski, S.J., Murphy, W.L., Schuler, L.A., Alarid, E.T., and Beebe, D.J. (2009). Biological implications of polydimethylsiloxane-based microfluidic cell culture. Lab on a chip *9*, 2132-2139.

Reul, N., Fournier, S., Boutin, J., Hernandez, O., Maes, C., Chapron, B., Alory, G., Quilfen, Y., Tenerelli, J., and Morisset, S. (2014). Sea surface salinity observations from space with the SMOS satellite: a new means to monitor the marine branch of the water cycle. Surveys in Geophysics *35*, 681-722.

Reyes, D.R., Iossifidis, D., Auroux, P.-A., and Manz, A. (2002). Micro total analysis systems. 1. Introduction, theory, and technology. Analytical chemistry *74*, 2623-2636.

Riebesell, U., Gattuso, J.-P., Thingstad, T., and Middelburg, J. (2013). Preface" Arctic ocean acidification: pelagic ecosystem and biogeochemical responses during a mesocosm study". Biogeosciences (BG) *10*, 5619-5626.

Roman, G.T., and Culbertson, C.T. (2006). Surface engineering of poly (dimethylsiloxane) microfluidic devices using transition metal sol-gel chemistry. Langmuir *22*, 4445-4451.

Roman, G.T., Hlaus, T., Bass, K.J., Seelhammer, T.G., and Culbertson, C.T. (2005). Sol-gel modified poly (dimethylsiloxane) microfluidic devices with high electroosmotic mobilities and hydrophilic channel wall characteristics. Analytical chemistry *77*, 1414-1422.

Ruhl, H.A., and Smith, K.L. (2004). Shifts in Deep-Sea Community Structure Linked to Climate and Food Supply. Science *305*, 513-515.

Sato, T., Stange, D.E., Ferrante, M., Vries, R.G., Van Es, J.H., Van den Brink, S., Van Houdt, W.J., Pronk, A., Van Gorp, J., and Siersema, P.D. (2011). Long-term expansion of epithelial organoids from human colon, adenoma, adenocarcinoma, and Barrett's epithelium. Gastroenterology *141*, 1762-1772.

Sato, T., Vries, R.G., Snippert, H.J., van de Wetering, M., Barker, N., Stange, D.E., van Es, J.H., Abo, A., Kujala, P., Peters, P.J*., et al.* (2009). Single Lgr5 stem cells build crypt-villus structures in vitro without a mesenchymal niche. Nature *459*, 262-265.

Scadden, D.T. (2006). The stem-cell niche as an entity of action. Nature *441*, 1075-1079.

Schilling, E. (2001). Basic microfluidic concepts.http://facultywashingtonedu/yagerp/microfluidicstutorial/basicconcepts/basicconceptshtm.

Schoene, N.W., and Kamara, K.S. (1999). Population doubling time, phosphatase activity, and hydrogen peroxide generation in Jurkat cells. Free Radical Biology and Medicine *27*, 364-369.

Schreiber, S.L. (1998). Chemical genetics resulting from a passion for synthetic organic chemistry. Bioorganic & medicinal chemistry *6*, 1127-1152.

Serra, M., Correia, C., Malpique, R., Brito, C., Jensen, J., Bjorquist, P., Carrondo, M.J.T., and Alves, P.M. (2011). Microencapsulation technology: a powerful tool for integrating expansion and cryopreservation of human embryonic stem cells. PLoS One *6*.

Seymour, J.R., Simó, R., Ahmed, T., and Stocker, R. (2010). Chemoattraction to Dimethylsulfoniopropionate Throughout the Marine Microbial Food Web. Science *329*, 342-345.

Shamir, E.R., and Ewald, A.J. (2014). Three-dimensional organotypic culture: experimental models of mammalian biology and disease. Nature Reviews Molecular Cell Biology *15*, 647-664.

Shim, J.-u., Patil, S.N., Hodgkinson, J.T., Bowden, S.D., Spring, D.R., Welch, M., Huck, W.T.S., Hollfelder, F., and Abell, C. (2011). Controlling the contents of microdroplets by exploiting the permeability of PDMS. Lab on a chip *11*, 1132-1137.

Sia, S.K., and Whitesides, G.M. (2003). Microfluidic devices fabricated in poly(dimethylsiloxane) for biological studies. Electrophoresis *24*, 3563-3576.

Siegenthaler, U., and Sarmiento, J. (1993). Atmospheric carbon dioxide and the ocean. Nature *365*, 119-125.

Skelley, A.M., Scherer, J.R., Aubrey, A.D., Grover, W.H., Ivester, R.H., Ehrenfreund, P., Grunthaner, F.J., Bada, J.L., and Mathies, R.A. (2005). Development and evaluation of a microdevice for amino acid biomarker detection and analysis on Mars. Proceedings of the National Academy of Sciences of the United States of America *102*, 1041-1046.

Smith, A.G. (1991). Culture and differentiation of embryonic stem cells. Journal of tissue culture methods *13*, 89-94.

Snell, T.W., and Morris, P.D. (1993). Sexual communication in copepods and rotifers. Hydrobiologia *255*, 109-116.

Song, H., Tice, J.D., and Ismagilov, R.F. (2003). A microfluidic system for controlling reaction networks in time. Angewandte Chemie *115*, 792-796.

Squires, T.M., and Quake, S.R. (2005). Microfluidics: Fluid physics at the nanoliter scale. Rev Mod Phys *77*, 977-1026.

Stevens Jr, L.C., and Little, C.C. (1954). Spontaneous testicular teratomas in an inbred strain of mice. Proceedings of the National Academy of Sciences of the United States of America *40*, 1080.

Subramanian, B., Kim, N., Lee, W., Spivak, D.A., Nikitopoulos, D.E., McCarley, R.L., and Soper, S.A. (2011). Surface Modification of Droplet Polymeric Microfluidic Devices for the Stable and Continuous Generation of Aqueous Droplets. Langmuir *27*, 7949-7957.

Takahashi, K., Tanabe, K., Ohnuki, M., Narita, M., Ichisaka, T., Tomoda, K., and Yamanaka, S. (2007). Induction of pluripotent stem cells from adult human fibroblasts by defined factors. cell *131*, 861-872.

Takahashi, K., and Yamanaka, S. (2006). Induction of pluripotent stem cells from mouse embryonic and adult fibroblast cultures by defined factors. cell *126*, 663-676.

Takayama, S., Ostuni, E., LeDuc, P., Naruse, K., Ingber, D.E., and Whitesides, G.M. (2001). Laminar flows - Subcellular positioning of small molecules. Nature *411*, 1016-1016.

Takayama, S., Ostuni, E., LeDuc, P., Naruse, K., Ingber, D.E., and Whitesides, G.M. (2003). Selective Chemical Treatment of Cellular Microdomains Using Multiple Laminar Streams. Chemistry & Biology *10*, 123-130.

Tateda, K., Ishii, Y., Matsumoto, T., and Yamaguchi, K. (2006). 'Break-point Checkerboard Plate' for screening of appropriate antibiotic combinations against multidrug-resistant Pseudomonas aeruginosa. Scandinavian Journal of Infectious Diseases *38*, 268-272.

Tatistcheff, H.B., Fritsch-Faules, I., and Wrighton, M.S. (1993). Comparison of diffusion coefficients of electroactive species in aqueous fluid electrolytes and polyacrylate gels: step generation-collection diffusion measurements and operation of electrochemical devices. The Journal of Physical Chemistry *97*, 2732-2739.

Taylor, A.H., Allen, J.I., and Clark, P.A. (2002). Extraction of a weak climatic signal by an ecosystem. Nature *416*, 629-632.

Taylor, G. (1953). Dispersion of Soluble Matter in Solvent Flowing Slowly through a Tube. Proceedings of the Royal Society of London A: Mathematical, Physical and Engineering Sciences *219*, 186-203.

Taylor, G. (1954). The dispersion of matter in turbulent flow through a pipe. Proceedings of the Royal Society of London Series A Mathematical and Physical Sciences *223*, 446-468.

Tesar, P.J., Chenoweth, J.G., Brook, F.A., Davies, T.J., Evans, E.P., Mack, D.L., Gardner, R.L., and McKay, R.D. (2007). New cell lines from mouse epiblast share defining features with human embryonic stem cells. Nature *448*, 196-199.

Teslaa, T., and Teitell, M.A. (2015). Pluripotent stem cell energy metabolism: an update. The EMBO journal *34*, 138-153.

Thorsen, T., Maerkl, S.J., and Quake, S.R. (2002). Microfluidic Large-Scale Integration. Science *298*, 580-584.

Thorsen, T., Roberts, R.W., Arnold, F.H., and Quake, S.R. (2001). Dynamic pattern formation in a vesicle-generating microfluidic device. Physical review letters *86*, 4163.

Toepke, M.W., and Beebe, D.J. (2006). PDMS absorption of small molecules and consequences in microfluidic applications. Lab on a chip *6*, 1484-1486.

Toh, A.G., Wang, Z., Yang, C., and Nguyen, N.-T. (2014). Engineering microfluidic concentration gradient generators for biological applications. Microfluidics and nanofluidics *16*, 1-18.

Torres, J., Prieto, J., Durupt, F.C., Broad, S., and Watt, F.M. (2012). Efficient Differentiation of Embryonic Stem Cells into Mesodermal Precursors by BMP, Retinoic Acid and Notch Signalling. PLoS ONE *7*, e36405.

Tout, J., Jeffries, T.C., Petrou, K., Tyson, G.W., Webster, N.S., Garren, M., Stocker, R., Ralph, P.J., and Seymour, J.R. (2015). Chemotaxis by natural populations of coral reef bacteria. ISME J.

Tumarkin, E., Tzadu, L., Csaszar, E., Seo, M., Zhang, H., Lee, A., Peerani, R., Purpura, K., Zandstra, P.W., and Kumacheva, E. (2011). High-throughput combinatorial cell co-culture using microfluidics. Integrative Biology *3*, 653-662.

Umbanhowar, P.B., Prasad, V., and Weitz, D.A. (2000). Monodisperse Emulsion Generation via Drop Break Off in a Coflowing Stream. Langmuir *16*, 347-351.

Unger, M.A., Chou, H.-P., Thorsen, T., Scherer, A., and Quake, S.R. (2000). Monolithic microfabricated valves and pumps by multilayer soft lithography. Science *288*, 113-116.

Upadhyaya, S., and Selvaganapathy, P.R. (2010). Microfluidic devices for cell based high throughput screening. Lab on a chip *10*, 341-348.

Varum, S., Rodrigues, A.S., Moura, M.B., Momcilovic, O., Easley, C.A.I.V., Ramalho-Santos, J., Van Houten, B., and Schatten, G. (2011). Energy Metabolism in Human Pluripotent Stem Cells and Their Differentiated Counterparts. PLoS ONE *6*, e20914.

Walsh, D.P., and Chang, Y.-T. (2006). Chemical genetics. Chemical reviews *106*, 2476-2530.

Wang, J., Sui, G., Mocharla, V.P., Lin, R.J., Phelps, M.E., Kolb, H.C., and Tseng, H.R. (2006). Integrated microfluidics for parallel screening of an in situ click chemistry library. Angew Chem Int Ed Engl *45*, 5276-5281.

Wang, J.D., Douville, N.J., Takayama, S., and ElSayed, M. (2012). Quantitative analysis of molecular absorption into PDMS microfluidic channels. Annals of biomedical engineering *40*, 1862-1873.

Wang, Y., Zhang, Z., Chi, Y., Zhang, Q., Xu, F., Yang, Z., Meng, L., Yang, S., Yan, S., and Mao, A. (2013). Long-term cultured mesenchymal stem cells frequently develop genomic mutations but do not undergo malignant transformation. Cell death & disease *4*, e950.

Warner, A., and Hays, G. (1994). Sampling by the continuous plankton recorder survey. Progress in Oceanography *34*, 237-256.

Whitesides, G.M. (2006). The origins and the future of microfluidics. Nature *442*, 368-373.

Wilson, J.L., and McDevitt, T.C. (2013). Stem cell microencapsulation for phenotypic control, bioprocessing, and transplantation. Biotechnol Bioeng *110*, 667-682.

Wray, J., Kalkan, T., Gomez-Lopez, S., Eckardt, D., Cook, A., Kemler, R., and Smith, A. (2011). Inhibition of glycogen synthase kinase-3 alleviates Tcf3 repression of the pluripotency network and increases embryonic stem cell resistance to differentiation. Nature cell biology *13*, 838-845.

Xu, X., Duan, S., Yi, F., Ocampo, A., Liu, G.-H., and Belmonte, J.C.I. (2013). Mitochondrial regulation in pluripotent stem cells. Cell metabolism *18*, 325-332.

Xu, Y., Shi, Y., and Ding, S. (2008). A chemical approach to stem-cell biology and regenerative medicine. Nature *453*, 338-344.

Yamada, Y., and Ikeda, T. (1999). Acute toxicity of lowered pH to some oceanic zooplankton. Plankton Biology and Ecology *46*, 62-67.

Yamanaka, S. (2012). Induced Pluripotent Stem Cells: Past, Present, and Future. Cell Stem Cell *10*, 678-684.

Yeh, P., Tschumi, A.I., and Kishony, R. (2006). Functional classification of drugs by properties of their pairwise interactions. Nature genetics *38*, 489-494.

Ying, Q.-L., Stavridis, M., Griffiths, D., Li, M., and Smith, A. (2003). Conversion of embryonic stem cells into neuroectodermal precursors in adherent monoculture. Nature biotechnology *21*, 183-186.

Ying, Q.-L., Wray, J., Nichols, J., Batlle-Morera, L., Doble, B., Woodgett, J., Cohen, P., and Smith, A. (2008). The ground state of embryonic stem cell self-renewal. Nature *453*, 519-523.

Yu, J., Vodyanik, M.A., Smuga-Otto, K., Antosiewicz-Bourget, J., Frane, J.L., Tian, S., Nie, J., Jonsdottir, G.A., Ruotti, V., and Stewart, R. (2007). Induced pluripotent stem cell lines derived from human somatic cells. Science *318*, 1917-1920.

Zec, H., Rane, T.D., and Wang, T.-H. (2012). Microfluidic platform for on-demand generation of spatially indexed combinatorial droplets. Lab on a chip *12*, 3055-3062.

Zeng, S., Li, B., Su, X.o., Qin, J., and Lin, B. (2009). Microvalve-actuated precise control of individual droplets in microfluidic devices. Lab on a chip *9*, 1340-1343.

Zhang, R., Xia, X., Lau, S., Motegi, C., Weinbauer, M., and Jiao, N. (2012). Response of bacterioplankton community structure to an artificial gradient of pCO2in the Arctic Ocean.

Zhao, T., Zhang, Z.-N., Rong, Z., and Xu, Y. (2011). Immunogenicity of induced pluripotent stem cells. Nature *474*, 212-215.

Zheng, B., and Ismagilov, R.F. (2005). A Microfluidic Approach for Screening Submicroliter Volumes against Multiple Reagents by Using Preformed Arrays of Nanoliter Plugs in a Three-Phase Liquid/Liquid/Gas Flow. Angewandte Chemie (International ed in English) *44*, 2520-2523.